Molecular Dynamics Simulation for Nanoparticle-Surface Collision

by

Milad Khodabakhshi

A thesis
presented to the University of Waterloo
in fulfillment of the
thesis requirement for the degree of
Doctor of Philosophy
in
Mechanical and Mechatronics Engineering (Nanotechnology)

Waterloo, Ontario, Canada, 2021

Examining Committee Membership

The following served on the Examining Committee for this thesis. The decision of the Examining Committee is by majority vote.

External Examiner: **Leung Wallace**
Professor, Dept. of Mechanical Engineering,
Hong Kong Polytechnic University

Supervisor(s): **John Z. Wen**
Professor, Dept. of Mechanical and Mechatronics Engineering,
University of Waterloo
Zhongchao Tan
Professor, Dept. of Mechanical and Mechatronics Engineering,
University of Waterloo

Internal-External Member: **Luis Ricardez Sandoval**
Associate Professor, Dept. of Chemical Engineering,
University of Waterloo

Internal Members:	**Jean-Pierre Hickey** Assistant Professor, Dept. of Mechanical and Mechatronics Engineering, University of Waterloo **Yimin Wu** Assistant Professor, Dept. of Mechanical and Mechatronics Engineering, University of Waterloo

Author's Declaration

I hereby declare that I am the sole author of this thesis. This is a true copy of the thesis, including any required final revisions, as accepted by my examiners.

I understand that my thesis may be made electronically available to the public.

Abstract

Nanoparticles are referred to as those particles with at least one dimension less than 100 nm. Their small sizes lead to high surface area to volume ratios, which results in physical and chemical properties different from their respective larger sized particles and bulk substances. Because of their unique and extraordinary properties, nanoparticles are synthesized and used in a wide range of industrial processes such as biomedicine, energy systems, environmental technologies, and water treatment. Meanwhile, these nanoparticles may become airborne, inhalable and cause air pollution. Therefore, removal of the dispersed nanoparticles from ambient air is essential to protect the public health. The collision of these nanoparticles with a surface needs to be addressed in developing such processes. Accordingly, understanding the collision dynamics and associated characteristics between nanoparticles and substrate surfaces is essential for the design of high-efficiency aerosol nanoparticle filters, as well as fabricating self-assembled nanoparticles, and developing advanced coating technologies, to name a few.

Laboratory equipment is inaccurate in quantifying the effects of different parameters on collision properties of nanoparticles with diameters less than 10 nm on solid surfaces. Additionally, it is impractical to describe for the adhesion behavior based on the dynamic equations of the particle motion because of a lack of information on the material properties. Meanwhile, numerical simulation can help provide a better understanding of the effects of various parameters at molecular scales on the nanoparticle-surface collision properties. Among various simulation techniques, molecular dynamics is especially powerful for the study of collision of nanoparticles because it allows a user to modify system conditions that may not be possible in experiments.

The main objective of this thesis is to investigate the effects of various parameters affecting the adhesion of nanoparticles on a solid surface. The effects of nanoparticle size and relative humidity of the ambient air are examined using molecular dynamics simulation. Air humidity can intervene in a particle-surface collision by forming a layer of water molecules on the surface. These water molecules act as a buffer layer that alter the collision condition. In this work, we study the effects of condensed water layer on the collision of 5-nm silver particles on a silver substrate. The coefficient of restitution is used to characterize the collision. Results indicate that the effects of air humidity on the collisional dynamics depend on the water layer thickness and the surface energy of the substrate. Air humidity can either increase or decrease the coefficient of restitution in the studied nanoparticle collisions. For a high surface energy substrate, the coefficient of restitution first increases then decreases by increasing the water layer thickness on the substrate when the impact velocity changes from 20 to 500 m/s. For a low surface energy substrate, the coefficient of restitution decreases because of a condensed water layer on the substrate at impact velocities less than 300 m/s. For higher impact velocities, the coefficient of restitution first increases, then decreases, with the condensed water layer thickness. Therefore, the air humidity reduces the adhesion between the nanoparticles and the substrate for a high surface energy substrate. For a low surface energy substrate, however, air humidity may increase or decrease the adhesion between the nanoparticle and the substrate, depending on the impact velocity.

In addition, the effects of adhesivity of particles to a surface on the nanoparticle-surface collisional dynamics are also investigated by changing the degree of particle-surface adhesion strength. Results show that particles accelerate because of the attraction force applied by the adhesive surface when the particles enter the interaction range of the surface. As a result, the particle velocity increases from its initial value to a higher impact velocity. However, the acceleration changes inversely with the particle size. A particle smaller than

2 nm in diameter accelerates and results in an impact velocity higher than its yield velocity even when the initial particle velocity is much lower than the yield velocity. During the collision, part of the total energy contributes to the plastic deformation of the sub-2nm particles, reducing the coefficient of restitution (CoR). For a particle larger than 2 nm in diameter, however, the impact velocity remains lower than the yield velocity when the initial velocity is lower than its yield velocity, resulting in elastic collision. Furthermore, this size dependent behavior of CoR intensifies with increasing adhesivity of the collision and becomes less significant for lower adhesivity. This work indicates that a sub-2 nm particle with a velocity lower than the yield velocity can collide the surface in its plastic deformation regime and adhere to the surface.

Acknowledgements

I would like to express my special appreciation to my supervisors, Prof. John Z. Wen and Prof. Zhongchao Tan, for their guidance and support. Your tremendous support and mentorship encouraged my research and allowed me to be grown up as a research scientist.

I would also like to thank my PhD committee members, Prof Leung Wallace from Hong Kong Polytechnic University, Prof. Luis Ricardez Sandoval, Prof. Jean-Pierre Hickey, and Prof. Yimin Wu from the University of Waterloo.

Finally, my deep and sincere gratitude to my family for their continuous and unparalleled love, help and support. I am grateful to my beloved mother for always being there for me and for giving me the opportunities and experiences that have made me who I am.

Thanks again to everyone who made this thesis possible.

Dedication

I would like to dedicate this thesis to my late father, even if he cannot see me graduate. Your memory will be eternal.

Table of Contents

List of Tables

List of Figures

Chapter 1

Introduction

1.1 Problem Statement

Nanoparticles are referred to as those particles with at least one dimension less than 100 nm. Their small sizes lead to high surface area to volume ratios, which results in different properties from bulk substances. Because of their unique and extraordinary chemical and physical properties, nanoparticles are synthesized and used in a wide range of industrial processes such as biomedicine [1], energy systems [2], environmental technologies [3], and water treatment [4].

In lots of these industrial processes, the interaction and collision of nanoparticles with a surface plays a crucial role. Therefore, understanding the collision of nanoparticles on a solid surface is important to several industrial processes such as nanoparticle filtration [5], antimicrobial surface treatment [6], agglomeration of nanoparticles [7], surface coating [8], and water purification [9], etc. Thus, the collision of nanoparticles on surfaces has become a subject of intense research in the past few decades [10, 11, 12, 13]. Depending on the kinetic energy of a colliding nanoparticle, its collision characteristics can be categorized into different regimes, including implantation [14], fragmentation [15], and adhesion/rebound [16].

The transition from adhesion to rebound of nanoparticles in their collision on surfaces is important to various processes. For example, the transition from adhesion to reflection of nanoparticles colliding on a surface was utilized in nanowire fabrication industries [17]. Moreover, the collision of energetic nanoparticles with high initial kinetic energy on a substrate could be used in surface coating technologies to provide a cover for the materials that both improve already existing properties of the material and add new properties to the material [18]. Moreover, the collision of energetic nanoparticles with high initial kinetic energy on a substrate could be used in surface coating technologies to provide a cover for the materials that both improve already existing properties of the material and add new properties to the material.

On the other hand, the widespread use of nanoparticles in industry causes the dispersal of unwanted nanoparticles in the air. Due to their small size, if inhaled, nanoparticles are hard to remove from the upper respiratory tract, and they can penetrate deep into the body. Long-time exposure to nanoparticles can cause pulmonary disease, fibrosis, and lung cancer [19, 5]. As a result, the dispersed nanoparticles in ambient air are considered as a major source of public health concern. Filtration is an effective method that removes aerosol particles from the air stream [20]. In a filtration process, particles are deposited and adhered upon collision with the filter media. Therefore, nanoparticle removal from the air stream takes place upon collision of nanoparticles on the surface of the filter media. As a result, the collision of nanoparticles with surfaces has been the subject of intense research in the past few years [5].

Nanoparticles, distinguishing themselves from micron-scale particles demonstrating continuum-regime characteristics [21], are of the utmost interest in investigating their collision and adhesion behavior. Adhesion of nanoparticles on a substrate is a complex physical process that depends greatly on several parameters, such as the size of these nanoparticles, the relative humidity of the ambient air, the surface characteristics of the substrate besides other geometrical and material properties [22].

Despite the large body of literature on the MD simulation of nanoparticle-surface collision dynamics (*see* Chapter 2), there is still lack of understanding on the effects of various parameters such as air moisture, particle size, chemical reactivity, etc. affect the collision process.

A comprehensive study on the collision of nanoparticles on a wet substrate should be performed. Air moisture or humidity, as an inevitable ingredient of ambient air, can intervene in the particle-surface collision by forming a condensed layer of water on their surfaces. This layer possesses a variable thickness under ambient conditions and acts as a buffer layer, which alters the collision condition. How humidity affects the collision depends strongly on the structural behavior of water molecules near the surface, which is mainly determined by the surface energy (or wettability) of the substrate [23, 24]. Therefore, research is also needed to investigate the structural water behavior as a function of the surface energy (or wettability) of the substrate.

Nanoparticle size is another parameter that affects the dynamics of the collision. The mechanical properties of nanoparticles such as stiffness and hardness are size-dependent, although the mechanical properties of microparticles are size-independent and are determined mainly by the bulk material properties [25]. Moreover, nanoparticles accelerate as they approach the surface due to the attractive force between the particle and the surface [26]. This particle acceleration affects the collision properties by increasing the impact velocity. Since the particle-surface attractive force depends on the particle size, the acceleration is size-dependent [26]. As a result, a comprehensive study on the effects of particle size on the collision dynamics of nanoparticles on surfaces is essential.

Due to challenges associated with their small size, it is difficult to experimentally investigate the effects of various parameters on the nanoparticle-surface collision dynamics. One of the challenges associated with the experimental methods is the accurate sizing of the nanoparticles. To study the collision dynamics of nanoparticles on surfaces, the size distribution of colliding nanoparticles should be accurately determined. However, it was shown that instrumental errors in determining the size of the nanoparticles may lead to misleading results in collision studies [27]. Another challenge is the generation of very small nanoprticles (sub-2 nm) using available experimental equipment. Only few experimental studies have reported on the collision properties of sub-2 nm particles [28, 29]. Moreover, due to the lack of a comprehensive information on the material properties, it is challenging to derive expressions for the adhesion energy between nanoparticle and surfaces based on dynamic equations of the particle motion. Therefore, all the theoretical studies on the particle-surface contact are based on the static adhesion energy calculations. Numerical simulations, on the other hand, can provide a detailed and reliable understanding of how varying parameters at molecular scales affects the nanoscales collisions. Among various simulation techniques, molecular dynamics (MD) is especially well suited to study the nanoparticle collision dynamics. MD is a deterministic method that allows tracking the atomic motions of the system and modifying the conditions that may not be readily varied experimentally. The movement of every single atom is monitored by solving the Newtonian equations of motion, and hence the dynamics of the simulated system can be revealed.

Research on collision dynamics of nanoparticles and solid surfaces is of great interest in developing many industrial applications such as aerosol nanoparticle filtration [5], fabrication of antibacterial surfaces [6], nanowire synthesis from self-assembly of nanoparticles on template surfaces [7], advanced coating technology [8], etc. Appropriately addressing of particle-surface interactions will help not only design suitable filtration and fabrication systems with the optimal interfacial properties but choose the proper operating parameters to improve the process efficiency.

1.2 Research Objectives

This research aims to provide a fundamental insight into nanoparticle-surface collision process using MD simulations in a range of parameters that are not observable by current laboratory equipment. To achieve this goal, a fundamental research is carried out on the interfacial behavior between the nanoparticles and a surface. A simulation framework is designed to model the nanoparticle-surface collision. A validated dataset is used to model the potential interaction between all the atom types used in the simulations. The results of the research could provide a deep insight into any industry processes that the nanoparticle-surface collision plays a role. The following objectives are determined to fulfill the main purpose of this project:

- Designing a simulation setup to model a collision process at the nanoscale
- Validating the potential functions and parameters for silver (Ag), oxygen (O), and hydrogen (H)
- Investigating the effects of air humidity on the collision dynamics of a silver nanoparticle on a silver substrate
  - Studying the effects of surface energy (or wettability) of a substrate on the structure of the condensed water molecules on that substrate

  - Investigating the effects of condensed water layer on the nanoparticle-surface collision dynamics
  - Investigating the effects of surface energy of the substrate on the collision of the nanoparticle on the wet substrate

- Investigating the effects of particle size on the coefficient of restitution of silver nanoparticles on silver a substrate
  - Calculating the yield velocity, the velocity at which the collision transforms from elastic to plastic regime, for sub-10 nm particles
  - Investigating the collision dynamics for adhesive collisions of sub-10 nm particles
  - Investigating the effects of different levels of particle-surface adhesivity on the collision dynamics

1.3 Thesis Structure and Research Approach

Figure 1.1 displays the overall structure of this thesis, which is organized into six chapters.

Chapter 1 presents an overview of the research topic and describes the motivation, opportunities, and objectives of the research. The information provided in Chapter 1 forms the basis of a comprehensive literature review, which is presented in Chapter 2. The review covers background knowledge about the fundamental concepts of the parameters affecting the nanoparticle-surface collision process, how the collision process has been modeled using MD simulations in the literature, water behavior near a surface ranged from superhydrophobic to superhydrophilic.

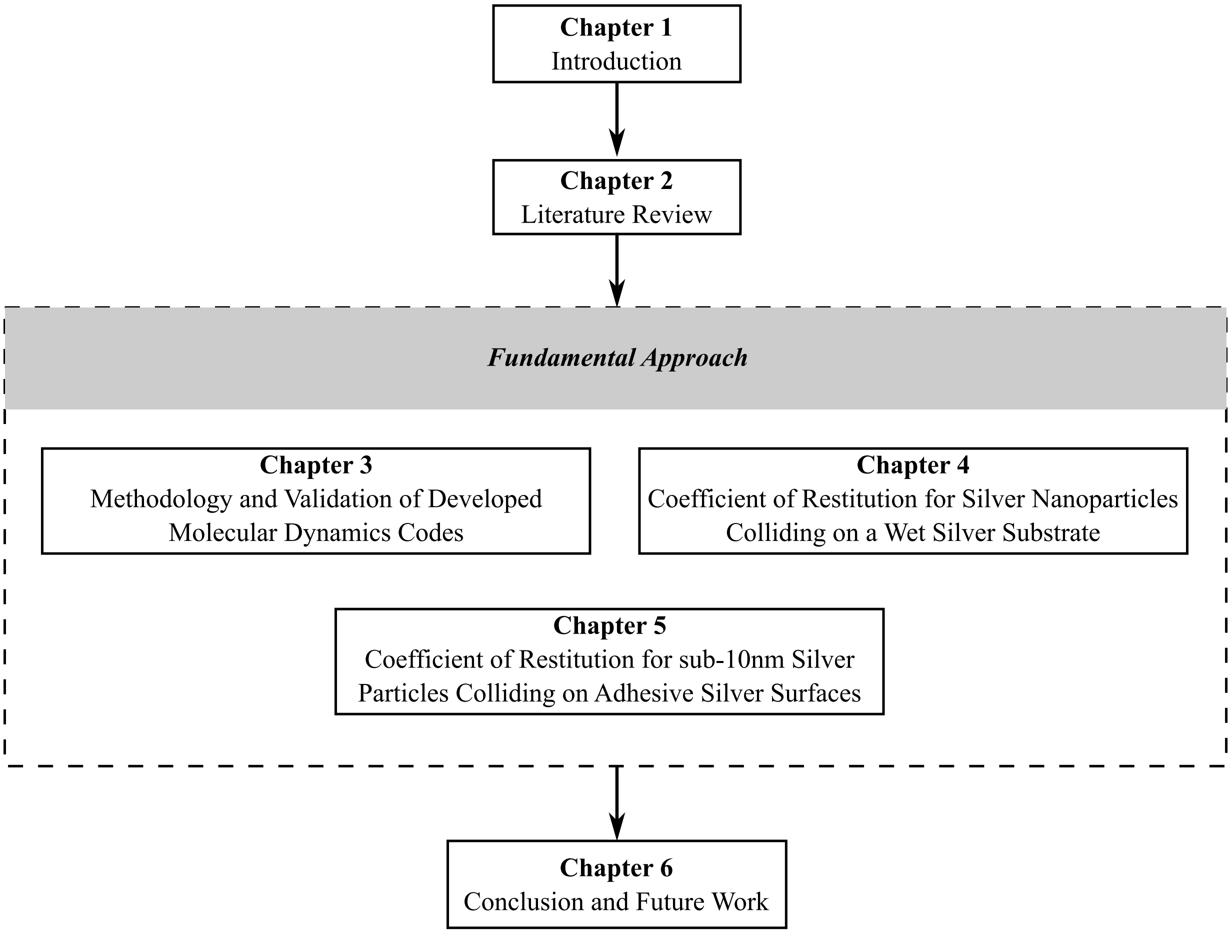

Figure 1.1: The big picture of the thesis structure.

Chapter 3 presents the model validation for the interatomic potentials used to model the interaction between all the atom types in this study. Validation of the models is the first and the most important step in performing molecular dynamics simulations with the ultimate goal of producing accurate and reliable results. In MD simulations, all the atoms interact for a while, where their interatomic interactions are often calculated using some prescribed potential functions. However, the validity of these functions and the force fields from which the parameters used in these functions are extracted should be proved first. To simulate a collision process using MD, it is first necessary to prove the validity of the potential functions, as well as the potential parameters used to calculate the interactions between all the atoms in the simulation box. The model is validated by several independent steps. At first, it is proven that the model has the ability to simulate a collision process at the nanoscale. After that, for each atom type, the model is validated by reproducing a specific property of the molecular and atomic structures containing that kind of atom. For silver atoms, the anisotropic stiffness constants (C_{11} and C_{22}) are calculated using MD simulations and the results are compared with the available experimental and numerical data in the literature. For the water molecules, the density of water is calculated using MD simulations and the results are compared with the previous experimental and numerical studies.

Chapter 4 explains the effects of air humidity on particle-surface collision using molecular dynamics simulations. Air humidity can intervene in a particle–surface collision by forming a layer of water molecules on the surface. These water molecules act as a buffer layer that alters the collision condition. The effects of condensed water layer on the collision of 5-nm Ag particles on an Ag substrate are investigated. The coefficient of restitution that is inversely proportional to the adhesion between the nanoparticle and the surface is used to characterize the collision. Results indicate that air humidity can either increase or decrease the coefficient of restitution in the studied nanoparticle collisions, depending on the condensed water layer thickness and the surface energy of the substrate. The surface energy of the substrate varies with its Lennard-Jones potential. For a high surface energy substrate (superhydrophilic and hydrophilic), the coefficient of restitution first increases then decreases by increasing the water layer thickness on the substrate when the impact velocity changes from 20 to 500 m/s. For a low surface energy substrate (superhydrophobic and hydrophobic), the coefficient of restitution decreases because of a condensed water layer on the substrate at impact velocities less than 300 m/s. For higher impact velocities, the coefficient of restitution first increases, then decreases, with the condensed water layer thickness.

Chapter 5 presents a molecular dynamics study on the collision of sub-10 nm silver (Ag) particles on a silver surface. The effects of adhesivity of collision on the nanoparticle-surface collisional dynamics are also investigated by changing the degree of particle-surface adhesion strength. Results show that particles accelerate because of the attraction force applied by the adhesive surface when the particles enter the interaction range of the surface. As a result, the particle velocity increases from its initial value to a higher impact velocity. The acceleration changes inversely with the particle size. A particle smaller than 2 nm in diameter accelerates and results in an impact velocity higher than its yield velocity even when the initial particle velocity is much lower than the yield velocity. During the collision, part of the total energy contributes to the plastic deformation of the sub-2nm particles, reducing the coefficient of restitution (CoR). For a particle larger than 2 nm in diameter, however, the impact velocity remains lower than the yield velocity when the initial velocities are lower than its yield velocity, resulting in elastic collision. Furthermore, this size dependent behavior of CoR intensifies with increasing adhesivity of the collision and becomes less significant for lower adhesivity. The results indicate that a sub-2 nm particle with a velocity lower than the yield velocity can collide the surface in its plastic deformation regime and adhere to the surface.

Chapter 6 summarizes the major findings of this research and discusses the future directions of the work.

Chapter 2

Literature Review

This chapter begins with an introduction to the basic concepts of nanoparticle-surface collision process. An overview of how the collision process could be investigated using MD simulations of nanoparticle-surface collision is presented afterwards. Then, all the parameters affecting the collision of nanoparticles on a solid surface are discussed from the literature. Finally, the limitations of the existing knowledge on MD studies of nanoparticle-surface collision are discussed. Based on these limitations, the effects of air humidity and nanoparticle size on nanoparticle collisions are introduced as the potential research gaps of this field.

2.1 Nanoparticle-Surface Collision

Nanoparticles are used in many industrial applications such as catalyst synthesis [30, 31], chemical detection [32], photo-electrical device fabrication [33], and advanced manufacturing [34]. Meanwhile, these nanoparticles may become airborne and inhalable, resulting in air pollution. Accordingly, understanding the collision between nanoparticles and substrate surfaces is important to high-efficiency aerosol nanoparticle filtration [5], effective antibacterial devices [6], self-assembly of nanoparticles [7], advanced coating technologies [8], and among others.

A particle-substrate collision can be quantified by Newton's coefficient of restitution (CoR), which is defined as the ratio of the rebound velocity (v_r) and the impact velocity (v_i):

$$CoR = \left|\frac{v_r}{v_i}\right| = \sqrt{\frac{KE_r}{KE_i}} = \sqrt{1 - \frac{E_{loss}}{KE_i}} \tag{2.1}$$

where KE_r and KE_i are the kinetic energy of the particle after and before the collision, respectively. The CoR represents the rate of velocity reduction of the particle in the collision process. The reason for this velocity reduction is the initial kinetic energy loss of the colliding particle. A smaller CoR indicates a greater velocity reduction or a greater kinetic energy loss of the incident nanoparticle. Therefore, CoR is inversely related to the energy loss of the particle.

The initial kinetic energy of a colliding nanoparticle dissipates through several mechanisms, including plastic deformation, rotation, vibration, thermal dissipation, and transfer energy to the substrate [35]. The energy loss, and as a result, the CoR of a collision depends on particle and surface properties, ambient conditions, etc. In order to investigate the particle-surface collision, it is first necessary to investigate the energy loss of a collision under different conditions, and consequently, the CoR of the nanoparticle colliding on a substrate.

Due to challenges associated with the small size of nanoparticles, it is challenging to experimentally investigate the effects of different parameters on nanoparticle-surface collision dynamics. Moreover, due to the lack of a comprehensive information on the material properties, it is challenging to derive expressions for the adhesion energy between nanoparticle and surfaces based on dynamic equations of the particle motion. Therefore, all the theoretical studies on the particle-surface contact are based on the static adhesion energy calculations. Numerical simulations can provide a better understanding of how varying parameters affects the nanoparticle collision process.

For micron or micro size systems, system behavior is studied based on the continuum assumption, while these assumptions are no longer valid for nanosized systems. Knudsen number (Kn) is the characteristic that checks for the type of system in terms of continuity. In general, the mean-free path (λ) is the average distance that each particle travels to reach other particles. Knudsen number is the ratio of the mean free path to the system characteristic length (L_s).

$$Kn = \frac{\lambda}{L_s} \tag{2.2}$$

If $K_n < 0.01$, the Navier-Stokes equations are solved based on the continuum assumption. For $0.01 < K_n < 0.1$, Navier-Stokes equations can be applied if the tangential component of the velocity at the boundaries are considered. If $K_n > 0.1$, the continuum assumption starts to break down, and finally, for $K_n > 10$, the continuum assumption completely breaks down, and the system follows a free molecular regime, at which the particles travel a considerable distance compared to the system's characteristic length before colliding the other particles [36]. For nanoscale systems, the mean free path of the system has the same order of magnitude of the characteristic length of the system, and the assumption of continuity is no longer valid. Therefore, to study the behavior of nano-sized systems, the use of continuity equations results in significant errors in the calculations. As a result, since the Knudsen number for nanoscale systems is around 10 or larger, the free-molecular assumption that the nanoparticle does not interact with other gas molecules is valid. In the field of sub-micron research, the Schrödinger equation is applicable to be applied to all systems of any scale and workspace. Although the Schrödinger equation is theoretically correct for nanoscale systems, due to high computational cost and complexity, it is only applicable for very small-scale systems. Therefore, a new strategy is needed for modeling nano-scale systems to predict the behavior of the system. Molecular dynamics is a promising method to numerically analyze the movements of atoms and molecules in a nanoscale system. The interaction between the atoms and molecules is modeled in this method, and their trajectories are predicted by solving Newton's equations of motion. MD is a deterministic method that allows tracking the atomic motions of the system and modifying system conditions that may not be readily varied experimentally. The motion of every single atom is monitored by solving the Newtonian equations of motion, and hence the dynamics of the system can be revealed. Therefore, MD simulation of the nanoparticle-substrate collision has been the subject of numerous recent research. Several studies have been performed on the effects of several parameters on the collision dynamics of a nanoparticle on a surface. The following section, discusses all the factors affecting the nanoparticle collision from MD simulations in the literature.

2.2 Factors Affecting Collision - MD Studies

Several factors affect the collision dynamics of nanoparticles on surfaces. These factors are summarized as follows:

- Dynamic characteristics of the nanoparticle

  - Impact velocity
  - Initial angular velocity
  - Angle of incidence
- Physio-chemical properties of particle and surface
  - Particle size
  - particle material (mechanical properties such as hardness)
  - Particle shape
  - Surface energy
  - Chemical reactivity
- Ambient conditions
  - Humidity

First, the dynamic characteristics of the moving particle affect the collision. Second, physical and chemical properties of the particle and substrate may also affect the collision. Last, ambient air conditions at which the collision takes place can affect the collision dynamics.

2.2.1 Effects of Dynamic Characteristics of Particle on Collision

Impact velocity

Impact velocity is one of the most important factors affecting the collision. The impact velocity is equal to thermal velocity of the particle, which follows a Maxwell-Boltzmann distribution. Awasthi *et al.* [22] found that the particle-surface adhesion probability is a bimodal function of the impact velocity (*see* Figure 2.1). Particles adhere to the surface at very low velocities but start to rebound from the surface at intermediate velocities. Further increasing the impact velocity increases, then decreases the probability of adhesion. This behavior was explained by the amount of energy loss in two collision regimes [37]. First, elastic regime with negligible deformation of the particle. Second, plastic regime, which the nanoparticle experiences plastic deformation. The adhesion energy depends on the contact area between the colliding nanoparticle and the surface. For low impact velocities, at which the deformation is negligible, the contact area and hence the adhesion energy, depends weakly on the impact velocity. As a result, the adhesion energy remains unchanged while the kinetic energy increases with increasing the impact velocity in the elastic regime. At higher impact velocities, the deformation grows substantially, which increases the contact area and adhesion energy. In this strong deformation regime, the adhesion energy initially dominates the kinetic energy of the nanoparticle as the deformation produces a large contact area. Eventually, the kinetic energy of the nanoparticle dominates the adhesion energy, which decreases the probability of adhesion [38].

Angular velocity of rotation

Prior to collision, nanoparticles in the air stream may collide with each other and gain rotational angular velocity. After revealing the effects of translational impact velocity, Awasthi *et al.* [39] also examined the effects of initial angular velocity of the particle on the collision dynamics. They found that the adhesion probability for nanoparticles with initial angular velocity increases compared to adhesion probability of non-rotating nanoparticles. It was also reported that the adhesion probability increases with increasing the initial angular velocity of the nanoparticles. The reason is that the degree of plastic

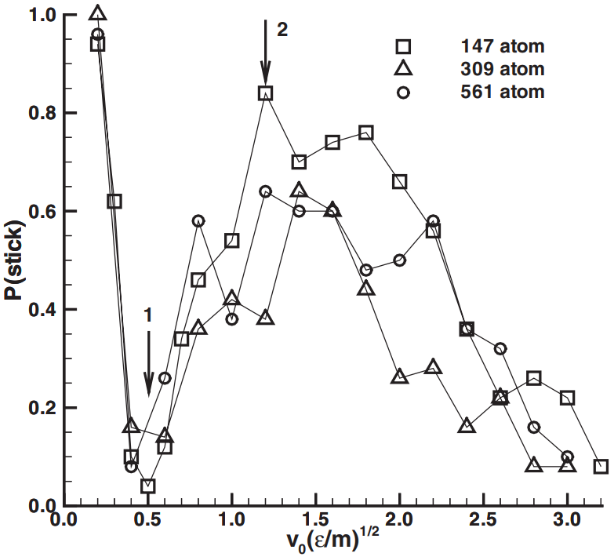

Figure 2.1: Sticking probability as a function of impact velocity for three particles with the number of atoms 147, 309, 561. The minimum and maximum in sticking probability are distinguished with arrows number 1 and 2, respectively. Adapted with permission from Ref. [22] Copyright 2006 Physical Review Letters.

deformation increases as the angular velocity increases. Therefore, the energy loss due to plastic deformation increases, resulting in higher adhesion probability.

Angle of collision

Since aerosol nanoparticles move randomly in air, they may obliquely collide the surface. Therefore, the nanoparticles may collide the surface with different angles. Angle of collision was investigated by Awasthi *et al.* [40]. They found that the adhesion probability is the same for oblique collisions with equal normal velocity component. This indicates that the adhesion probability is mainly determined by the normal component of the impact velocity. Therefore, for an oblique impact, the CoR is defined as the ratio of normal velocity components after and before collision. The fact that the rotational kinetic energy of the particles after rebound is negligible, is also consistent with these results. This suggests that the transnational kinetic energy is not transferred to the rotational motion for oblique collisions. Therefore, the tangential component of velocity is approximately maintained after the rebound. It has recently been shown that the oblique collision of conductive nanoparticles on the V-shaped grooves etched on a silicon surface can be used in nanowire fabrication technology [7].

2.2.2 Effects of Physio-chemical Properties of Particle and Surface on Collision

Particle size

Due to high surface area to volume ratio, nanoparticles usually show size-dependent physical properties distinctly different from those of bulk materials. Takato *et al.* [25] studied the size and the impact velocity (v_i) dependence of the coefficient of restitution (CoR) for two identical argon nanoparticles using MD simulations. In their simulations, only the repulsive interaction between the particles is considered, to make sure that the only energy loss mechanism that can change the CoR is the plastic deformation. Figure 2.2a shows the CoR for different particle sizes and impact velocities. As shown, a sharp crossover is recognized between elastic and plastic deformation regimes, where the impact velocity reaches yield velocity (v_Y). When the impact velocity is lower than the yield velocity, the energy loss is negligible since the collision is mainly elastic, and the CoR remains close to unity. However, by increasing the impact velocity to values higher than the yield velocity, the energy of the moving particles dissipates through plastic deformation, and

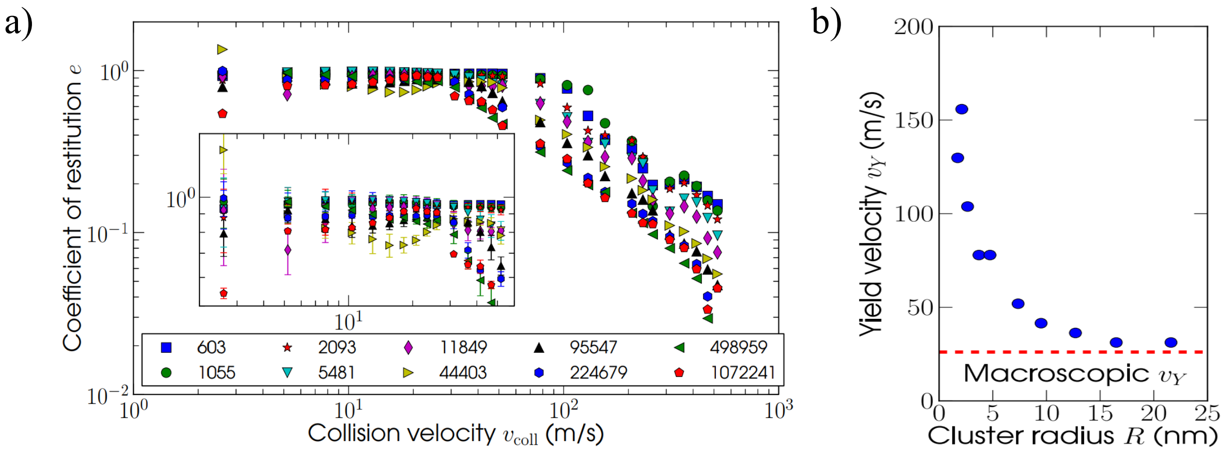

Figure 2.2: (a) Coefficient of restitution as a function of impact velocity for nanoparticles with different sizes. The change in slope, which shows the onset of plastic deformation, occurs at the yield velocity. (b) Yield velocity as a function of particle size. Adapted with permission from Ref. [25] Copyright 2014 Physical Review E.

consequently, the CoR decreases roughly. Figure 2.2b displays the yield velocity for each particle size. The results show that the physical properties of nanoparticles, such as hardness, is size-dependent. The yield velocity decreases by increasing the particle size, which indicates that the hardness of the particles decreases with increasing their size until it approaches its macroscopic value. The results of this study provide valuable information of size-dependent CoR for purely repulsive nanoparticles. However, there is a different scenario for the collision between adhesive nanoparticles. The attractive force between adhesive nanoparticles accelerates the nanoparticles [26]. This acceleration increases the impact velocity, which affects the collision dynamics. Therefore, a comprehensive study on the collision between nanoparticles with different levels of adhesivity is required.

Sato *et al.* [41] also found that the energy loss of a nanoparticle colliding on a surface depends on particle size. The reason is that the mechanical properties of nanoparticles, which affects the CoR are size-dependent. It was found that the energy loss of the small particles is largely due to the energy transfer to the surface. It is probably due to the fact that small particles do not have many internal degrees of freedom compared to bigger particles. To explain the reason for this phenomenon, they modeled both the particle and the substrate with an imaginary spring, and each of them was assigned a spring constant. Due to the low internal degrees of freedom, small particles have a high spring constant compared to the substrate with higher internal degrees of freedom. In fact, the initial kinetic energy of the particle that is mainly stored as the elastic energy of the substrate with a smaller spring constant, cannot be completely recovered in the rebound phase, sine the spring constants are not compatible. In this study, the energy loss mechanisms for particles with different sizes are discussed; however, the effects of particle size and the degree of adhesivity of the collision on the CoR is still unclear. Therefore, further research is needed to fully investigate the adhesive collision of nanoparticles with different sizes.

Particle hardness

The imaginary spring can also be considered to study the effect of the particle material on the collision dynamics [41]. According to the imaginary spring explanation presented in the preceding section, the imaginary spring constant increases with increasing the hardness of the nanoparticle. Therefore, the stored energy in the particle cannot be effectively retrieved after collision. As a result, the energy lose increases with increasing the nanoparticle harness. Therefore, the CoR decreases with increasing the particle material hardness.

2.2.3 Particle orientation

Due to their atomic structures, nanoparticles are not perfect spheres. The nanoparticles usually have various shapes with lots of asperities on their surfaces. Therefore, the CoR of a moving particle depends on its orientation prior to the collision. It was shown by Schoner *et al.* [42] that the main properties of the collision such as coefficient of restitution, contact force, plastic deformation of the particle, and adhesion probability depend on the orientation of the nanoparticle prior to collision. Therefore, for each numerical study on nanoparticle-surface collision, the orientation of the nanoparticle should be changed randomly, and the average value should be reported as the final result. This eliminates the effects of particle orientation on the results.

Surface energy

Awasthi [38] showed that for a dry collision the sticking probability increases with increasing the attraction strength between the particle and substrate. In their study, the attraction strength between the particle and the surface atoms was modeled using the modified LJ potential:

$$E_i^{LJ} = 4\varepsilon \left[\left(\frac{\sigma}{r_{ij}} \right)^{12} - C \left(\frac{\sigma}{r_{ij}} \right)^{6} \right] \tag{2.3}$$

The constant C is applied to the attractive part of the LJ potential to modify the particle-surface attraction force, although the atoms inside the particle and inside the substrate interact via the standard LJ potential with $C = 1$. The adhesion probability strongly depends on the attraction energy of the substrate, and the transition from adhesion to rebound of the particle is observed as the factor C decreases from 0.7 to 0.2. Figure

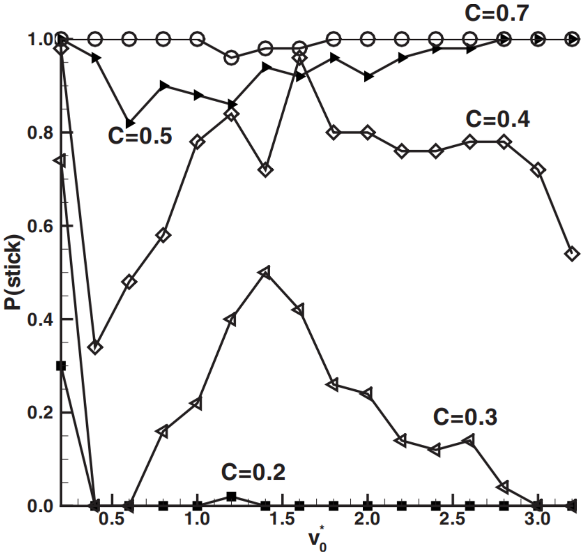

Figure 2.3: The particle-substrate adhesion probability versus impact velocity for different C values. Adapted with permission from Ref. [38] Copyright 2007 Physical Review B.

2.3 shows that the bimodal behavior of adhesion probability, which was observed in their previous study, disappears outside the range of $0.3 < C < 0.4$. The reason is that the kinetic energy of the rebounding particle dominates the attraction energy when the surface attraction is low (C is low), and the attraction energy dominates the kinetic energy of the particle when the surface attraction is high (C is high). When either the kinetic energy of the rebounding particle or the attraction energy dominates, it suppresses the effect of the other one and causes the bimodal behavior, which is a result of the balance of these two energies, no longer be observed.

The attraction force between the particle and the surface increases the impact velocity of the particle. This velocity increase affects the collision dynamics. However, as mentioned in Section 2.2.2 this velocity increase is size-dependent. Therefore, the effects of attraction strength between the particle and surface should studied for particles with different sizes.

Chemical reactions between particle and surface

Most studies assume that the collision properties at the nanoscale are mainly determined by the van der Waals (vdW) or electrostatic interactions between nanoparticle and surface. However, in some cases, the chemical reactivity between the particles and the surface also plays an important role in determining the collision characteristics.

Quadery *et al.* [43] studied the collision of two silica (SiO2) nanoparticles to examine the effects of chemical reactivity on their adhesion behavior. According to their results, the sticking probability is lower for hydroxylated nanoparticles compared to the nonhydroxylated ones. The presence of dangling bonds belong to the unsaturated Si atoms on the surface of the nanoparticle results in chemical bond formation between nanoparticle and surface. The strong bond formation increases the kinetic energy dissipation and, consequently, the adhesion efficiency between the nanoparticles. Since the energy dissipation increment was attributed to the chemical bond formation due to the dangling bonds, effective passivation their using hydroxylation agents reduces the probability of the particle adhesion. It was shown that surface hydroxylation could reduce the adhesive forces and, consequently, the energy dissipation upon collision. The results indicate that the probability of adhesion depends on whether the surface is hydroxylated.

It was also revealed by Sure *et al.* [44] that the adhesion dynamics of a nanoparticle on a substrate depends on the level of chemical reactivity between them. The collision between a 10-nm Si particle and a Si substrate was examined. The presence of dangling bonds on the surface of both particle and substrate leads to the formation of covalent bonds and increases the energy dissipation upon collision. To reduce the surface reactivity, the surface of the particle or substrate was fully coated by hydrogen atoms. The hydrogen atoms saturate the dangling bonds on the surface of the nanoparticle. As a result, the

Si-Si bond formation is hindered during the collision. Therefore, the poor reactivity of the H-passivated particles prevents the adhesion of colliding Si nanoparticles on the substrate.

Quadery *et al.* [43] and Sure *et al.* [44] reported that the strong chemical bond formation between two SiO2 or Si nanoparticles increases the kinetic energy loss, and as a result, affects the CoR during the collision. Both studies considered dry collisions between nanoparticles, however, if nanoparticles with dangling bonds on their surfaces become in close contact with water molecules, bond formation may also occur between the unsaturated surface atoms and the water molecules. It was reported by Cicero *et al.* [23] that when a silicon carbide (SiC) nanoparticle, containing unsaturated surface atoms, gets in close contact with water molecules, chemical bonds are formed between the dangling bonds and the oxygen atoms of water molecules. As a result, the water molecules dissociate, and proton transfer due to this chemical reaction leads to the formation of H3O+ ions. Similar results were reported by Ma *et al.* [45] about the formation of chemical bonds between the unsaturated Si atoms and the water molecules. Covalent bond formation applies an adverse force against the detachment of the nanoparticle from the surface and acts as an energy dissipation mechanism. Therefore, the effects of the chemical reaction on the collision must be considered when dealing with a particle, which contains unsaturated surface atoms on a wet substrate.

2.2.4 Effects of Ambient Conditions on CoR

Humidity

Water moisture or humidity, as an inevitable ingredient of ambient air, can intervene in the particle-surface collision and affect the adhesion of the particle on the surface. The humidity effects on the particle-surface interfacial behavior are clearly determined for microparticles in the literature. Many studies have shown that the adhesion of microparticles to a surface increases with increasing moisture content of the ambient air [46]. The increase in adhesion is attributed to the capillary force caused by the condensed water layer on the surface. Although the effects of humidity for microparticles is straightforward and always results in adhesion increment, uncertainties still remain about the nanosized particles. Some experimental studies reported on the effects of humidity on the particle-surface adhesion. Kim *et al.* [29] studied the effects of humidity on the impact of 3-70 nm particles on glass fibers. They showed that unlike microparticles, the adhesion of the nanoparticles to the surface is independent of the humidity. Bateman *et al.* [47] reported that the adhesion energy increases for particles with the size range of 90 to 370 nm at high relative humidity levels, while its effect is not considerable at low relative humidity. Similarly, Stein *et al.* [48] showed that for a 250 nm particle, the adhesion energy increases at high relative humidity and remains unaffected at low humidity levels. Therefore, despite the straightforward effects of humidity on microparticle collisions, its effects on the nanoparticle collisions are complicated and controversial. The humidity always increases the adhesion energy between particle and surface at the microscale. However, at the nanoscale, the humidity effects could be different depending on various parameters.

Accordingly, the effects of humidity on the nanoparticle-surface adhesion varies at high and low relative humidity. Therefore, relative humidity (RH) is one of the parameters that affect the nanoparticle-surface adhesion under the wet conditions. Depending on the relative humidity, the thickness of the condensed water layer on the surface changes [49]. Surface material is another parameter that is important in studying the effects of humidity on the nanoparticle-surface interfacial behavior. Different materials have different surface energies that can affect the dynamics of the collision by affecting the water structure near the surface. In fact, how the condensed layer affects the interfacial behavior between the nanoparticle and surface depends on the water's structural behavior near the substrate, which strongly depends on the surface energy or surface wettability of the substrate [24]. Therefore, studying the wettability of the surface is another importance parameter in studying the effects of humidity on the nanoparticle-surface collision.

Surface wettability is a property of surfaces that shows how a water droplet behaves on that surface. Modifying the wettability of surfaces is of great interest in developing many industrial applications such as antibacterial surfaces [6], airborne nanoparticle filtration [5], printing, clothing, painting, lubrication, and semiconductor [50, 51, 52]. As reported by Shafrin and Zisman [53], the surface wettability mainly depends on the outermost chemical groups of the substrate. Usually, atoms more than a few atomic layers below the surface have negligible effects on wettability. Difference in wettability between surfaces with a similar structure is due to differences in the outermost layer covering the surface of the substrate. Changing the outermost chemical groups transforms a high-energy surface into a low-energy surface of the same substrate material.

A typical approach to evaluate the surface wettability of a substrate is by the water contact angle measurement. Figure 2.4 shows the water contact angle (θ) is the angle between the exterior of a droplet and the surface of a substrate. For a droplet on a surface, the balance between cohesive and adhesive forces determines the contact angle. Adhesive forces are the attraction forces between the water molecules and the surface atoms, and the cohesive forces are the attraction forces between the water molecules their selves. The attraction forces between the water molecules and the surface increases with increasing the degree of surface wettability. Therefore, the water molecules tend to spread out over the surface, and the contact angle decreases. Therefore, the contact angle is inversely proportional to the surface wettability or surface energy [53].

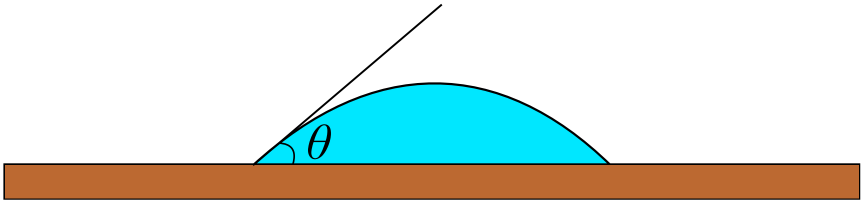

Figure 2.4: Water contact angle (θ) on a surface.

2.3 Surface Classification Based on Wettability

A solid-liquid interface forms when a water droplet comes in contact with a surface. The final shape of the droplet is determined by the competition between the cohesive and adhesive forces. Cohesive forces within the liquid sticks the water molecules together. Adhesive forces are the attraction forces between the droplet and the surface. Cohesive forces are determined by the liquid-liquid interaction strength, and adhesive forces are determined by the solid-liquid interaction strength. Assuming that the liquid is always water, the cohesive force is constant. The solid-liquid attraction strength is also determined by the surface energy of the surface.

A surface could be classified into four main categories shown in Figure 2.5. Surface wettability is determined by the surface energy level of the substrate. The energy content of a solid depends on the nature of the solid itself. Since hard solids such as metals, ceramics, and glasses are held together with strong interatomic interactions (metallic, covalent, and ionic), a large amount of energy is needed to break the bulk of the solid, and, the term “high energy” is used for these solid types. The wettability of these surfaces is high for most liquids, including water. The degree of wetting changes depending on the level of the surface energy. The adhesive force strength increases with increasing the surface energy of the substrate, resulting in a contact angle of less than 10°. In this case, the

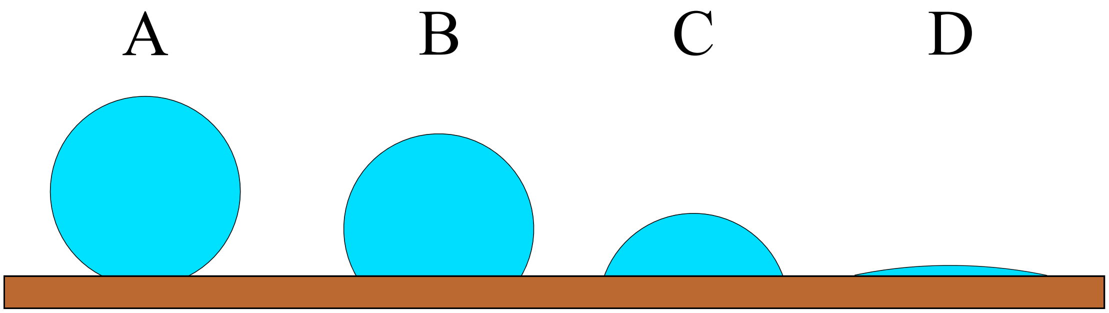

Figure 2.5: Surface classification based on wettability.

surface is called “superhydrophilic”. By decreasing the surface energy of the substrate, the adhesive interactions, and consequently, the wettability of the surface decreases. As a result, the drop balls up, and the contact angle increases. Such surfaces fall in the category of “hydrophilic”, and the contact angle is in the range of 10° to 90°. In this case, the surface energy is high enough that the fluid spreads over a large area of the surface. Weak molecular crystals such as hydrocarbons and fluorocarbons are the type of solids, where the molecules are held together by weak physical forces of vdW and hydrogen bonds. Since the molecular structures of these solids are held together by weak interactions, a low amount of energy is required to break them; thus, they are named ”low energy” surfaces. Depending on the surface energy, the contact angle of a water droplet on a low energy surface ranges from 90° to 180°. For the contact angle in the range of 90° to 150°, the surface wetting is low, that the fluid minimizes contact area with the surface and compact droplet is formed. Superhydrophobic surfaces (lotus effect) have contact angles higher than 150°, resulting in almost no contact between the water droplet and the surface. Contact angles and the strength of their liquid-liquid and solid-liquid interactions are described in Table 2.1.

The control of the interfacial behavior between a liquid and a surface is essential in

Table 2.1: Surface properties associated with its degree of wettability.

Surface type	Contact angel	Degree of wettability	Adhesive to cohesive interaction ratio
A	150°< θ <180°	Superhydrophobic	Very weak
B	90°< θ <150°	Hydrophobic	Weak
C	10°< θ <90°	hydrophilic	Strong
C	θ <10°	Superhydrophilic	Very strong

many technological processes. In the contact of a liquid droplet on a surface, three cases of completely wetting, partially wetting, and non-wetting may occur. As reported by Shafrin and Zisman [53], the surface wettability is mainly determined by the outermost chemical groups of the solid. Usually, atoms more than a few atom diameters below the surface do not influence wettability. Differences in wettability between surfaces with a similar structure are due to differences in the outermost layer covering the surface of the substrate. Changing the outermost chemical groups transforms a high-energy surface into one with the wetting properties characteristic of a low-energy surface of the same surface composition and packing.

2.4 Water Structure at a Solid Interface

Research on solid-liquid interfacial behavior is of great interest in the development of several industry processes. In particular, for any kind of technological process that the nanoparticle-surface comes in contact in a humid environment, the water structural behaves near the surface is important. Therefore, in order to investigate the effects of humidity on the collision of a nanoparticle on a substrate, the structure of water molecules near the surface should be studied. The water structure near a surface highly depends on the surface wettability. On both hydrophobic [54, 55] and hydrophilic [55, 56] surfaces, interfacial layers of water with properties different from those of bulk water have been reported.

Cicero *et al.* [23] presented a microscopic model for the interfacial behavior between liquid water and a hydrophilic surface. The surface material used in their simulations is silicon as a proper semiconductor for biocompatible devices. Figure 2.6 shows that a thin water layer with a density higher than the bulk water is formed near a hydrophilic substrate. The structure and dynamics of this layer have been compared to those of amorphous ice [57] and supercooled water [54]. For a hydrophilic substrate (with high surface energy), the attraction force between the substrate and the water molecules is strong, and the tendency of the surface to absorb water molecules is high. As a result, the water molecules adjacent to the substrate adhere strongly to the surface. Normal hydrogen bonds between the water molecules break down and are replaced by new hydrogen bonds, forming a dense water layer next to the surface. In other words, due to the strong attraction force between the water molecules and the surface atoms, the water molecules tend to stay close to the surface and a high-density water layer is formed near the surface. Only molecules with a distance less than 3 Å from the surface are strongly affected, and the thickness of this dense water layer is around 3 Å.

Instead, weakening of the attraction force between water molecules and the substrate results in weakening of H-bonds [58] between the water molecules in the dense layer on hydrophobic surfaces. Therefore, a water-vapor interfacial region is formed near the surface. By decreasing the surface energy of the substrate, the attraction energy between the substrate atoms and the water molecules decreases. Therefore, the attraction between the water molecules and the surface decreases, and the density of the adjacent water layer decreases. Jensen *et al.* [55] investigated the water structure near a hydrophobic and hy-

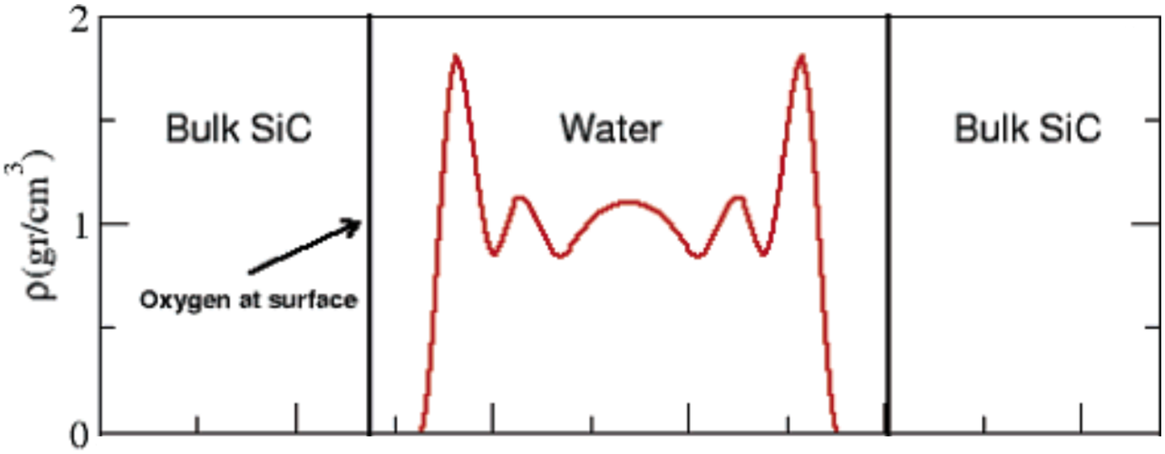

Figure 2.6: Water density as a function of vertical distance z from the hydrophilic substrate. Adapted with permission from Ref. [23] Copyright 2005 Journal of American Chemical Society.

drophilic surface and provided a comparison between them. Figure 2.9 shows the structure of the water molecules near a hydrophobic and hydrophilic surface. For the hydrophilic surface, the water molecules are absorbed strongly by the surface, and a thin dense water layer is created near the surface. However, for a hydrophobic surface, the water-surface interaction is weak and there is an interfacial vapor phase in the water-surface connection.

2.5 Knowledge Gap and Research Needed

Despite a relatively large body of literature, more research on the collision dynamics of nanoparticles on the surface of the filter media is still needed. The accuracy of the available equipment to determine the size of the nanoparticles and the difficulty to produce sub-2 nm particles makes experimental approaches challenging to study the collision of

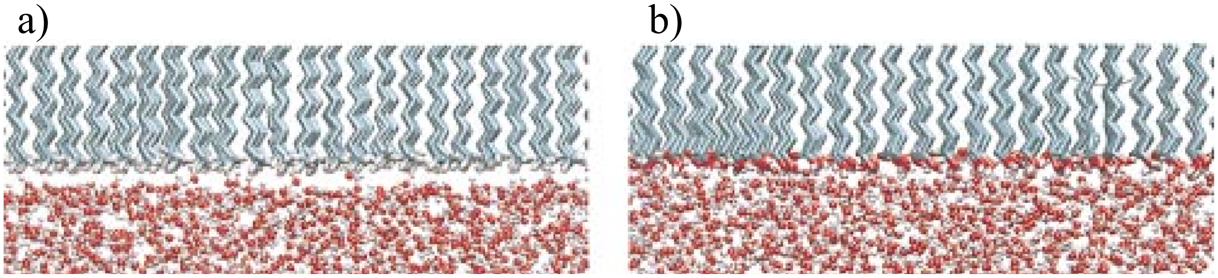

Figure 2.7: Water structure near (a) hydrophobic and (b) hydrophilic substrate. Adapted with permission from Ref. [55] Copyright 2014 Journal of Chemical Physics.

nanoparticles on a surface. Theoretical studies are also challenging due to the lack of data of material properties of nanoparticles. Therefore, numerical studies could be helpful to provide complementary data in particle-surface collision. The numerical studies based on continuum theory fails to study nanoparticle collision because the continuum assumption is no longer valid at nanoscales. Among all the simulation techniques, molecular dynamics simulations are the most promising approach to study a nanoscale system. The effects of several parameters such as impact velocity, particle orientation, angular velocity of the particle, etc. on the particle-surface collision dynamics are addressed in earlier MD studies. However, the effects of several parameters such as air humidity, particle size, surface energy of the colliding objects are still unclear.

All the earlier MD studies on the particle-surface collision dynamics are exclusively for dry surfaces, and little research has been focused on the effects of air humidity on the nanoparticle collisions. In reality, a water film may be formed at the particle-substrate interface, and it may interfere the collision between the particle and the surface. The water film can affect the quality of the products in material synthesis or the efficiency of air filtration. It is well-known in the literature that the adhesion of micron or larger particles to a surface always increases with relative humidity (RH) or water content in the air.

However, the effects of relative humidity on the adhesion of nanoparticles on a surface is still controversial. For example, Miguel *et al.* [46] found that the adhesion of micron particles to a surface is enhanced by increasing the moisture content of ambient air. This effect was attributed to the capillary force of the condensed water layer on the surface. Wang *et al.* [59] however investigated the effects of relative humidity on the deposition rate of aerosolized SiO2 nanoparticles in a test chamber. Their study shows a size-dependent effect of RH: for particles smaller than 70 nm in diameter, the deposition rate decreases as the RH increases; for larger ones, the deposition rate increases with rising RH. Kim *et al.* [29] found that RH had little impact on the collection efficiency of nanosized NaCl particles in the range of 3-70 nm in diameter. Thus, the effects of RH on the nanoparticle-substrate collision deserves further investigations.

Moreover, there is limited information on the dependence of particle-surface collision dynamics on nanoparticle size and adhesion force for nanoparticle collisions, especially for those involving sub-10 nm particles. Jung *et al.* [26] reported that the particle-surface adhesion force increased the impact velocities of sub-10 nm particles, depending on the particle size and the surface energy of the colliding objects. Nonetheless, the effects of the velocity increase on the nanoparticle collisions deserve further investigation. Thus, more research is needed to understand the effects of particle-surface adhesion force on the adhesive collisions of sub-10 nm particles on surfaces with different surface energies.

Chapter 3

Methodology and Validation of Developed Molecular Dynamics Codes

Validation of the computer models is the first and the most important step in development of a model with the purpose of producing accurate and reliable results. In MD simulations, all the atoms interact for a while, where their interatomic interactions are often calculated using some prescribed potential functions. However, the validity of these functions and the force fields from which the parameters used in these functions are extracted should be proved first. This research aims to investigate the effects of several parameters such as relative humidity, particle size, etc. on the collision of a nanoparticle on a substrate utilizing MD simulations. To simulate a collision process using MD, it is first necessary to prove the validity of the potential functions, as well as the potential parameters used to calculate the interactions between all the atoms in the simulation box. The model validation is achieved through several independent steps. At first, it is proved that our model has the ability to simulate a collision process at the nanoscale. After that, for each atom type, the model is validated by reproducing a specific property of the molecular and atomic structures containing that kind of atom. Besides, for water molecules, the results of a relevant study are also reproduced.

3.1 MD Simulation of nanoparticle collisions

As discussed in Chapter 2, Knudsen number is the main characteristic which determines whether the free-molecular regime is valid (*see* Eq. 2.2). The mean free path of air, at an atmospheric condition and relative humidity of 0-100 %, is in the range of 67.8-68.03 nm [60]. The diameter of the nanoparticles in this study is in the range of 1.6-7.6 nm. Therefore, for the particles considered in this study, the Knudsen number would take a value between 8.94 to 42.44. As a result, since the Knudsen number is around 10 or larger, the free-molecular assumption that the nanoparticle does not interact with other gas molecules is valid. Therefore, the interactions between the particle and the surrounding air molecules are not considered in this work. In an actual collision process, multiple nanoparticles may approach the surface at the same time. The approaching nanoparticles may collide to each other prior to collision, which may alter their impact velocity and their orientation prior to collision. The collision of each nanoparticle is modeled over a wide range of impact velocities to make sure that each nanoparticle's velocity (which is altered after the collision with other nanoparticles) is effectively covered. Moreover, nanoparticles which are not perfect spheres, collide the surface with different orientations. The actual collision outcome is the statistical average of the nanoparticles colliding on the surface with different orientations. In order to eliminate the effects of nanoparticle orientation prior to collision and improve the statistical accuracy of the results, up to 12 trials are performed. The nanoparticle is re-oriented prior to collision between each trial. Therefore, although the collision of a single nanoparticle on a surface is modeled, the reported results for each system condition is averaged over up to 12 distinct collisions. Therefore, it is reasonable to not model the collision of multiple nanoparticles on the surface. However, multiple collisions of nanoparticles on a surface or collision of nanoparticles on previously deposited nanoparticles on a surface could be studied as a future work.

The general simulation framework to model a collision process is depicted in Figure 3.1. For each simulation, it is first necessary to create an empty box with dimensions of $L_{b,x}$, $L_{b,y}$, and $L_{b,z}$. All the atoms needed for the simulation should be placed in this box. A substrate with dimensions of $L_{s,x}$, $L_{s,y}$, and $L_{s,z}$ is used to model the collision. A nanoparticle with the radius of r_p is also located at the distance of d above the substrate. Silver is chosen as the material of the particle and substrate. Silver is chosen as the material of the particle and substrate. Physical and optical properties of a material can be considerably altered by collision and deposition of nanoparticles on that material. In this content, the physical properties of silver substrates appear to be tunable using the collision and deposition of silver nanoparticles on the surface of that silver substrate [61]. Therefore, the silver-on-silver collision of nanoparticles on surfaces is considered in this study. The details about the size of the particle and substrate, which depends on the system conditions, are provided in each chapter. At the beginning of the simulation, the nanoparticle should be placed outside the interaction field of the substrate.

Usually, the size of MD systems is around several hundred nanometers. Since MD simulations are very time-consuming, it is impossible to simulate such a big system. This problem can be solved by applying periodic boundary conditions. To eliminate the finite-size effects of the simulation box, periodic boundary conditions are applied to the x and y

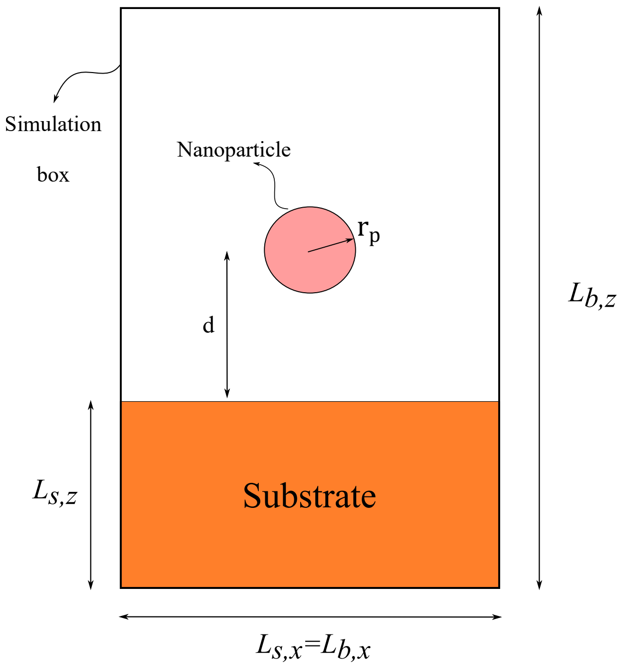

Figure 3.1: Schematic representation of the general simulation framework to model a nanoparticle-surface collision process.

directions. Figure 3.2 shows that by applying the periodic boundary condition, the central cell A (which is the simulated cell in Figure 3.1) is repeated indefinitely in the x and y directions. Each atom in cell A has its own image in the adjacent cells. When an atom crosses cell C from cell A, its image enters from cell H to cell A. In addition, the atoms in a cell interact with the image of adjacent cell atoms. Therefore, the periodic boundary condition enables modeling of an infinite system by modeling the interaction between the atoms inside a single cell (*see* Figure 3.2).

The length of the substrate in the x- and y-directions should be large enough that the picture of the particle in the nearby cells won't affect the particle behavior. The length of the substrate in the z direction ($L_{s,z}$) should be high enough to ensure that the energy

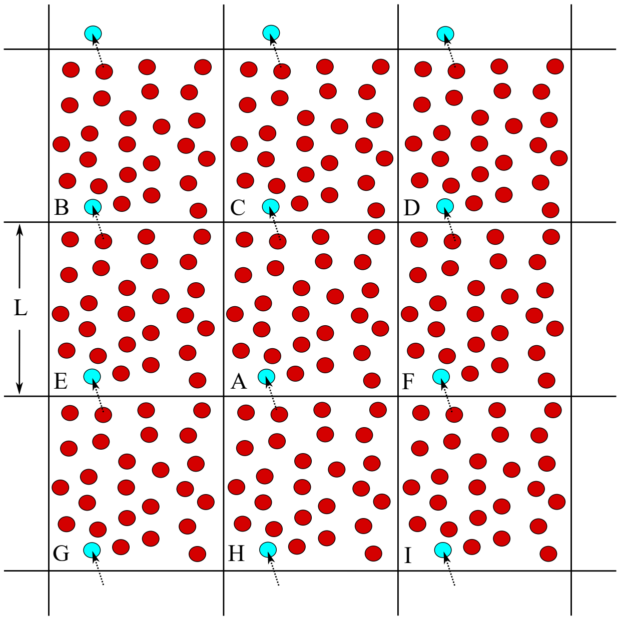

Figure 3.2: Periodic boundary conditions for a two-dimensional MD system. The Simulation cell A, with the size of L × L is replicated in the x and y directions. The circles show the cut-off area around each circle. Each arrow represents the atoms crossing between two cells.

from the cluster impact is absorbed by the substrate properly. The outermost layer of the substrate should be fixed to prevent the movement of the substrate while the rest of the substrate is left to vibrate normally.

All the simulations should start from the Maxwell-Boltzmann velocity distribution at temperature of T. At first, the system should be equilibrated under the NVT (constant number, volume, and temperature) ensemble at a contact temperature of T. The duration of the NVT ensemble should be long enough to ensure that the system reaches isothermal steady state. Then, to initiate the collision process, the desired initial velocity should be applied to the particle. Since the duration of the collision process is usually around few picoseconds, and also the interaction between the particle and the surrounding air molecules is not considered, it is reasonable to assume that the energy of the system is conserved during the collision. Therefore, Newtonian dynamics under the NVE (constant number, volume, and energy) ensemble should be used to model the collision process. However, since the substrate is connected to the nearby atoms through periodic boundary conditions, its heat conduction should not be ignored. Therefore, the temperature of the few atomic layers on top of the fixed part of the substrate should be regulated. Therefore, during the NVE ensemble, Langevin dynamics, [62] which controls the temperature of the system like a thermostat at a temperature of T, is applied to these layers. This block of Langevin atoms regulates the temperature of the rest of atoms in the simulation box, which follows a Newtonian dynamics. Both the Newton and Langevin equations of motion are integrated with a velocity Verlet algorithm.

3.2 Validation of a nanoparticle collision

First of all, we need to develop a MD simulation model which is able to accurately model a nanoparticle collision process. The developed model should be able to repeat the results of previous studies in MD simulation of nanoparticle collisions. For this purpose, the results reported by Takato *et al.* [63] are repeated. They studied the impact velocity (v_i) dependence of the coefficient of restitution (CoR) of two identical nanoparticles using MD simulations. The diameter of both nanoparticles is equal to 3.2 nm. The system setup is depicted in inside of Figure 3.3. The interatomic potential between all the atoms in the simulation box is modeled using standard (6,12) LJ potential.

$$U = 4\varepsilon\left[\left(\frac{\sigma}{r}\right)^{12} - \left(\frac{\sigma}{r}\right)^{6}\right] + \varepsilon_1 \tag{3.1}$$

where $\varepsilon = 1.654 \times 10^{-21}$J is the potential energy depth, and $\sigma = 3.405$ Å is the zero-across distance potential [63]. For the interaction between the atoms that reside inside each nanoparticle, the cut-off radius of $r_1 = 2.5\sigma$ is considered. For the interaction between the atoms in different nanoparticles the cut-off radius of $r_2 = 2^{1/6}\sigma$ is considered to exclude the adhesion part of the potential at $r_{ij} > r_2$. The LJ potential is shifted to zero by adding the constant energy of ε_1 to Equation 3.1. The impact velocity of $v_i \epsilon\, [2.6 - 517]$ m.s^{-1} is considered. Figure 3.3 compares the results of the under validation MD simulations with the results reported by Takato. As shown, the CoR reported by Takato *et al.* is accurately reproduced using the developed MD code, which shows the ability of the developed model to simulate a nanoparticle collision process.

3.3 Validation of Water Interaction Potential

Despite the simple molecular structure, water exhibits complex and unusual behaviors. Numerous molecular models have been proposed to justify the properties of water under various conditions. The development of molecular water models has a long history. The first attempts in this regard relate to Bernal and Fowler's study in 1933 [64]. The modern development of molecular water models in computer simulations began in 1970, and many of the models used today were developed in 1980. In 1981, Berendsen *et al.* [65] proposed the SPC model. The more sophisticated TIP3P and TIP4P models were also introduced in 1983 [66]. In the SPC/E model [67], which is an extended SPC model, the polarization effects of water are also taken into account.

Each molecular model of water is capable of reproducing one or more physical properties of water, such as density, radial distribution function (RDF), dipole moment, and so on.

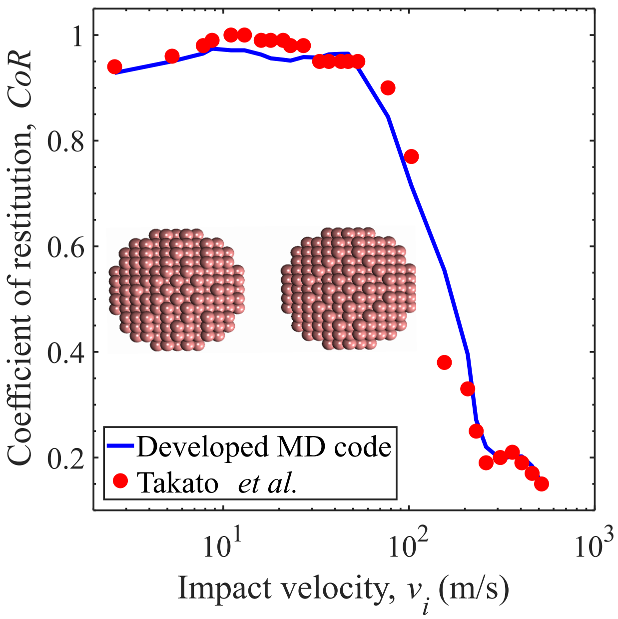

Figure 3.3: Coefficient of restitution *versus* impact velocity for two colliding nanoparticles. The red circles show the results reported by Takato *et al.* [63], and the blue curve shows the results from MD simulations.

In fact, none of the models are able to reproduce all the physical properties of water. In this project, the modified TIP3P water model is used to simulate the water molecules [68]. This water model is selected due to its low computational cost and its ability to accurately reproduce physical properties of bulk water. The first step is to validate the simulation results based on this model. One procedure is to check whether the model can reproduce the correct water density. The water density based on the modified TIP3P at $P = 1$ atm and $T = 298$ K is reported to be 1.009 kg.m^{-3} in the literature [68]. To calculate the water density, the reservoir shown in Figure 3.4a with initial volume of $V = 70 \times 70 \times 70$ Å^3 was filled with water. The number of water molecules in the reservoir was chosen in a way that the initial density becomes 0.95 Å^3. This way, the initial water density differs from its standard value. If we equilibrate the system under the constant Number, Pressure, and Temperature (NPT) ensemble, the volume of the box will change. If the density reaches its standard value, the model can reproduce the water properties correctly. The system was equilibrated under the NPT ensemble, and the water density profile is plotted in Figure 3.4b. It shows that the density reaches its standard value after a while. The average water density is calculated using Eq. 3.2

$$\rho = \frac{N_{H_2O} \times 18.0154}{0.602 \times V_{fill}} \approx 1.00861 \; kg.m^{-3} \tag{3.2}$$

The calculated water density is in agreement with the number reported in the literature 1.009 $kg.m^{-3}$ (0.04 % error), which shows the validity of the developed code for the TIP3P water model.

The validity of the model is also checked for the other water model, TIP4P2005 [69]. A reservoir similar to that shown in Figure 3.4a is filled with water with the same initial density. The system was equilibrated under the NPT ensemble at $P = 1$ atm and $T = 283 - 373$ K, and the density was calculated. The results are plotted in Figure 3.5 and are compared with the results reported in literature. There is an agreement with the results from MD simulations and the results reported by Ma *et al.* [70]. Therefore, the validity of the model for TIP4P-2005 model is also proved.

The validity of the TIP3P model is double-checked with a second procedure. The results reported by Liu *et al.* [71] are reproduced to show the validity of the simulations to model the water molecules based on the modified TIP3P model. They studied pressure-driven water transport inside a nanochannel formed by two graphene layers. The simulation system is shown in Figure 3.6a. The nanochannel thickness and length are $d = 10$ Å and $L = 51$ Å respectively. Both water reservoirs are 40, 37, and 38 Å in the x, y, and z

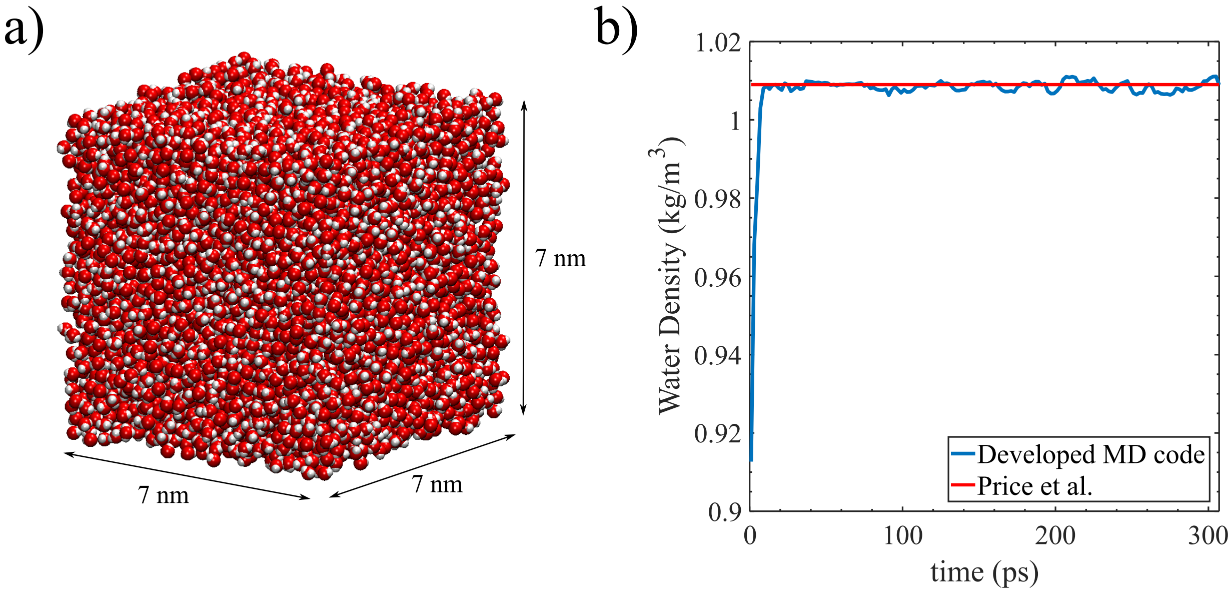

Figure 3.4: (a) Water box with dimensions of 7×7×7 nm^3. (b) Water density profile based on the modified CHARMM TIP3P water model [68].

directions, respectively. Each reservoir contains 1880 water molecules to produce a mass density of 1 $g.cm^{-3}$. The modified TIP3P model was adopted to construct water molecules. In our simulations, the system setup was selected exactly based on the values reported by the paper. All the simulations were performed under the NVT ensemble, at a constant temperature of 300 K. Initially, the water molecules are equilibrated for 50 ps with a time step of 0.5 fs. Subsequently, a pressure difference is applied on the system to create flow through the nanochannel. With the pressure gradient imposed, the simulation is conducted for 250 ps to obtain a steady condition. Then, the simulation is performed for another 250 ps for data collection. The dependence of water flow rate, Q, on the applied pressure gradient ΔP, for both the results of the paper and the simulation results. As shown in Figure 3.6b, there is an agreement between the results reported by Liu *et al.* and the

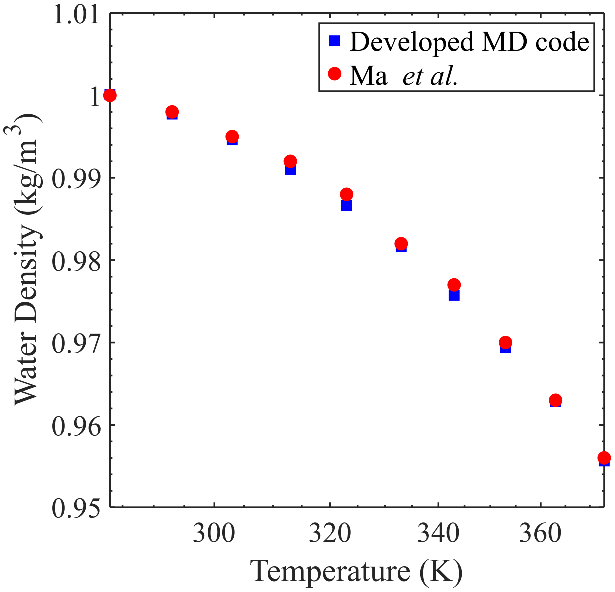

Figure 3.5: Water density profile as a function of temperature. TIP4P-2005 is used to model water molecules. The results from MD simulations (blue line) is compared to the results reported by Ma *et al.* [70].

results of the developed MD code.

3.4 Validation of Silver Interaction Potential

In this project, silver is considered as the material of both particle and substrate because it is frequently used in experimental studies of nanoparticle collision. In addition, the interatomic potential parameters for silver are fully developed in the literature [72]. The interaction potential between the atoms of the particle and substrate is modeled using an embedded atom model, EAM potential [73]. To validate the EAM potential interaction between silver atoms, the results of the study published by Mousavi *et al.* [74] are repro-

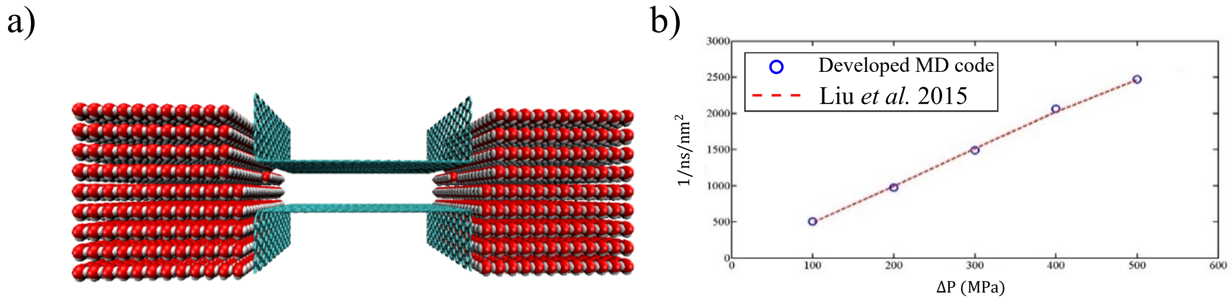

Figure 3.6: (a) Configuration of the system setup. (b) Water flow rate, Q, versus pressure difference, ΔP. The blue circles represent the simulation results, and the dashed red line stands for the results of the paper [71].

duced. In their study, the anisotropic elastic stiffness constants, C_{11} and C_{12}, of silver are reported at different temperatures using EAM potential. The elastic stiffness constant is a characteristic to quantify the strain rate in a material as a function of stress that is applied to that material. Their simulations are repeated exactly with the same procedure reported in their paper, to reproduce the anisotropic elastic stiffness constants of silver.

Figure 3.7 displays the simulation framework to calculate the anisotropic stiffness constants of a silver substrate. To calculate the anisotropic elastic stiffness constants, C_{11} and C_{12}, a cube made of silver atoms is considered. The silver substrate is 50 Å in all three directions. Applying a uniaxial tensile strain rate of 10^{-3} ps^{-1} in the x direction leads to stress components of σ_{xx}, σ_{yy}, σ_{zz} [75]. The relationship between (ε_{xx}, ε_{yy}, ε_{zz}), (σ_{xx}, σ_{yy}, σ_{zz}), and elastic stiffness constants of (C_{11}, C_{12}) could be quantified using the stress-strain equation series as follows:

$$\sigma_{xx} = C_{11}\varepsilon_{xx} + C_{12}\left(\varepsilon_{yy} + \varepsilon_{zz}\right) \tag{3.3}$$

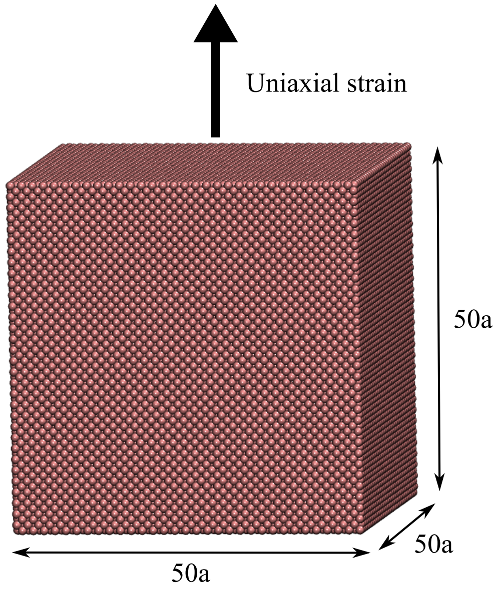

Figure 3.7: Simulation framework showing the silver substrate for calculation of the anisotropic elastic stiffness constants C_{11} and C_{12}.

$$\sigma_{yy} = C_{11}\varepsilon_{yy} + C_{12}\left(\varepsilon_{xx} + \varepsilon_{zz}\right) \tag{3.4}$$

$$\sigma_{zz} = C_{11}\varepsilon_{zz} + C_{12}\left(\varepsilon_{xx} + \varepsilon_{yy}\right) \tag{3.5}$$

The strain in the y- and z-directions is controlled to be zero under the NVT ensemble to have $\varepsilon_{yy} = \varepsilon_{zz} = 0$. Therefore, the stress-strain equations could be simplified as:

$$\sigma_{xx} = C_{11}\varepsilon_{xx} \tag{3.6}$$

$$\sigma_{yy} = C_{12}\varepsilon_{xx} \tag{3.7}$$

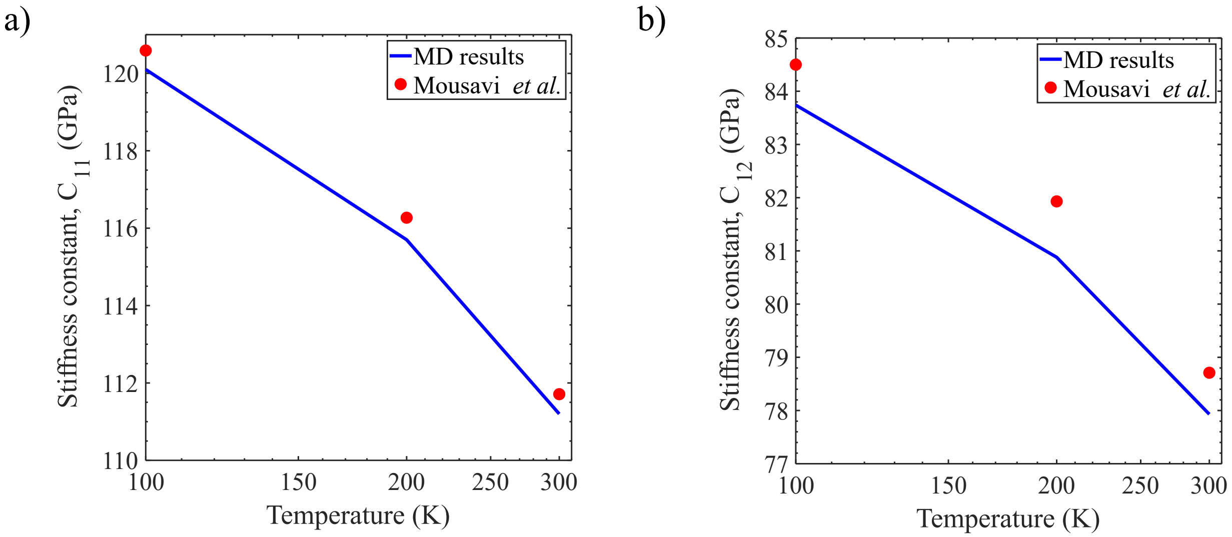

Figure 3.8: Anisotropic elastic stiffness constants of (a) C_{11} and (b) C_{12} of silver [74].

By plotting the stress-strain curves, C_{11} and C_{12} can be calculated from Equations 3.6 and 3.7. The parameters of σ_{xx} and σ_{yy} could be obtained from the MD simulations and having the value of ε_{xx}, C_{11} and C_{22} could be calculated. As shown in Figure 3.8, the MD simulation results are consistent ($\sim$ 1.5 % error) with the results reported by Mousavi *et al.* [74].

3.5 Summary

A simulation setup to study the aerosol filtration process using MD simulations was developed in this chapter. Because modeling of a real filtration process is not possible using MD simulations, several assumptions were considered to simplify the system. Therefore, the aerosol filtration process was simplified as the collision of a single nanoparticle on a flat rigid substrate. The potential parameters for the interaction between all the types presented in the simulation box (Ag, O, H) were validated by repeating the results of previous experimental and numerical studied. The embedded atom model (EAM) for the interaction energy between the silver atoms was validated. The water-water interaction energy was also validated using TIP3P and TIP4P water models.

Chapter 4

Coefficient of restitution for silver nanoparticles colliding on a wet silver substrate

Air humidity can intervene in a particle-surface collision by forming a layer of water molecules on the surface. These water molecules act as a buffer layer that alters the collision condition. In this chapter, we study the effects of condensed water layer on the collision of 5-nm silver particles on a silver substrate by molecular dynamics simulations. The coefficient of restitution is used to characterize the collision. Results indicate that the effects of air humidity on the collisional dynamics depend on the water layer thickness and the surface energy of the substrate. The surface energy of the substrate varies with its Lennard-Jones potential that is used to describe the particle-water, particle-substrate, and water-substrate interaction energies. Air humidity can either increase or decrease the coefficient of restitution in the studied nanoparticle collisions. For a high surface energy substrate, the coefficient of restitution first increases then decreases by increasing the water layer thickness on the substrate when the impact velocity changes from 20 to 500 m/s. For a low surface energy substrate, the coefficient of restitution decreases because of a condensed water layer on the substrate at impact velocities less than 300 m/s. For higher impact velocities, the coefficient of restitution first increases, then decreases, with the condensed water layer thickness. Therefore, the air humidity reduces the adhesion between the nanoparticles and the substrate for a high surface energy substrate. For a low surface energy substrate, however, air humidity may increase or decrease the adhesion between the nanoparticle and the substrate, depending on the impact velocity.

The results presented in this chapter are published in the Journal of *Applied Surface Science* [76].

4.1 Problem Statement

Nanoparticles are used in many industrial applications such as catalyst synthesis, chemical detection, photo-electrical device fabrication, and advanced manufacturing. Meanwhile, these nanoparticles may become airborne and inhalable, resulting in air pollution. Accordingly, understanding the interaction energies between nanoparticles and substrate surfaces is important to high-efficiency aerosol nanoparticle filtration [5], effective antibacterial devices [6], self-assembly of nanoparticles [7], advanced coating technologies [8], and among others.

A particle-substrate collision can be quantified by Newton's coefficient of restitution (CoR), which is defined as the ratio of the rebound velocity and the impact velocity (*see* Eq. 2.1). A small CoR indicates a great velocity reduction or energy dissipation over the collision. Adhesion occurs when CoR is nearly zero, indicating a complete conversion of incident kinetic energy to dissipated energy. Thus, highly accurate and sensitive analytical and numerical approaches are needed for characterizing changes of the kinetic and potential energy of molecules and atoms at interested lattices and on the interface.

CoR for micron particles can be calculated using the velocity terms that depend on the bulk properties of the incident particle, substrate, and surrounding fluid. This approach, however, fails for nanoparticles [77]. When the incident kinetic energy (or impact velocity) is small, part of the thermal energy of the colliding nanoparticles is transformable into the translational kinetic energy; this should be taken into account [78]. There are numerous analytical studies on the collision dynamics of nanoparticles on surfaces. Sato *et al.* [41], using molecular dynamics (MD) simulation, studied the effects of particle size and material properties on energy dissipation for particles colliding on a substrate. They found that the hardness of the particle relative to that of the substrate affects energy dissipation and CoR. Alternatively, Ayesh *et al.* [17] studied the collision of bismuth particles on the silicon substrate, and they found that liquid deformed more than that of solid particles, which led to a small CoR of liquid particles. In addition, Suri *et al.* [44] carried out large-scale atomistic simulations focusing on 5-nm pristine and hydrogen passivated Si nanospheres. They found that hydrogen passivation of each particle prevents the formation of Si-Si covalent bonds and decreases the energy dissipation during collision, although the collision of two pristine Si nanoparticles results in the formation of such bonds in the contact region. Other studies [35, 26] focused on energy transfer during collision by analyzing the contributions of particle size, velocity, and angle of incidence to the adhesion probability. In general, the impact velocity affects the CoR by influencing energy dissipation and incident energy. The significance of the critical velocity, however, varies with the size of incidental nanoparticles.

Despite a relatively large body of literature on the collision between nanoparticles and substrate surfaces, all these earlier works are exclusively for dry surfaces, and little research has been focused on water content in the air [10]. In reality, a water film may be formed at the particle-substrate interface, and it may interfere the collision between the particle and the surface. The water film can affect the quality of the products in material synthesis or the efficiency of air filtration. It is well-known in the literature that the adhesion of micron or larger particles to a surface always increases with relative humidity (RH) or water content in the air. However, the effects of relative humidity on the adhesion of nanoparticles on a surface is still controversial. For example, Miguel *et al.* [46] found that the adhesion of micron particles to a surface is enhanced by increasing the moisture content of ambient air. This effect was attributed to the capillary force of the condensed water layer on the surface. Wang *et al.* [59] also investigated the effects of relative humidity on the deposition rate of aerosolized SiO_2 nanoparticles in a test chamber. Their study showed a size-dependent effect of RH: for particles smaller than 70 nm in diameter, the deposition rate decreases as the RH increases; for larger ones, the deposition rate increases with rising RH. In contrary, Kim *et al.* [29] found that RH had little impact on the collection efficiency of nanosized NaCl particles in the range of 3-70 nm in diameter. Thus, the effects of RH on the nanoparticle-substrate collision deserves further investigations.

To address the role of air humidity, water-surface interfacial behaviors can be studied using MD simulation by integrating the parameters which were obtained empirically. An accurate description of nanoparticle-substrate interaction energy requires a valid database of inter- and intra-molecular forces. Recently, nanoparticles and substrates made of silver were used as a model system to study interfacial phenomena [41, 42].

The main objective of this chapter is to understand how a water layer on the surface affects the CoR of incident nanoparticles, with impact energies between soft-landing and fragmentation regimes, in which the nanoparticle hits the surface elastically, or experiences a severe plastic deformation but is not fragments into pieces, respectively. First, this work reveals the properties of the water layer on the silver surface through implementing the validated silver-silver and silver-water molecular potential data via MD simulation. Then, we investigate the energy dissipation mechanisms and examined how the water film affects the CoR of the incident nanoparticles. Additionally, the surface hydrophobicity is investigated by varying the surface energy of the silver substrate to change so that the surface changes from hydrophilic to hydrophobic. Although the second objective is achieved using a method reported in literature, which requires manual adjustment of the surface molecular potentials, the model predictions and result analyses are expected to provide a general guidance on modifying the wettability of silver surfaces via mechanical or chemical approaches.

4.2 Model Description

4.2.1 Numerical Simulation Method

The collision of a nanoparticle on a dry or wet substrate is investigated using MD simulations, which were experimentally validated for coefficient of restitution in a collision process [79]. Figure 4.2 presents the simulation framework, which is 130 Å in the x- and y-directions and 392 Å in the z-direction. The box contains 55588 to 88855 atoms, depending on the thickness of the water layer. Such a simulation box size is large enough to avoid its finite-size effects on the results.

Silver is chosen as the particle and substrate materials because it is frequently used in experimental studies of nanoparticle collision. In addition, the interatomic potential parameters for silver are fully developed in the literature [72]. The substrate and the nanoparticles are cut out from a grid of a face centered cubic (FCC) structure. The radius of the nanoparticles is $r_p = 25$ Å and the size of the substrate is 130 Å, 130 Å, and 50 Å along the x-, y-, and z- directions, respectively. This size of substrate is large enough to ensure that simulation results are not distorted by artificial boundaries of the substrate, and the energy from the collision is absorbed by and propagated through the substrate. We checked the results for the collision of nanoparticles with the impact velocity of 500 m/s for a larger substrate with dimensions 1.5 times larger in all three directions (*see* Figure 4.4a). No significant difference were observed between the results. The thickness of the condensed water layer on the surface changes in the range of 0 to 21 Å for relative humidity changing from 0 to 100 % [49]. The initial thickness of the water layer on the substrate (L_w) is in between 0 and 21 Å [49]. The minimum water-layer thickness is 5 Å to form a uniform water layer. A Python code was developed to generate the water molecules on the substrate. To place the water layer on the substrate, a prespecified domain was considered on top of the substrate (*see* Figure 4.1a). The size of the domain in the x - and y-directions is equal to the size of the substrate in that directions (130 Å). The size of the domain. in the z -direction is equal to the initial thickness of the water layer (L_w). A distance of 2.5 Å was considered between the box and the substrate to prevent the overlap of water molecules and the silver atoms of the substrate. The number of water molecules inside the box was chosen such that the water density inside the occupied volume be equal to 0.997 gr/cm^3. To generate the water molecules, the oxygen atom of each water molecule was placed randomly inside the box. A minimum distance of 4.4 Å was considered between each pair of oxygen atoms to prevent the overlap of water molecules. After generating all the oxygen atoms inside the box, the hydrogen atoms were bonded to each oxygen atom with the O-H bond length and H-O-H bond angle based on the m-TIP3P [68] water model [68]. Based on the m-TIP3P water model, the O-H bond length is 0.9572 Å and the H-O-H

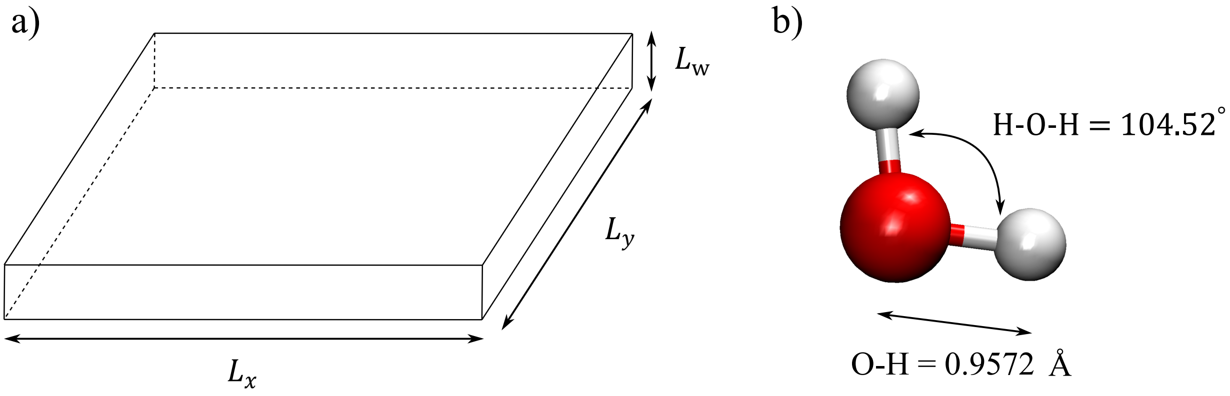

Figure 4.1: (a) Schematic representation of the prespecified domain used to generate water molecules using the Python code. (b) bond and angle values for a water molecule based on the TIP3P model [68].

bond angle is 104.52° (*see* Figure 4.1b). Therefore, the first hydrogen atom is attached to each oxygen atom with a bond length of 0.9572 Å, and the other hydrogen atom is attached to the same oxygen atom in a way that the H-o-H bond angle is 104.52°. It should also be noted that both O-H bonds of each water molecule should be in the same plane.

The interaction energy between the nanoparticle and the surrounding air molecules is ignored in this model. This simplification is reasonable because the diameter of the nanoparticles (50 Å) is much smaller than the mean free path of the air, which is in the range of 678-683 Å under normal conditions [60].

The silver atoms of both nanoparticle and substrate are bonded together inside an FCC crystalline structure; their metallic interatomic potential interaction is modeled using the embedded atom method (EAM) [73], which gives the potential energy U_i of atom i

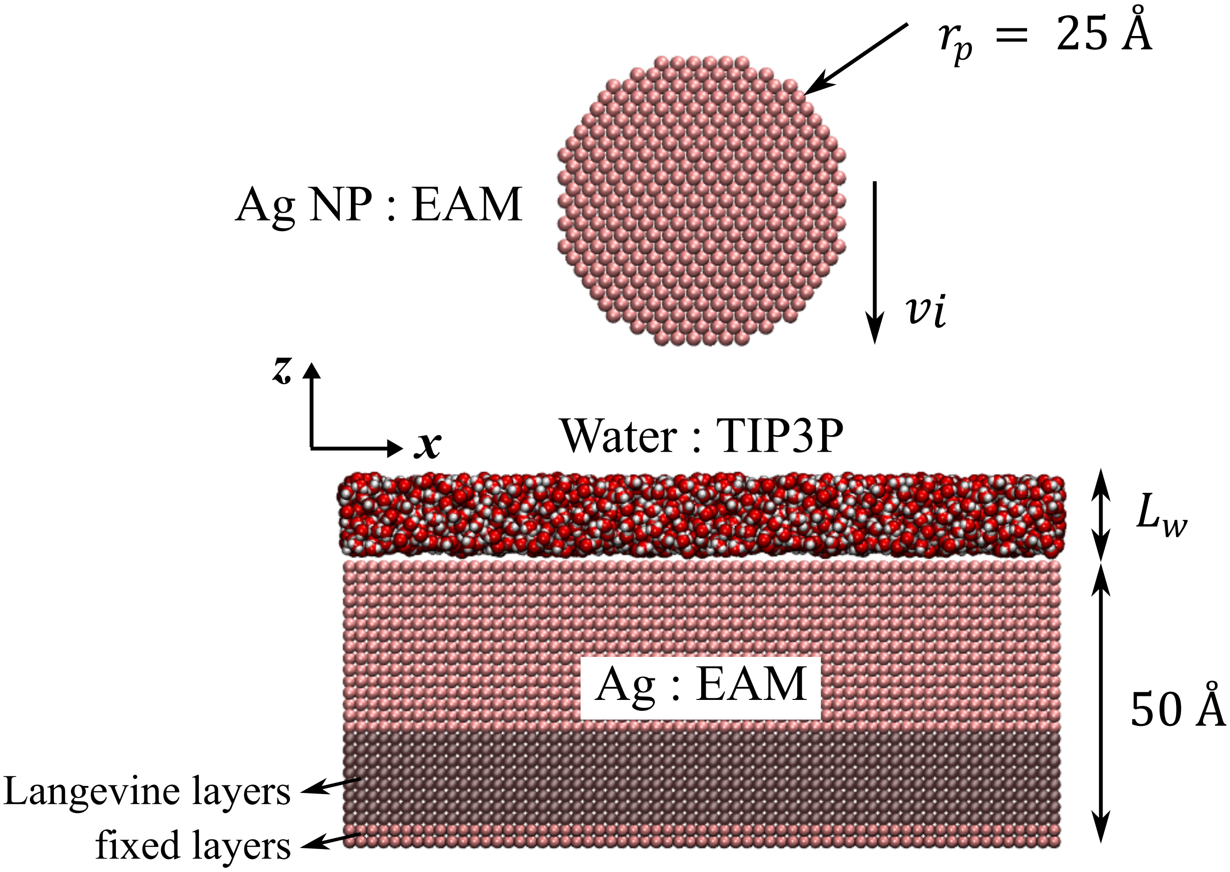

Figure 4.2: Simulation geometry and molecular interaction energy modes for a silver nanoparticle colliding on a wet silver substrate.

$$U_i^{EAM} = F\left(\sum_{j\neq i} \rho\left(r_{ij}\right)\right) + \frac{1}{2}\sum_{j\neq i} \phi\left(r_{ij}\right) \tag{4.1}$$

where F is an embedding energy function, ρ denotes the electron charge density function, and ϕ is a pair-wise potential function, with an interatomic distance of r_{ij}. The material parameters for silver reported by Foiles *et al.* [72] are used for the modeling of silver atoms.

The standard Lennard-Jones (LJ) relationship (*see* Eq. 3.1) is used for the van der Waals (vdW) interaction energy between particle-substrate, particle-water, and water-substrate atoms. The cut-off distance is 10 Å for LJ potential interaction. The Columbic potential is used to calculate the electrostatic interaction energy between oxygen and hydrogen atoms,

$$U_i^C = \frac{kq_iq_j}{r_{ij}} \tag{4.2}$$

where k is the Coulomb's constant, and q is the atomic partial charges. Long-range electrostatic interaction energies are calculated using a particle-particle particle-mesh (PPPM) method, with a cut-off distance of 12 Å and a root-mean-square accuracy of 10^{-4}.

Table 4.1 summarizes all LJ pair interaction energies and the partial charges for all atoms in the simulation box. Mix arithmetic [80] is used to calculate the values of ε and σ for O-H, O-Ag, H-Ag, and Ag-Ag pairs on water-water, water-particle, water-substrate, and particle-substrate interaction energies. Same as in an earlier work [9], the potential parameters for water molecules are chosen based on the modified TIP3P model [68]. In addition, the SHAKE algorithm is used to fix the internal geometry of each water molecule.

Table 4.1: Lennard-Jones potential and Columbic parameters for all atoms in the simulation box [68, 81].

Atom type	ε (kcal.mol^{-1})	σ Å	q (e)
Oxygen	0.1521	3.150	-0.834
Hydrogen	0.0461	0.400	+0.417
Silver	7.9466	2.644	0.000

The surface attraction energy of the nanoparticle or substrate is controlled by manipulating the LJ parameter, ε, of their silver atoms. For the particle, the LJ parameter of $\varepsilon_p = 0.3178$ kcal.mol^{-1} is considered to enable weak adhesive collisions. Two values of 7.9466 and 1.2714 kcal.mol^{-1} for the LJ parameter of the substrate, ε_s, stand for the substrates with high and low surface energy (or wettability), respectively. The first value of 7.9466 is from literature [81]; while the second value of 1.2714 was determined by changing the surface from a high-energy to a low-energy one until reaching a hydrophobic surface. The surface hydrophobicity is determined by the relative value of the adhesive and cohesive forces, which are the water-water and water-surface interaction energies, respectively. Decreasing the surface energy of the substrate by decreasing its ε_s parameter reduces the attraction energy between the substrate and the water molecules. As a result, the water-surface adhesive forces are reduced compared to the water-water cohesive forces. Therefore, the water molecules tend to be sticked to each other, leading to a more hydrophobic substrate. Figure 4.3 displays the water contact angle for both surfaces, which is calculated using MD simulations. For the substrate with $\varepsilon_s = 7.9466$ kcal.mol^{-1}, which is from literature [81], the water contact angle is approximately 9.6°, which is in agreement with the experimental measurement for water contact angle on a pristine silver surface [82]. The water contact angle for the substrate with $\varepsilon_s = 1.2714$ kcal.mol^{-1} is 24°, which produces a more hydrophobic surface.

The interaction energy strength of the nanoparticle or substrate is reduced by assuming that a partial oxide layer created on their surface weakening the surface interaction energy [53]. As reported by Shafrin and Zisman [53], atoms below the surface do not influence surface energy. Differences in surface energy between substrates that are similar in the bulk structure result from the varying outermost layer that covers the surface of the substrate. Modifying the outermost layer can transform a high-energy surface into one with the

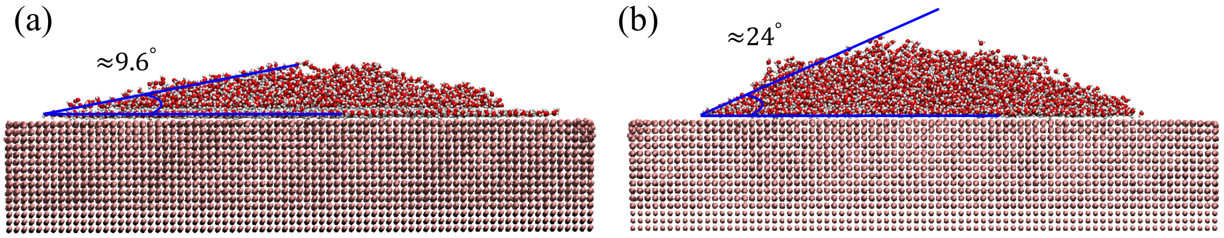

Figure 4.3: Water contact angle for surfaces with (a) $\varepsilon_s = 7.9466$ kcal.mol^{-1}, and (b) $\varepsilon_s = 1.2714$ kcal.mol^{-1}.

wetting characteristics of a low-energy surface of the same material. Therefore, the surface energy of the particle or substrate is modified by controlling the ε parameter of its atoms.

All equations are solved using the LAMMPS package [83]. At the initial condition of each simulation, the nanoparticles are located outside the interaction energy range of the substrate and water molecules above the substrate. All the simulations begin with the Maxwell-Boltzmann velocity distribution for all atoms at 300 K. Two outermost atomic layers of the substrate are fixed to prevent the movement of the substrate while the other layers are left to vibrate normally. The NVT ensemble with a Nose-Hoover thermostat was initially used, which maintains the system temperature at 300 K. The time duration of the NVT ensemble is 100 ps to ensure that the system reaches an isothermal steady state.

At thermal equilibrium, a desired impact velocity in the range $v_i \ \epsilon \ [20, 500]$ m.s^{-1} (to cover both elastic and plastic regimes) is applied to the z component of each atom that the particle consists of. Therefore, the particle impacts the plane at v_i with the atoms fluctuating because of thermal noise. During collision, the bottom two layers remain fixed in time, and Langevin dynamics [62] is applied to the next eight atomic layers to control the substrate temperature. All other atoms are followed by Newtonian dynamics. The

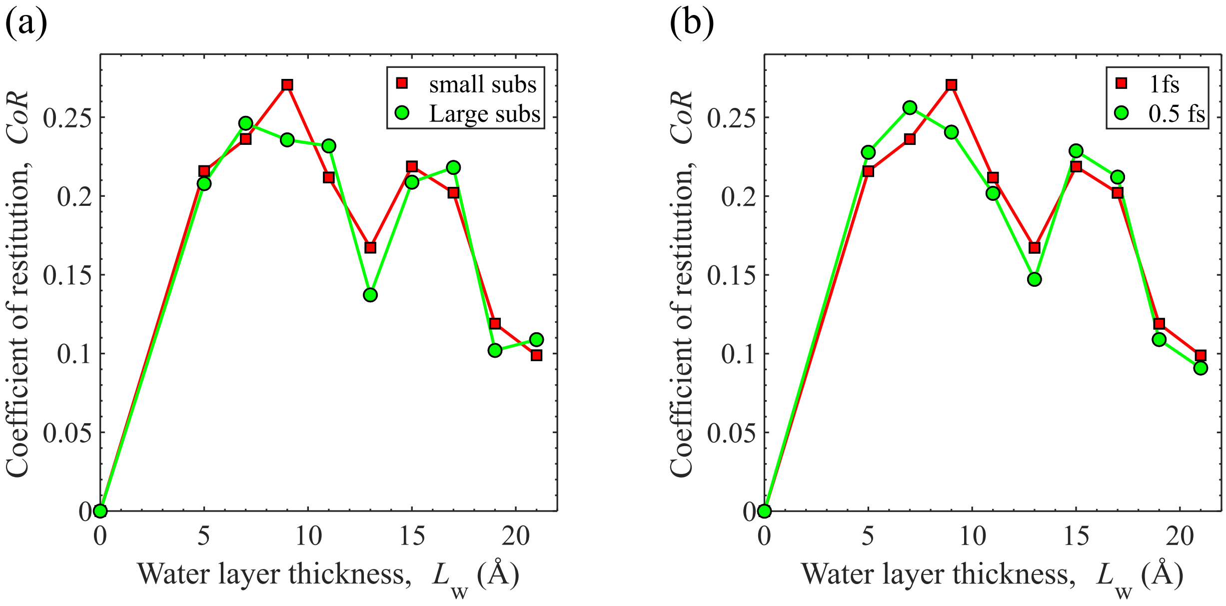

Figure 4.4: Coefficient of restitution (CoR) for the collision of nanoparticles with impact velocity of 500 m/s to show the independency of the results of (a) time-step, and (b) size of the substrate.

block of Langevin atoms controls the temperature of the rest of atoms in the simulation box that follows Newtonian dynamics. Both Newton and Langevin equations of motion are integrated with a velocity Verlet algorithm with a time step of 1 fs. Additionally, the CoR of nanoparticles colliding on the substrate with the impact velocity of 500 m/s are modeled with a smaller timestep of 0.5 fs (*see* Figure 4.4b). No considerable difference was observed between the results for the small (0.5 fs) and large (1fs) time steps.

4.2.2 Dynamics of the System

The coefficient of restitution (CoR) is defined as the ratio of the rebound velocity to the impact velocity. Equation 4.3 shows that the CoR represents the energy dissipation during the collision. The mechanisms of energy dissipation during the collision is analyzed based on the energy balance for the particle before and after a collision. During the collision,

$$KE_i + U_i = KE_r + U_r + E_c + E_{th} \tag{4.3}$$

where KE_i, U_i, KE_r, U_r, E_c, and E_{th} are kinetic energy before collision, potential energy before collision, kinetic energy after collision, potential energy after collision, and the potential energy arising from the particle-substrate contact between the particle and the surface of the substrate, and the thermal energy dissipation into the block of Langevin atoms substrate due to vibration of atoms, respectively. There is a change in the internal potential energy of the particle because of its plastic deformation. The interaction energy between the particle and the surface of the substrate accounts for the attractive molecular forces. Therefore, the kinetic energy dissipation is mainly due to the contact interaction energy between the particle and surface, the plastic deformation of the particle, and the thermal dissipation (*see* Equation 4.4)

$$E_{diss} = KE_i - KE_r = (U_i - U_r) + E_c + E_{th} \tag{4.4}$$

The dissipation mechanisms are illustrated in Figure 4.5. It is crucial to examine the effects of all the parameters on the dissipation mechanisms for nanoparticle collisions. Air humidity is one of the parameters that affect the collision dynamics by affecting E_c,

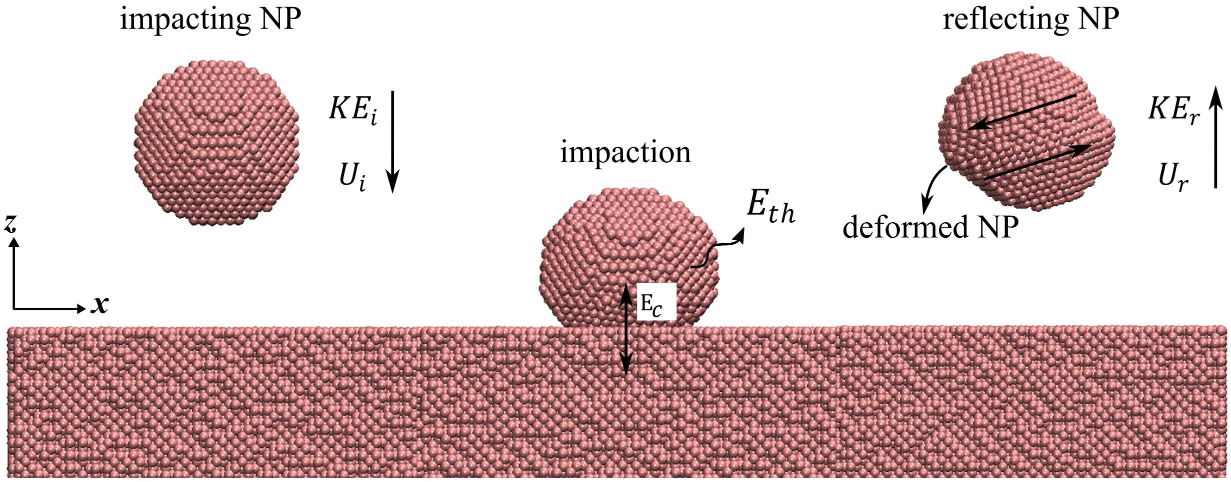

Figure 4.5: Schematic of the dissipation mechanisms when a nanoparticle collides on a substrate.

$(U_i - U_r)$, and E_{th}. For wet collisions, the plastic deformation and the thermal dissipation changes because the particle is in contact with the water molecules rather than the solid substrate. The contact interaction energy (E_c) also changes, since in addition to the particle-substrate interaction energy (E_{ps}), it also results from the particle-water interaction energy (E_{pw})

$$E_C = E_{ps} + E_{pw} \tag{4.5}$$

With this model, we first studied the water-substrate interfacial behavior, followed by the effects of water layer thickness on the collision behavior of a nanoparticle on a silver substrate. Finally, the effects of surface energy of the substrate on the collision behavior is reported.

4.3 Results

4.3.1 Water Density Profile at a Solid Interface

The water layer on the substrate is initially relaxed to reach equilibrium state prior to applying the impact velocity to the particle. Figure 4.6a shows the snapshots of the simulation framework of the water-substrate interface at equilibrium, when the water molecules tend to form a layered structure on the substrate. For $L_w = 5$ Å, only one dominant water layer is formed on the substrate. With increasing L_w, the water molecules above the first layer form another layer, resulting in a double layer structure on the substrate. Above this double layer, the water molecules form no specific arrangement other than bulk-like water structure. This is similar to the double-layer structure of water molecules near a graphene surface [24].

Figure 4.6b shows the distribution of the water density as a function of the distance from the surface (z). There are two peaks in the density profile, one being at $z = 2.5$ Å and another at 5.5 Å, which indicates that the water molecules form a double-layer structure on the silver substrate. For $L_w = 5$ Å, there is only one dominant peak at $z = 2.5$ Å, and increasing the number of water molecules (increasing L_w) results in the second peak at $z = 5.5$ Å. These characteristic peaks of the water molecules remain unchanged even as the number of water molecules increases, implying that the double-layer structure of water is maintained at the silver/water interface. There is no clear peak observed when z is greater than 8 Å, and the water density gradually reaches to its bulk value of 1 g.cm^{-3} or so.

The double-layer structure of water molecules on the substrate is attributed to the surface energy of the substrate. The pristine silver substrate has a high surface energy

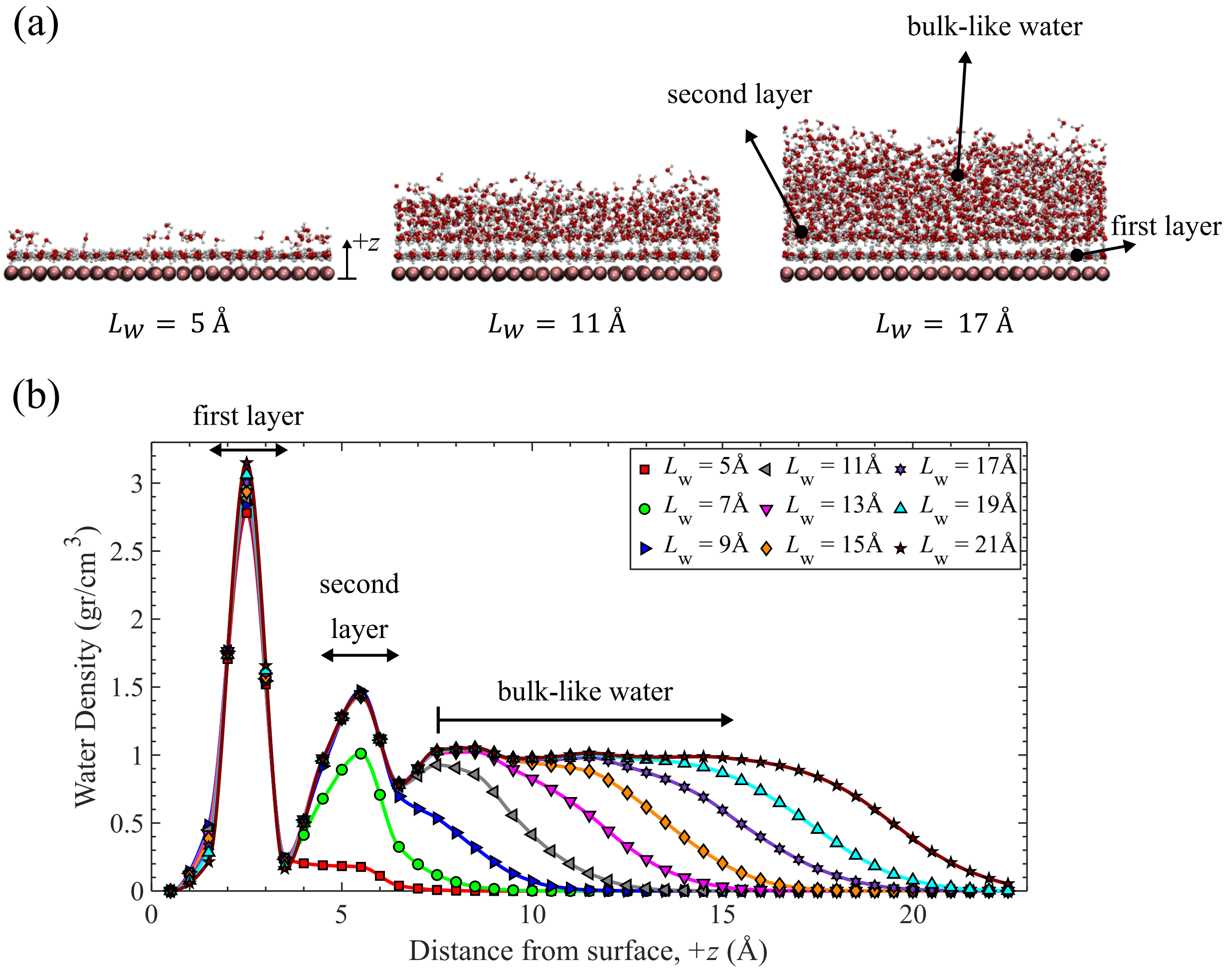

Figure 4.6: Water density profile near the high-energy substrate: (a) snapshots of MD simulations of a water layer with the initial thickness of L_w on a silver substrate; (b) water density profile near a silver substrate at different water layer thicknesses.

that absorbs the water molecules nearby and forms a compact water layer (the first layer) with a great density [24]. The orientation of hydrogen bonds in the first and second layers of water is plotted in the Figure 4.7. The orientation of O-H bonds in the first layer is

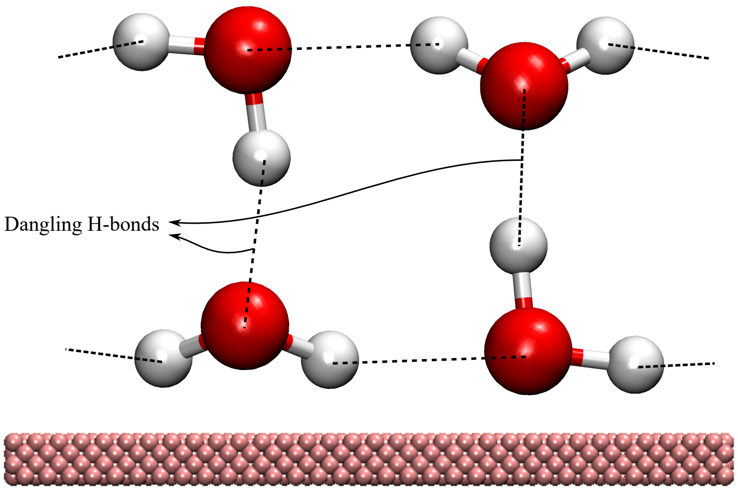

Figure 4.7: Orientation of hydrogen bonds in the first and second layers of water near the silver substrate.

parallel or normal to the silver substrate, hydrogen atoms in the first layer is arranged in such way that some hydrogen bonds dangle outside of this layer [24]. These dangling hydrogen bonds, interacting with other water molecules, form the second water layer on top of the substrate. The orientation of O-H bonds in the second layer is parallel or normal to the silver substrate such that some hydrogen bonds dangle toward the first layer with no hydrogen bonds dangling outside of the second layer. This means that the hydrogen bonds in the second layer are saturated with the hydrogen bonds in the first layer; therefore, there is no dangling H-bond beyond the second layer [24]. Consequently, the water molecules above the second layer are normally arranged in a bulk-like water structure, and no clear peaks present beyond the second layer.

As shown in Equation 3.1, the attractive term of LJ potential decays with interatomic distance to the inverse power of six, indicating that the LJ attraction decays considerably with increasing interatomic distance. As a result, the attraction applied to the water molecules in the second layer is lower than that applied to those in the first layer because the distance between the second layer and the substrate is greater than that between the first layer and the same substrate. Therefore, the density of the second layer is lower compared to that of the first layer, which the density of the first layer is so high that it behaves like a solid layer at a room temperature [57]. The LJ interaction energy between the substrate and the water molecules decreases considerably for z greater than 8 Å. As a result, the water molecules above the second layer are weakly affected by the substrate.

4.3.2 Effects of Condensed Water Layer on Particle-surface Collision

Coefficient of restitution for high-energy substrate

Figure 4.8 shows the coefficient of restitution (CoR) for the collision of a 5-nm particle on a silver substrate. Figure 4(a) displays the CoR as a function of water layer thickness. According to Figure 4.8a, the CoR for dry collisions (*i.e.*, $L_w = 0$) is zero for all impact velocities, which indicates that the particle always adheres to the dry substrate. When $L_w > 0$, however, the CoR is greater than zero. This means that the collision can result in particle rebound when there exists a water layer on the substrate. By increasing the water layer thickness on the substrate, the CoR first increases and then decreases until the particle adheres to the substrate again when CoR approaches 0.

The impact velocity affects the CoR and the water layer thickness at which the particles re-adhere to the substrate. The CoR is also depicted in Figure 4.8b as a function of the impact velocity to illustrate the dependency of CoR on impact velocity. The CoR displays a bimodal behavior as a function of the impact velocity. The CoR increases with the

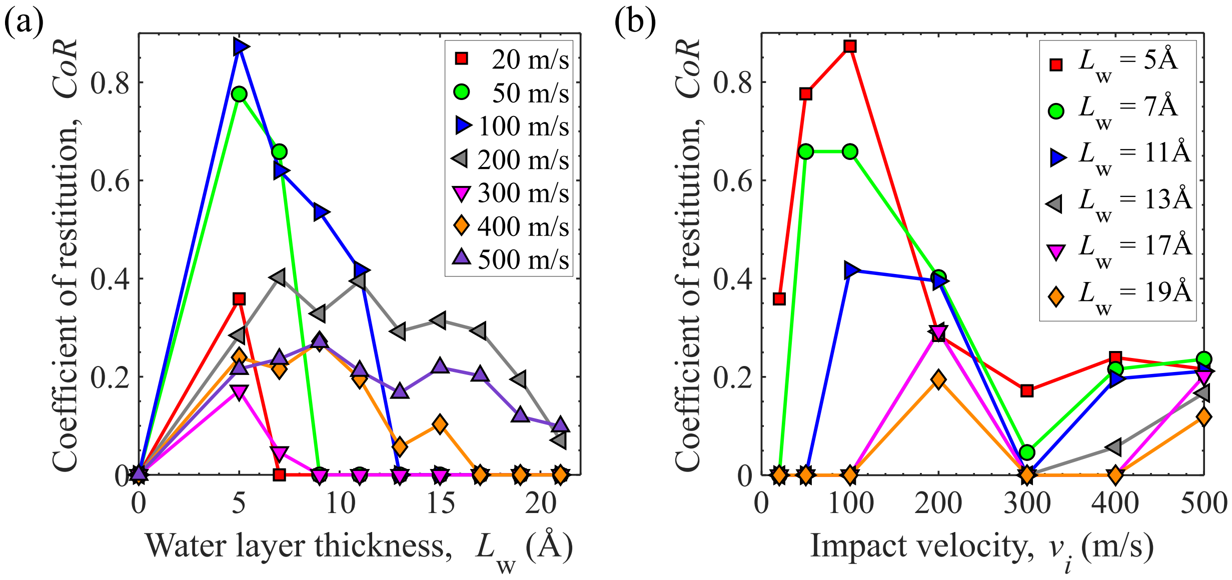

Figure 4.8: Coefficient of restitution (CoR) of the 5-nm particle colliding on the silver substrate as a function of (a) water layer thickness, and (b) impact velocity.

impact velocity in the range of 20-100 m.s^{-1}. It decreases for the impact velocities of 200 and 300 m.s^{-1}, and it increases again for the impact velocities of 400 and 500 m.s^{-1}. This bimodal behavior was also reported previously in the study of collision of nanoparticles on a dry substrate [22].

To better understand the effects of water layer thickness on CoR, the dependence of the dissipation mechanisms on water layer thickness are discussed below because according to Equation 2.1 the CoR depends on energy dissipation.

Dissipation mechanisms for high-energy substrate

(a) Particle-substrate interaction energy. Figure 4.9 shows how the particle-substrate interaction energy (E_{ps}) changes as a result of the condensed water layer on the substrate. Figure 4.9a displays the average potential interaction energy between the particle and silver substrate as a function of the water layer thickness (L_w). The particle-substrate interaction energy drops quickly as a water layer is formed near the substrate with $L_w = 5$ Å. However, it becomes saturated for the water layer thickness beyond 5 Å. As shown in Figure 4.9a, when L_w changes from 0 to 5 Å, the interaction energy decreases from -7.58 to -0.32 eV for the impact velocity of 20 m.s^{-1}, and from -70.80 to -5.35 eV for the impact velocity of 500 m.s^{-1}. The values of E_{ps} for other velocities fall into these two ranges. Further increasing the water layer thickness does not considerable change the particle-substrate interaction energy.

The reduction in particle-substrate interaction energy could be attributed to the formation of the dense water layer near the surface, which separate the nanoparticle from the substrate (*see* Figure 4.9b). Figure 4.9c displays the closest distance between the particle and substrate as a function of L_w, for different values of impact velocity. The closest distance between the particle and substrate increases and saturates with increasing the water layer thickness on the substrate. As discussed in Section 4.3.1, the water molecules form a layered structure near the substrate. The first layer has such a high density that it behaves like a solid layer even at a room temperature. On the contrary, the second layer has a density that is much lower than the first layer, although it is higher than the bulk water density. During the collision, the nanoparticle penetrates through the bulk-like layer and the second layer before reaching the first layer of water molecules. However, it cannot breakthrough the strong hydrogen bonds between the water molecules in the first

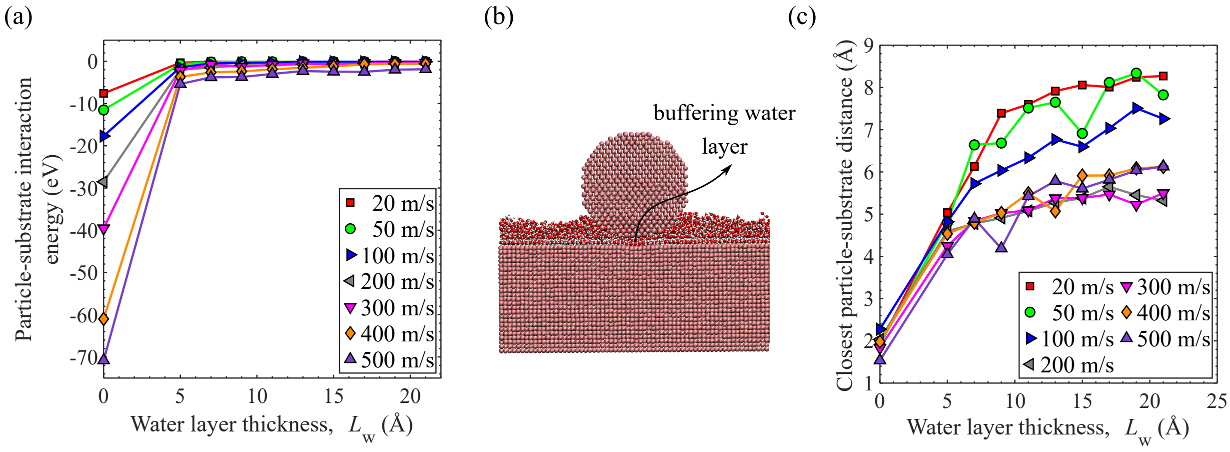

Figure 4.9: Effects of condensed water layer on the particle-substrate interaction energy (E_{ps}): (a) average particle-substrate interaction energy *versus* water layer thickness at different impact velocities for a high-energy substrate; (b) schematic of the layered water molecules separating the nanoparticle from the substrate during the collision. (c) The shortest distance between the particle and the high-energy substrate as a function of the condensed water layer thickness for different impact velocities.

layer near the substrate. Therefore, the closest distance between the particle and substrate increases then saturates with increasing the water layer thickness.

For dry collisions, because the particle directly contacts with the high-energy silver substrate, there is a strong interaction energy between them. As discussed in Section 4.3.1, the water molecules form a layered structure near the substrate. The first layer has such a high density that it behaves like a solid layer even at room temperature. On the contrary, the second layer has a density that is much lower than the first layer, although it is higher than the bulk water density. When $L_w = 5$ Å, only the first layer is formed. But the second layer and the bulk-like water layer may be formed with increasing L_w. During the collision, the nanoparticle penetrates through the bulk-like layer and the second layer before reaching the first layer of water molecules. However, it cannot breakthrough the strong hydrogen bonds between the water molecules in the first layer near the substrate. As illustrated in Figure 4.9b, the dense water layer adjacent to the substrate behaves like a buffer, separating the nanoparticle from the substrate. Therefore, the distance between the nanoparticle and the substrate increases, which decreases their interatomic interaction energy. Note that the increment of the distance between the particle and the substrate is around 1.5 Å. Such a slight increment in distance between the particle and the substrate greatly reduces their interatomic interaction energy because LJ potential is a short-range interaction energy. Therefore, the energy dissipation through particle-substrate interaction energy decreases considerably in the presence of a water layer on the substrate (*see* Figure 4.9a).

It should also be noted that E_{ps} increases with increasing impact velocity for both dry and wet contacts. The particle deformation increases at the deepest contact point as the impact velocity increases. As a result, the contact area between the particle and substrate increases, increasing their interatomic interaction energy. However, due to the short-range of the LJ potential interaction, the effect of velocity on the particle-substrate interaction energy (E_{ps}) is much stronger for dry than for wet collisions when the particle is not in direct contact with the substrate. Therefore, by increasing impact velocity from 20 to 500 m.s^{-1}, E_{ps} changes from -7.58 to -70.80 eV for dry collisions, and from -0.07 to -1.86 eV for wet collisions at $L_w = 21$ Å. The particle-substrate interaction for other values of water layer thicknesses falls into these two ranges.

(b) Particle-water interaction energy. The particle-water interaction energy (E_{pw}) during a collision consists of viscous and capillary interaction energies, which are applied to the nanoparticle during the colliding and rebounding stages, respectively. Figure 4.10

shows the particle-water interaction energy for different values of water layer thickness. The particle-water interaction energy is zero before the collision because the particle is not in contact with the water molecules. The particle-water interaction energy increases gradually when the particle approaches the surface until reaching its maximum value at the deepest particle-surface contact point. If the collision results in rebound, the particle gradually detaches from the water molecules. Therefore, the particle-water interaction energy decreases after the deepest contact point and approaches to zero again. However, if the collision results in adhesion, the particle remains in contact with the water molecules. Therefore, the particle-water interaction energy remains unchanged or decreases slightly until approaching a non-zero value for a collision which results in adhesion. It should be noted that for impact velocity of 20 m/s the particle-water interaction energy remains unchanged when the water layer thickness changes from 15 to 21 Å. The reason is that the particle's kinetic energy is not high enough to overcome the capillary force. Therefore, the particle sticks to the water molecules on the surface and cannot rebound from the surface and as a result, the particle-water interaction energy remains unchanged. As shown in Figure 4.10, the magnitude of E_{pw} increases by increasing the water layer thickness for all the impact velocities. Increasing the water layer thickness (L_w) increases the number of water molecules on the substrate. Then the particle is in contact with more water molecules during the collision, which increases the interaction energy applied to the particle during both colliding and rebounding stages. As a result, both viscous and capillary interaction energy increase with L_w. Since the interaction energy applied to the particle by the water molecules dissipates the initial collision energy of the particle, the thicker water layer, the more energy dissipation. Similar results were reported by Xiao et al. [49] that the capillary force increases by the ambient relative humidity or the condensed water layer thickness.

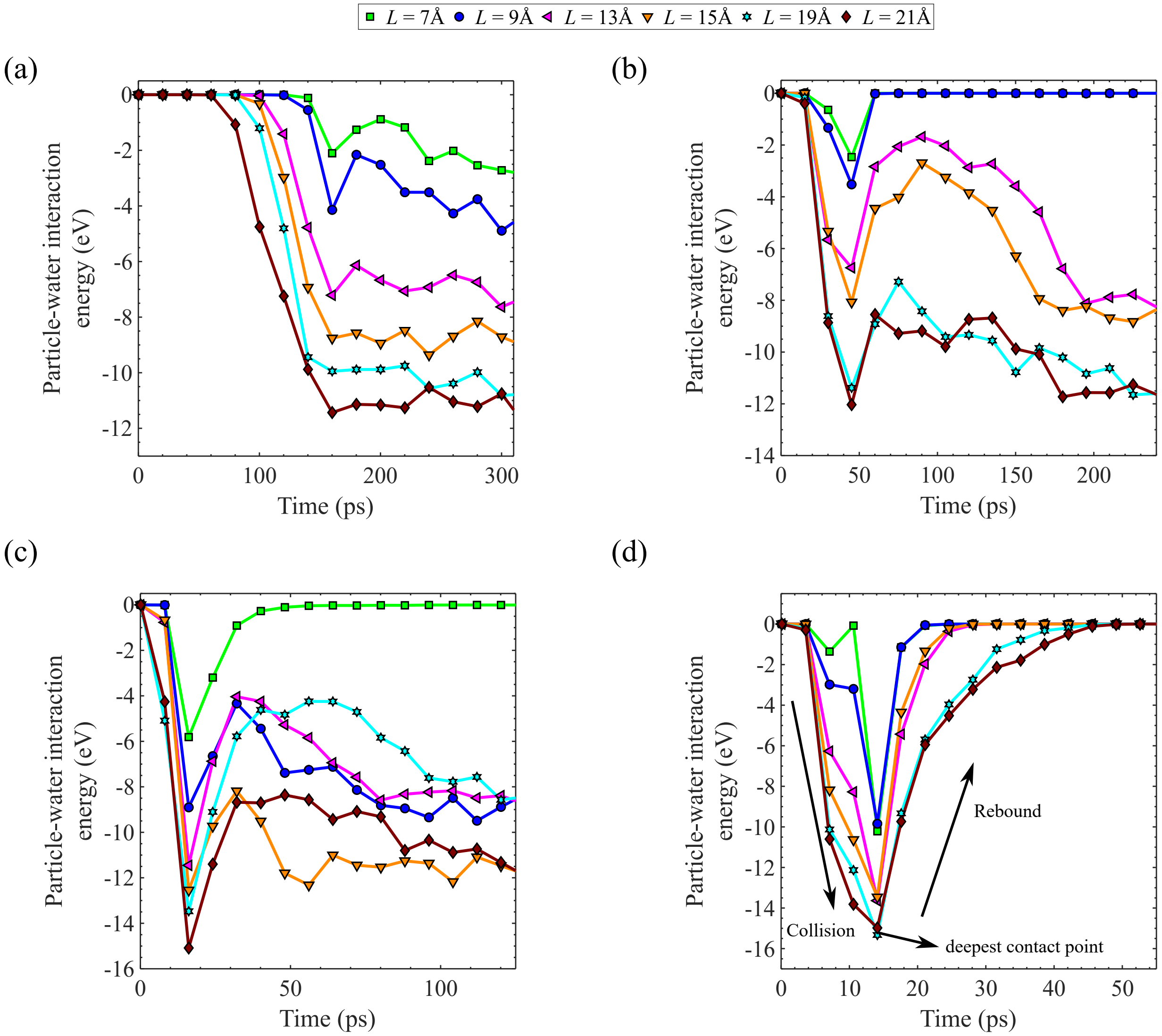

Figure 4.10: Particle-water interaction energy (E_{pw}) at different water layer thicknesses for a high-energy substrate. The impact velocity is (a) $v_i = 20$ m.s^{-1}, (b) $v_i = 100$ m.s^{-1}, (c) $v_i = 300$ m.s^{-1}, and (d) $v_i = 500$ m.s^{-1}. When the collisions result in adhesion, there is a subsequent relaxation of E_{pw} as the nanoparticle begins to equilibrate with the water layer.

(c) Plastic deformation of the nanoparticle. In this study, plastic deformation of the nanoparticle is characterized by its radius of gyration (*see* Figure 4.11). Figure 4.11a shows the radius of gyration of the nanoparticles versus water layer thickness for different impact velocities. Both elastic and plastic collision regimes are observed for the range of velocities presented. The particle collides on the surface elastically at $v_i < 200$ m/s, and plastically at $v_i > 300$ m/s. Although the velocity above which the particle undergoes an elastic to plastic deformation depends on the particle size and material, the same transition from elastic to plastic deformation has been reported in previous studies [25, 63]. For example, Takato *et al.* [25] have reported that the transition from elastic to plastic regime occurs at the velocity of 155 m/s to 25 m/s for argon particles with radius ranging from 1.73 to 21.5 nm, respectively. The deformation of the particle for a low-speed impact ($v_i = 200$ m.s^{-1}) is reversible, and the shape of the nanoparticle is retrieved after the collision. In this elastic collision regime, the collision remains elastic for all water layer thicknesses. In contrary, the deformation of the particle for a high-speed impact ($v_i = 300$ m.s^{-1}) is irreversible, and it experiences a permanent structural change. In this plastic collision regime, the collision energy of the particle is high enough to change the atomic structure in the particle. In the plastic deformation regime, however, the degree of plastic deformation may decrease with increasing water layer thickness.

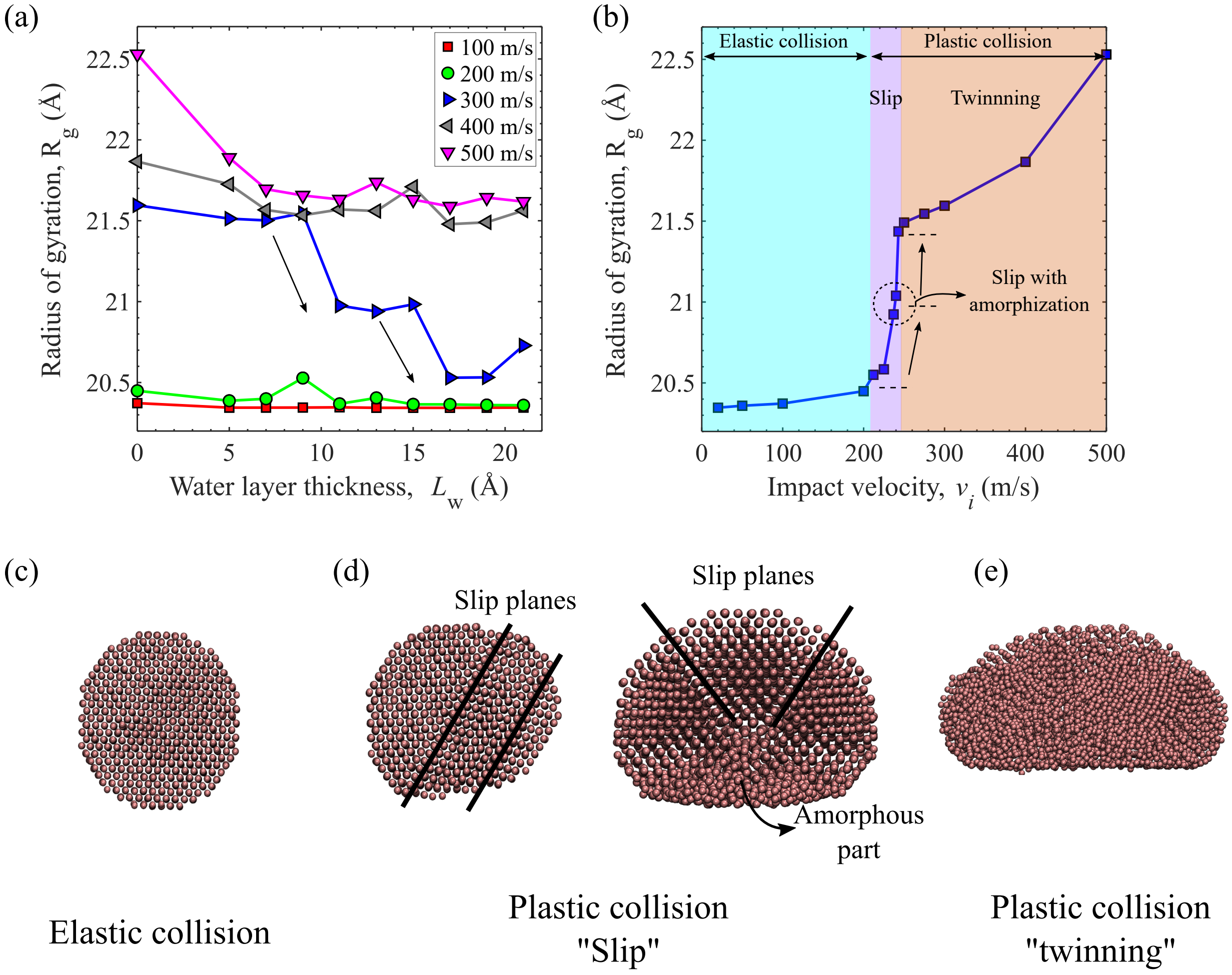

Figure 4.11: Radius of gyration of the colliding nanoparticle on a high-energy substrate as a function of (a) water layer thickness for wet collisions, and (b) impact velocity for dry collisions. Three types - (c) elastic, (d) plastic ”slip”, and (e) plastic ”twinning” - deformation regimes are recognized according to the radius of gyration of the colliding nanoparticles.

We investigated the deformation modes of the colliding nanoparticles on a dry substrate to understand the effects of condensed water layer thickness on the radius of gyration. Figure 4.11b shows the radius of gyration *versus* impact velocity for nanoparticles colliding on a dry substrate. In the elastic collision regime for the impact velocity lower than 200 m.s^{-1}, the nanoparticle returns to its original shape (*see* Figure 4.11c). The nanoparticles undergo plastic deformation for higher impact velocities. Depending on the impact velocity, the nanoparticles experience two types of plastic deformation, slip or twining [25]. The energy dissipation of colliding nanoparticles in the plastic collision regime depends on both the degree of permanent deformation and the corresponding deformation mode [25].

A nanoparticle with an impact velocity in the range of 200-243 m.s^{-1} undergoes a slip plastic deformation (*see* Figure 4.11d), where the atoms of the nanoparticle move along the slip planes. Depending on the impact velocity, two types of slip deformation may take place: slip with preserving the crystalline structure (left side of Figure 4.11d) and slip with partial amorphization (right side of Figure 4.11d). For impact velocities between 200 and 225 m.s^{-1}, the crystalline structure of the nanoparticle is preserved, although the nanoparticle is deformed along the slip plane(s). When the impact velocity increases to 237-240 m.s^{-1}, the crystalline structure of some parts of the nanoparticle is distorted and the structure becomes partially amorphous on multiple slip planes. The radius of gyration gradually changes in each velocity range, but it quickly jumps when the impact velocity increases from 225 to 237 m.s^{-1}. The reason is that the type of slip deformation changes and the crystalline structure of the nanoparticle is no longer preserved when the impact velocity increases from 225 to 237 m.s^{-1}.

A nanoparticle undergoes twinning deformation for $v_i = 243$ m.s^{-1}. The nanoparticle is compressed along the collision axis and elongated along the direction perpendicular to the collision direction (*see* Figure 4.11e). Consequently, the nanoparticle is flattened, and the strong impact alters the crystal structure of the nanoparticle. The radius of gyration increases quickly when the impact velocity changes from 240 to 243 m.s^{-1} because the deformation shifts from slip plastic to twinning plastic. However, the degree of plastic deformation increment slows down in twinning deformation ($v_i = 243$ m.s^{-1}). The reason is that the crystalline structure of the whole nanoparticle is distorted at the impact velocity of 243 m.s^{-1}; further increase in impact velocity flattens the nanoparticle more.

In the presence of a water layer on the substrate, the viscous force between the water molecules and the nanoparticle reduces the velocity of the nanoparticle. As a result, the particle velocity before reaching the solid substrate (v_i') becomes lower than its initial value (v_i). The thicker the water layer, the great reduction in the velocity, and the lower v_i'. For a wet collision, the degree of plastic deformation depends not on v_i but v_i'. Since $v_i' < v_i$ the degree of plastic deformation may decrease with a water layer on the substrate.

The collision for $v_i \leq 200$ m.s^{-1} is elastic in dry condition. Since the dry collision is in elastic regime for this velocity range, the collision still results in elastic deformation in the wet condition, although v_i' is lower than v_i. The kinetic energy of the particle is insufficient to make permanent structural changes in the particle. Therefore, the plastic deformation and the resultant energy dissipation through this mechanism is negligible regardless of the condensed water layer. In this elastic collision regime, energy loss mainly arises from contact interaction energy (E_c).

The collision energy becomes high enough to permanently change the atomic structure of the nanoparticle when the impact velocity reaches 300 m.s^{-1}. As a result, the deformation of the nanoparticle changes from elastic to plastic when the impact velocity increases from 200 to 300 m.s^{-1}. Figure 4.11b shows that a dry collision at 300 m.s^{-1} results in twinning deformation and that the deformation type remains twinning even the impact velocity drops to 243 m.s^{-1}. This result indicates that the radius of gyration drops slightly as long as the deformation type remains twinning. With a water layer on the substrate, although, v_i' continuously decreases with the water layer thickness, v_i' remains higher than the velocity that enables twinning deformation when $L_w \leq 9$ Å. Consequently, the degree of plastic deformation decreases slightly as the water layer thickness changes from 0 to 9 Å. When the water layer thickness increases from 9 to 11 Å, v_i' becomes low enough that the type of deformation changes from twinning to slip, with amorphization occurring in some parts of the nanoparticle, as illustrated in the left side of Figure 4.11d. Therefore, the radius of gyration drops quickly when the water layer thickness changes from 9 to 11 Å. Further increasing L_w from 11 to 15 Å, v_i' continues decreasing, but the type of deformation is still slip with partial amorphization. Therefore, the radius of gyration remains the same when L_w increases from 11 to 15 Å. Finally, increasing the water layer thickness to values higher than 15 Å, no amorphization occurs in the nanoparticle and the slip deformation occurs while the crystalline structure of the nanoparticle is preserved. Therefore, the radius of gyration quickly drops again when L_w increases from 15 to 17 Å.

For $v_i = 400$ m.s^{-1}, v_i' remains higher than 332 m.s^{-1}, which is higher than the threshold for twinning deformation. Therefore, the reduction rate of radius of gyration remains low since the type of deformation is the same (twinning) regardless of water layer thickness, although v_i' decreases because of the water layer on the substrate.

It is worth mentioning that there are slight fluctuations in some points in the Figure 4.11a, for example, at impact velocities of $v_i = 200, 300$ and 400 m.s^{-1} combined with water layer thicknesses of $L_w = 9, 21$ and 15 Å, respectively. The reason is that the nanoparticle is not a perfect sphere and there are some asperities at the surface of the nanoparticle. Therefore, a slight rotation of the nanoparticle prior to the collision may affect the collision behavior slightly, as indicated by the fluctuations in the diagram. Moreover, the persistent movement of water molecules changes the instantaneous thickness of water layer at each position on top of the substrate. Therefore, the thickness of the water layer where the collision takes place may be slightly higher or lower than the average value of water layer thickness, which can also slightly affect the CoR.

(d) Vibrational thermal dissipation. The vibrational movement of all the atoms inside the system increases because of the collision (*see* Figure 4.12a). As a result, the temperature of the system increases and leads to the thermal dissipation of the impact energy of the nanoparticle. Figure 4.12b shows the temperature profile of the system after the collision as a function of the water layer thickness for different values of impact velocity. The system temperature decreases with the condensed water layer thickness until it saturates. The reason is that, in wet collisions, the nanoparticle gets in contact with the soft surface of the water molecules instead of contacting the hard surface of the substrate. As a result, Figure 4.11a shows that plastic deformation of the particle decreases, which also decreases the vibrational movement of its atoms. Moreover, for high values of impact energy, more energy is transferred to the vibrational movement of atoms in the system, and as a result, the system temperature and the resultant energy dissipation increases with the impact velocity.

4.3.3 Effects of Surface Energy of Substrate on Particle-surface Collision

To this point, the collision of a 5-nm particle on an ideal silver substrate was modelled under dry and wet conditions. The ideal silver substrate is treated as a flat surface without asperity, contamination, or functional group on the surface. In reality, however, a real silver substrate may have asperities, contaminations, or functional groups, which affect its surface energy [53]. The surface energy of the substrate affects the behavior of water near the substrate and the particle-substrate interaction energy. Therefore, surface energy of

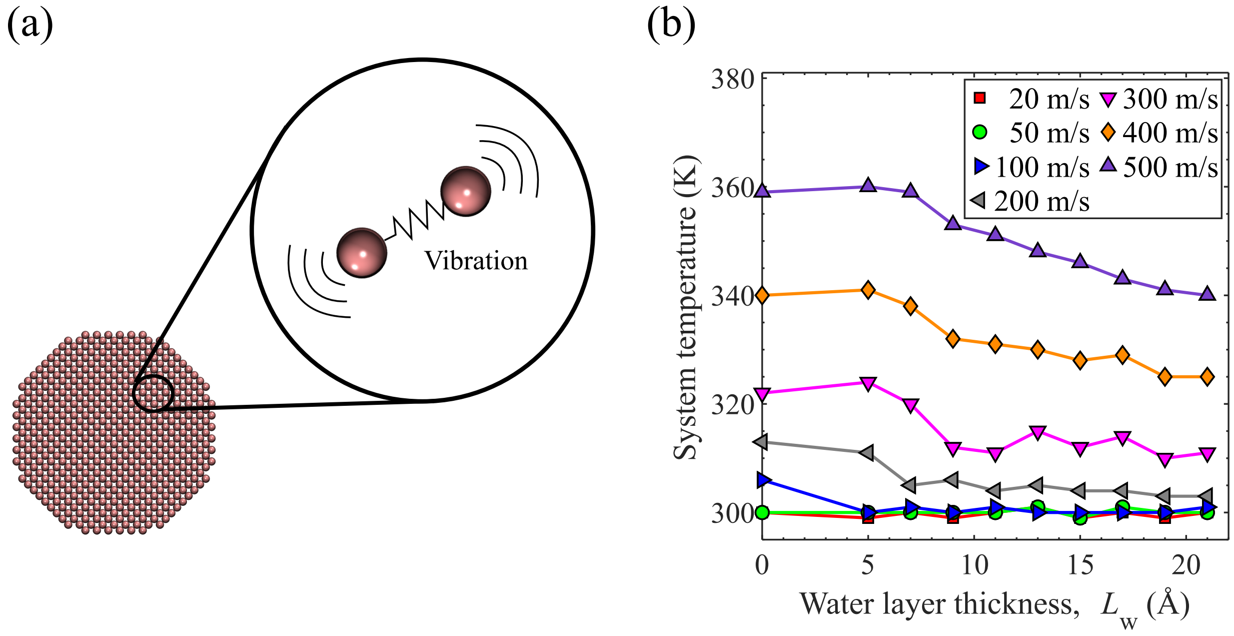

Figure 4.12: (a) Schematic of atomic thermal vibration; (b) Temperature profile of the system after collision of the nanoparticle on a high-energy substrate as a function of water layer thickness for different values of impact velocity.

the substrate is a dominating factor in particle-substrate collision, with or without water layer. It is, therefore, crucial to examine the case in which the substrate is replaced by one with a low surface energy, for example, $\varepsilon_s = 1.2714$ kcal.mol^{-1} (*see* Section 4.2.1).

Coefficient of restitution for low-energy substrate

Figure 4.13 shows the coefficient of restitution of colliding nanoparticles on a low-energy substrate as a function of water layer thickness. Depending on the impact velocity, the coefficient of restitution may increase or decrease with increasing the water layer thickness.

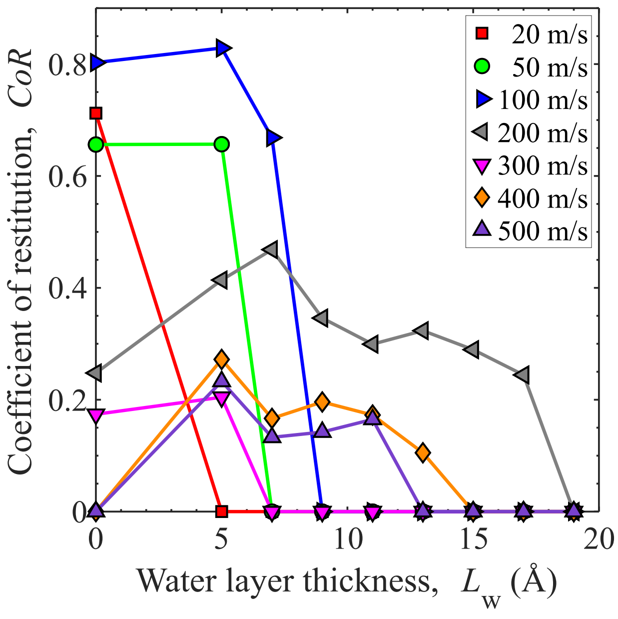

Figure 4.13: Coefficient of restitution of a nanoparticle colliding on a low-energy substrate *versus* water layer thickness, at different impact velocities.

For collisions with an impact velocity $v_i \leq 300$ m.s^{-1}, the particle rebounds from the substrate in dry collisions, as indicated by the non-zero coefficients of restitution, but the particle-surface contact becomes more adhesive in wet condition. For the impact velocity $v_i \geq 400$ m.s^{-1}, however, the particle adheres to the dry substrate. With increasing the water layer thickness on the substrate, the coefficient of restitution first increases then decrease. This result implies that the presence of a water layer on the substrate may reduce the adhesion of the particle to the substrate for high-speed impacts. Similar to results presented for the high-energy substrate, it is necessary to investigate the dependence of the dissipation mechanisms on the water layer thickness on the low-energy substrate to understand the relationship between water layer thickness and the CoR for colliding nanoparticles on a low-energy substrate.

Dissipation mechanisms for low-energy substrate

(a) Particle-substrate interaction energy. Figure 4.14a displays the average potential interaction energy, between the particle and low-energy substrate, as a function of the water layer thickness (L_w). Similar to the particle-substrate interaction for a high-energy substrate, the particle-substrate interaction energy experiences a quick drop at the point of $L_w = 5$ Å, then reaches saturation by continuing to increase the water layer thickness to values higher than 5 Å. For dry collisions, the particle comes into direct contact with the low-energy substrate. Therefore, the interatomic interaction energy between the particle and substrate is applied from a short distance. As shown in Figure 4.14a, for dry collisions, the average particle-substrate interaction energy changes from -0.99 to -17.46 eV, when the impact velocity changes from 20 to 500 m.s^{-1}. The thin water layer near the substrate ($L_w = 5$ Å) considerably weakens the particle-substrate interaction energy. Figure 4.14a shows that when L_w changes from 0 to 5 Å, the magnitude of interaction energy decreases from -0.99 to -0.17 eV for the impact velocity of 20 m.s^{-1}, and from -17.46 to -4.09 eV for the impact velocity of 500 m.s^{-1}. The values for other velocities fall into these two ranges.

Figure 4.14b displays the water density profile *versus* vertical distance z from the substrate. The density distribution shows two major peaks at $z = 2.5$ and 5.5 Å, indicating that similar to the high-energy substrate, the water molecules form a double-layer structure near the substrate. Both peaks are less sharp compared to the high-energy substrate. Although, the substrate is a low-energy one, the double-layer structure is formed in this case but with lower density compared to the high-energy substrate. In fact, the water-substrate interaction energy is still stronger than the water-water interaction energy, leading to the formation of the layered structure near the surface of the substrate. The first layer with density higher than that of bulk water that it behaves like a solid layer at room

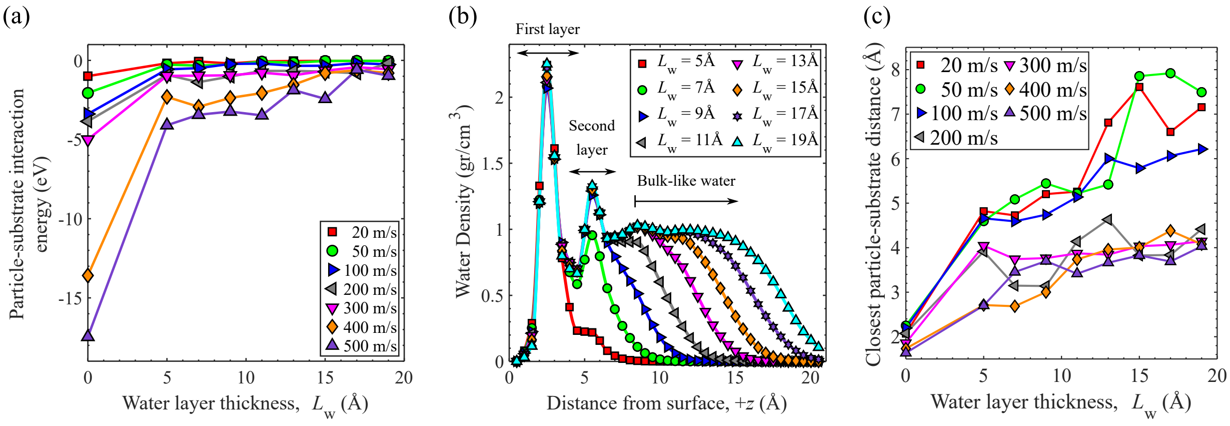

Figure 4.14: The dependence of particle-substrate interaction energy on the water layer thickness. (a) Average particle-substrate interaction energy as a function of the water layer thickness at different impact velocities for the low-energy substrate. (b) Water density profile near the low-energy substrate at different water layer thicknesses. (c) The shortest distance between the particle and the low-energy substrate as a function of the condensed water layer thickness for different impact velocities.

temperature. Independent of the initial thickness of the water layer, the thickness of this dense layer is always around 1.5 Å. This dense layer prevents the particle to get in direct contact with the substrate. Therefore, the interatomic interaction energy between particle and substrate decreases since their interatomic distance increases. Since LJ is a short-range potential interaction, such a slight distance increment is enough to reduce the particle-substrate interaction energy. Therefore, in the presence of a water layer on the substrate, the particle-substrate interaction energy decreases considerably.

Same as the high-energy substrate, the particle-substrate interaction energy is also a function of the impact velocity. By increasing the impact velocity from 20 to 500 m.s^{-1}, the particle-substrate interaction energy increases from -0.99 to -17.46 eV for dry collisions, and from -0.02 to -0.96 eV for wet collisions at $L_w = 19$ Å. The particle-substrate interaction energy for other values of water layer thickness falls into these two ranges. The reason is the same as what discussed in Section 4.3.2.

It is also worth mentioning that the particle-substrate interaction energy for both low- and high-energy substrates differs considerably in dry collisions while they are almost the same in wet collisions (see Figures 4.9a and 4.14a).

(b) Particle-water interaction energy. Figure 4.15 displays the time evolution of the Particle-water interaction energy at different values of water layer thickness and impact velocity. Both the viscose and capillary interaction energies increase by increasing the water layer thickness for all values of impact velocity. Therefore, the particle-water interaction energy and the resultant energy dissipation increases with increasing the water layer thickness.

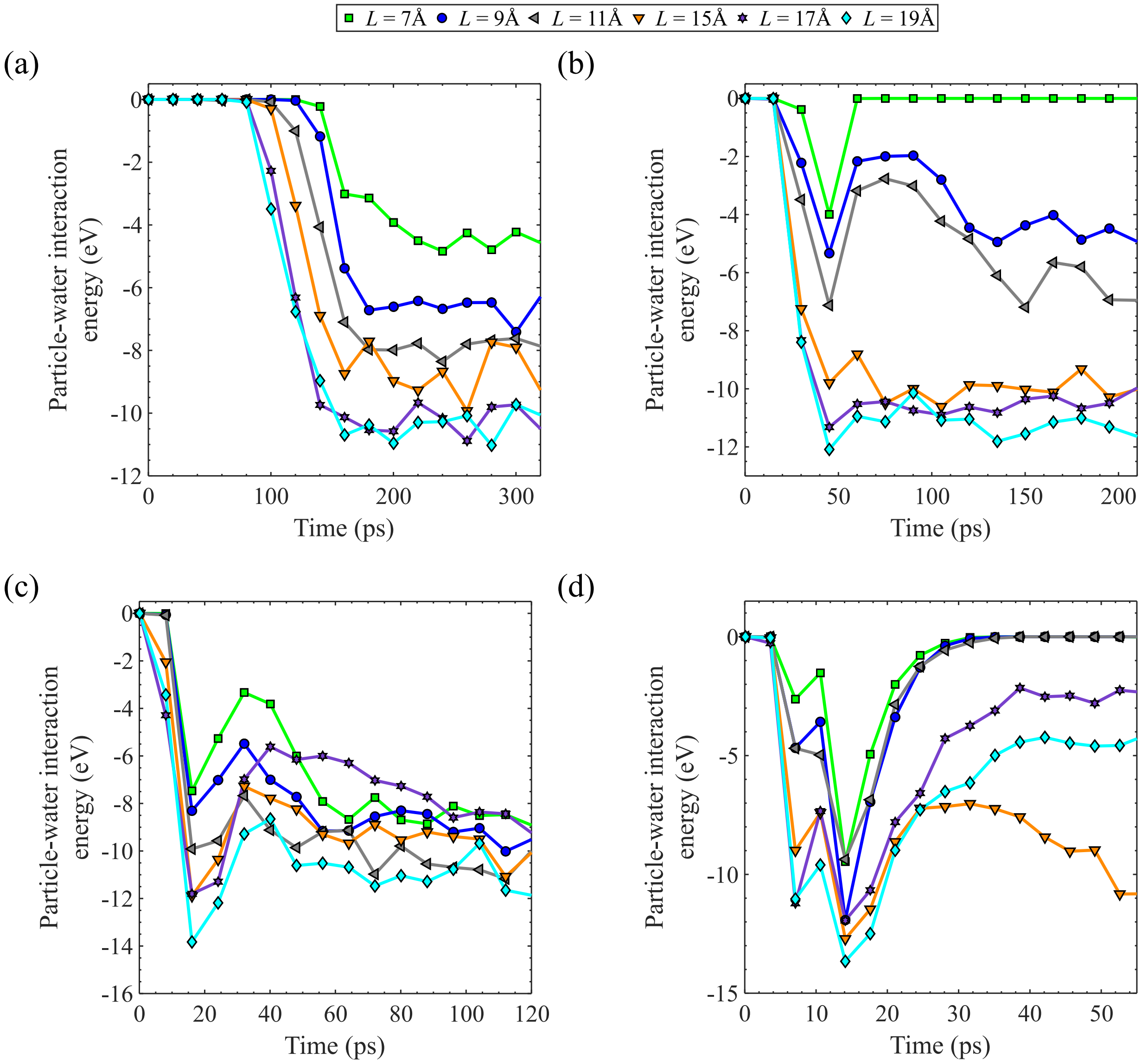

Figure 4.15: Particle-water interaction energy (E_{pw}) at different water layer thicknesses for a low-energy substrate. The impact velocity is (a) $v_i = 20$ m.s^{-1}, (b) $v_i = 100$ m.s^{-1}, (c) $v_i = 300$ m.s^{-1}, and (d) $v_i = 500$ m.s^{-1}. When the collisions result in adhesion, there is a subsequent relaxation of E_{pw} as the nanoparticle begins to equilibrate with the water layer.

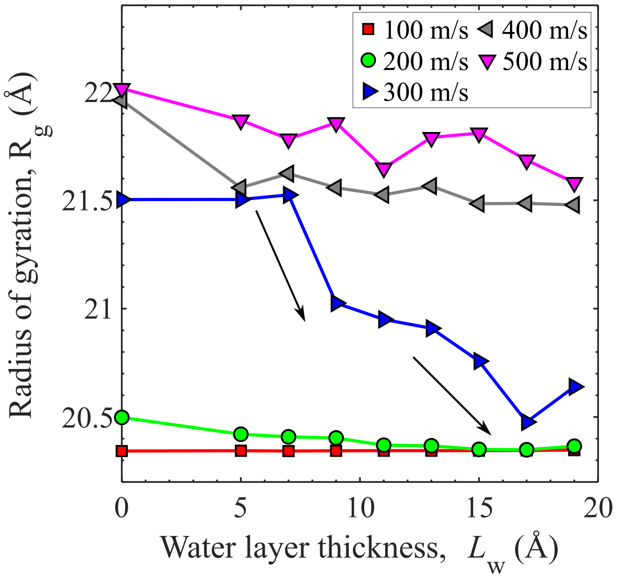

Figure 4.16: Radius of gyration of colliding nanoparticles on the low-energy substrate *versus* water layer thickness at different impact velocities.

(c) Plastic deformation of the nanoparticle. Figure 4.16 shows the radius of gyration (R_g) of colliding nanoparticles on a low-energy substrate *versus* water layer thickness at different impact velocities. Similar to the radius of gyration for a high-energy substrate, two elastic and plastic collision regimes are observed for the studied impact velocities.

For an impact at $v_i \leq 200$ m.s^{-1}, the collision results in elastic deformation for any water layer thickness because the dry collision is in elastic regime. Regardless of the water layer, the plastic deformation and the resultant energy dissipation is negligible. In this elastic collision regime, energy loss mainly arises from contact interaction energies (E_c).

The deformation regime of the nanoparticle changes from elastic to plastic when the impact velocity increases to 300 m.s^{-1}. In this plastic deformation regime, the degree of plastic deformation decreases with increasing the water layer thickness. Similar to the deformation on a high-energy substrate (*see* Figure 4.11b), a dry collision at $v_i = 300$ m.s^{-1} results in twinning deformation. In wet collisions, however, the plastic deformation is determined by v_i', which decreases by increasing the water layer thickness on the substrate. Specifically, the radius of gyration remains almost constant when the water layer thickness is less than 7 Å because v_i' is still higher than the velocity required to enable twinning deformation. However, by increasing L_w from 7 to 9 Å, the radius of gyration drops quickly, because v_i' becomes low enough to change the type of deformation from twinning to slip, with amorphization occurring in some parts of the nanoparticle. Further increasing L_w from 9 to 13 Å, the radius of gyration decreases slightly because the type of deformation remains slip with partial amorphization. On the contrary, when L_w is thicker than 13 Å, the radius of gyration drops quickly, since no amorphization occurs in the nanoparticle and slip deformation occurs where the crystalline structure of the nanoparticle is preserved.

For $v_i \geq 400$ m.s^{-1}, the dependence of the radius of gyration on L_w is exactly the same as the high-energy substrate, where the radius of gyration decreases slightly with L_w. The reason is that, for all the values of studied water layer thickness, the velocity of the particle prior to reaching the substrate (v_i') always remains higher than 295 m.s^{-1} which is higher than the velocity above which the particle experiences twinning deformation.

(d) Vibrational thermal dissipation. Figure 4.17 shows the temperature profile of the system after the collision as a function of the water layer thickness for different values of impact velocity. Like the temperature profile for the high-energy substrate, the system temperature decreases with the condensed water layer thickness until it saturates. Moreover, the system temperature and the resultant energy dissipation increases with the impact velocity.

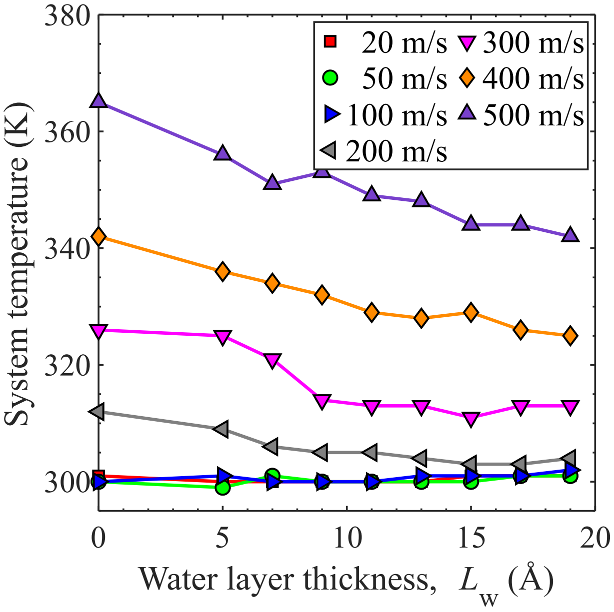

Figure 4.17: Temperature profile of the system after collision of the nanoparticle on a low-energy substrate, as a function of water layer thickness for different values of impact velocity.

4.4 Discussion

For a high-energy substrate, the CoR first increases then decreases with L_w for all values of impact velocity. As shown in Figure 4.8a, the CoR of a nanoparticle colliding on a high-energy substrate first increases, then decreases, with increasing water layer thickness (L_w) on the substrate. As CoR is a representative of the kinetic energy dissipation of the nanoparticle, how CoR changes with the water layer thickness can be explained by the mechanisms of kinetic energy dissipation of the nanoparticle. The collision energy of the nanoparticle dissipates through 1) particle-substrate interaction energy, 2) particle-water interaction energy, 3) plastic deformation, and 4) thermal dissipation. A water layer on the substrate affects all these three mechanisms.

For a dry collision where the nanoparticle comes into direct contact with the high-energy substrate, the energy dissipation through particle-substrate interaction energy is very strong (*see* Figure 4.9a) that it dissipates all the kinetic energy of the colliding nanoparticle and causes its adhesion to the substrate. Therefore, particles with different impact velocities up to 500 m/s colliding on a high-energy surface under dry conditions stick onto the surface ($CoR = 0$) meaning that all the kinetic energy of the particle is lost to dissipation.

For low values of water layer thickness, the particle-substrate interaction energy and the resultant energy dissipation decreases considerably. Depending on impact velocity, energy dissipation through plastic deformation of the nanoparticle and the thermal vibration either decreases or remains unchanged in the presence of a water layer on the substrate (*see* Figure 4.11a and Figure 4.12b). The energy dissipation through plastic deformation decreases slightly for impact velocities higher than 400 m/s. The water molecules on the substrate exert an interaction energy to the particle in wet collisions, which dissipates the initial kinetic energy of the colliding nanoparticle. Although, the particle-water interaction energy is applied to the nanoparticle, the energy dissipation through this mechanism is considerably lower than the reduction in the energy dissipation through particle-substrate interaction energy. Therefore, among four mechanisms of energy dissipation, E_{ps} decreases considerably, plastic deformation and thermal vibration decrease slightly or remain unchanged, and U_{pw} increases slightly. Since the dissipation reduction through the first three mechanisms is more severe than its increment through E_{pw}, the overall energy dissipation decreases and consequently, the coefficient of restitution increases.

Continuing to increase the water layer thickness (L_w) does not further reduce the particle-substrate interaction energy. Therefore, the energy dissipation through this mechanism which has been decreased dramatically at $L_w = 5$ Å saturates for higher values of L_w. Plastic deformation of the particle also remains unchanged for $v_i \leq 200$ m/s, it decreases for the case of $v_i = 300$ m/s, and it saturates for higher values of impact velocity. However, according to Figure 4.10, the particle-water interaction energy increases continuously with the water layer thickness. Since the energy dissipation through two other mechanisms are almost saturated, and it increases continuously through particle-water interaction energy, the total energy dissipation increases continuously with L_w. This goes on until the total energy dissipation exceeds the collision energy, and as a result, the particle adheres to the substrate again.

The effects of condensed water layer on the CoR for colliding nanoparticles depends on the surface energy of the substrate. For the high-energy substrate, CoR first increases then decreases with L_w for all the impact velocities. However, for the low-energy substrate, how the CoR changes with L_w depends on the impact velocity. For impact velocities lower than 300 ms^{-1}, the CoR decreases with L_w. On the other hand, for higher values of impact velocity, the CoR first increases, then decreases with L_w.

Surface energy of the substrate affects the CoR of a colliding nanoparticle by affecting the particle-substrate interaction energy. According to Figure 4.9 and Figure 4.14, the particle-substrate interaction energy for high-energy substrate is much higher than that for the low-energy one in dry collisions. However, the particle-substrate interaction energy for both surfaces almost equals in wet collisions.

First, the results for dry collisions are discussed. According to Figure 4.13, in dry collisions, the particle rebounds when $v_i \leq 300$ m.s^{-1}, and it adheres to the substrate for impact velocities of $v_i = 400$ m.s^{-1} and 500 m.s^{-1}. According to Figure 4.16, the dry collision is mainly elastic for low-speed impacts at $v_i \leq 200$ m.s^{-1}, while, for higher values of impact velocity, the impact energy of the nanoparticle is high enough to make permanent structural changes in the nanoparticle. As a result, the degree of plastic deformation and the resultant energy dissipation of the colliding nanoparticle increases with the impact velocity. Moreover, the nanoparticle gets more squeezed at the deepest contact point as the impact velocity increases. Therefore, the contact area between the particle and the dry substrate increases, which increases the particle-substrate interaction energy. Therefore, as shown in Figure 4.14a, the average particle-substrate interaction energy increases from -0.99 to -17.46 eV when the impact velocity increases from 20 to 500 m.s^{-1} in dry collisions. The thermal energy dissipation also increases with the impact velocity (*see* Figure 4.12b). As a result, the total energy dissipation through mechanisms of plastic deformation, particle-substrate interaction energy, and thermal vibrations increases by increasing the impact velocity. Increasing the energy dissipation results in adhesion of the nanoparticle to the dry substrate for high- speed impacts at $v_i \geq 400$ m.s^{-1}. Since, for a low-energy substrate, the dry collision results in two distinct regimes of rebound ($v_i \leq 300$ m.s^{-1}) and adhesion ($v_i \geq 400$ m.s^{-1}), each regime should be discussed separately at the presence of a water layer on the substrate.

For impact velocities in the range of $v_i \leq 300$ m.s^{-1}, by increasing the water layer thickness from 0 to 5 Å, the particle-substrate interaction energy decreases from -0.99 to -0.17 eV and from -4.99 to -0.97 eV for impact velocities of 20 m.s^{-1} and 300 m.s^{-1}, respectively. The value for other impact velocities falls into these two ranges. The particle-substrate interaction energy becomes saturated for water layer thicknesses beyond $L_w = 5$ Å. Therefore, energy dissipation through particle-substrate interaction energy decreases while L_w changes from 0 to 5 Å, and it saturates for higher values of water layer thickness. Similarly, the energy dissipation through plastic deformation of the particle and thermal vibration; it either remains unchanged or decreases first then saturates with increasing the water layer thickness. However, for wet collisions, the water molecules on the substrate also apply an additional interaction energy to the nanoparticle during the loading stage (viscous interaction energy) and unloading stage (capillary interaction energy). Since the substrate is a low-energy one, the reduction in the particle-substrate interaction energy in wet collisions is much lower compared to a high-energy substrate. Therefore, when a water layer with the thickness of $L_w = 5$ Å is formed on the substrate, although the energy dissipation through the first three mechanisms decreases, the energy dissipation through the particle-water interaction energy compensates for its reduction. Therefore, according to Figure 4.13, for low values of L_w, particle adhesion to the substrate remains constant (or increases slightly for $v_i = 200$ m.s^{-1}). However, as the water layer thickness increases, the particle-water interaction energy increases continuously. Therefore, the energy dissipation increases through this mechanism continuously and the coefficient of restitution decreases until the CoR drops to zero which indicates the adhesion of the nanoparticle to the substrate.

For high-impact velocities at $v_i = 400$ m.s^{-1} and 500 m.s^{-1}, the presence of a 5 Å thick water layer on the substrate decreases the average particle-substrate interaction energy from -13.58 to -2.30 eV and from -17.46 to -4.09 eV, respectively. The particle-substrate interaction energy almost saturates for higher values of L_w. According to Figure 4.14a and Figure 4.15, by changing L_w from 0 to 5 Å, the reduction in the particle-substrate interaction energy is much higher than the particle-water interaction energy. Besides, for this velocity range, plastic deformation of the nanoparticle and the thermal energy dissipation also decrease in wet collisions. As a result, for low values of water layer thickness around $L_w = 5$ Å, the overall energy dissipation decreases, which increases the CoR of the colliding nanoparticle. By increasing L_w, the particle-substrate interaction energy, the plastic deformation, and the thermal dissipation saturate, while the particle-water interaction energy increases continuously. Therefore, the total energy dissipation of the nanoparticle increases, which decreases the CoR until the nanoparticle adheres to the substrate again.

Finally, it could be concluded that the effects of air humidity on the adhesion of nanoparticles on a substrate depends on the substrate material. The nanoparticle adhesion to a high-energy substrate decreases under wet conditions. However, for a low-energy substrate, the effects of humidity on the nanoparticle adhesion on the substrate depends on the impact velocity. The adhesion of nanoparticle to a low-energy substrate increases with humidity for low-speed impacts, and it decreases for high-speed impacts. Because the movement velocity of nanoparticles in an airstream falls into a velocity range determined by the Maxwell-Boltzmann distribution, the overall effect of humidity on the nanoparticle-surface adhesion is determined over the velocity range of the nanoparticles colliding on the surface. If the adhesion reduction for high-speed impact dominates the adhesion increment for low-speed impact, the overall particle-surface adhesion decreases, and *vice versa*. That's why the nanoparticle-surface adhesion increases, decreases, or remains unaffected as a result of air humidity in experimental studies [59, 29].

4.5 Summary

In summary, our MD simulations show that, depending on the ambient conditions and surface properties of the substrate, condensed water layer can either increase or decrease the nanoparticle adhesion on the substrate. It was shown that the coefficient of restitution of 5-nm particles on a wet substrate depends on the thickness of the condensed water layer on the substrate, surface energy of the substrate, and impact velocity. Depending on the surface energy of the substrate and impact velocity, the coefficient of restitution for nanoparticles colliding on a substrate either increases or decreases with increasing the thickness of the condensed water layer on the substrate. For a high-energy substrate, the coefficient of restitution of the colliding nanoparticles first increases, then decreases by increasing the water layer thickness on the substrate. This kind of behavior was observed for the whole range of studied velocity $v_i \in [20-500]$ m.s^{-1}. However, for a low-energy substrate, the effects of condensed water layer thickness on the coefficient of restitution depend on the impact velocity. The nanoparticle rebounds from a low-energy and dry substrate for impact velocities lower than 300 m.s^{-1}. The coefficient of restitution decreases by increasing the thickness of the condensed water layer until the nanoparticle adheres to the substrate. The water layer thickness at which the nanoparticle adheres to the low-energy substrate depends on the impact velocity. For higher impact velocities, the nanoparticle adheres to the low-energy dry substrate. The coefficient of restitution first increases with the condensed water layer thickness, then decreases until the nanoparticle adheres to the substrate again. The change of the coefficient of restitution with respect to water layer thickness for both high- and low-energy substrates was explained by three mechanisms of translational kinetic energy dissipation of the colliding nanoparticles: particle-substrate interaction energy, particle-water interaction energy, and plastic deformation of the nanoparticle. The particle-substrate interaction energy decreases on a wet substrate because of the formation of a dense water layer near the substrate: the water layer acts as a buffer separating the nanoparticle from the substrate. The particle-water interaction energy continuously increases with increasing water layer thickness on the substrate. Plastic deformation of the nanoparticle also decreases or remains unaffected in wet conditions.

Chapter 5

Coefficient of restitution for sub-10 nm silver particles colliding on adhesive silver surfaces

This chapter presents a molecular dynamics (MD) study on the collisional dynamics of sub-10 nm silver (Ag) particles on a silver surface. The effects of adhesivity of particles to a surface on the nanoparticle-surface collisional dynamics are also investigated by changing the degree of particle-surface adhesion strength. Results show that particles accelerate because of the attraction force applied by the adhesive surface when the particles enter the interaction range of the surface. As a result, the particle velocity increases from its initial value to a higher impact velocity. However, the acceleration changes inversely with the particle size. A particle smaller than 2 nm in diameter accelerates and results in an impact velocity higher than its yield velocity even when the initial particle velocity is much lower than the yield velocity. During the collision, part of the total energy contributes to the plastic deformation of the sub-2nm particles, reducing the coefficient of restitution (CoR). For a particle larger than 2 nm in diameter, however, the impact velocity remains lower than the yield velocity when the initial velocities are lower than its yield velocity, resulting in elastic collision. Furthermore, this size dependent behavior of CoR intensifies with increasing adhesivity of the collision and becomes less significant for lower adhesivity. This work indicates that a sub-2 nm particle with a velocity lower than the yield velocity can collide the surface in its plastic deformation regime and adhere to the surface.

5.1 Problem Statement

The coefficient of restitution (CoR) for macroscale collisions is often considered constant, and it is determined using the bulk properties of the particle and the surface. However, nanoscale CoR depends on impact velocity, particle size, and the degree of adhesion between the nanosized solid objects [84]. The impact velocity can affect the CoR of nanoparticles by changing the deformation regime. Elastic or plastic deformation occurs at a low or high impact velocity, respectively. The yield velocity (v_Y), defined as a critical velocity above which the particle undergoes plastic deformation, separates these two regimes of deformation. As one of the kinetic energy loss mechanisms, plastic deformation reduces the CoR (*see* Eq. 2.1). This suggests that CoR rapidly decreases when the impact velocity exceeds the yield velocity [25].

The yield velocity also indicates the strength of a nanoparticle, and it increases with decreasing nanoparticle size [63]. The yield velocity for the nanoparticles is size-dependent and its value is much higher than that for macroscopic particles [85], although the yield velocity for a macroscopic collision mainly depends on the material of the colliding particle. A small nanoparticle may withstand a large impact velocity before yielding.

Adhesive force is another factor that affects the CoR for a nanoparticle collision because of the large surface area to volume ratio of nanoparticles. Adhesive force primarily depends on the contact area and surface energy of the contacting objects, where the contact area may increase with increasing impact velocity by flattening the nanoparticles [86, 26].

In addition, the adhesion force affects the impact velocity of the colliding nanoparticle [26]. An attraction force is applied to the particle when it enters the van der Waals (vdW) interaction range of the surface [38]. The attractive force increases the impact velocity while the nanoparticle is approaching the surface [26]. This increase in velocity affects the CoR by changing the energy loss due to plastic deformation of the colliding nanoparticle. Additionally, this increase in impact velocity also increases the contact area between the colliding objects because the colliding particle undergoes a plastic deformation.

There is limited information on the dependence of CoR on impact velocity, nanoparticle size, and adhesion force for nanoparticle collisions, especially for those involving sub-10 nm particles. Jung *et al.* [26] reported that the particle-surface adhesion force increased the impact velocities of sub-10 nm particles, depending on the particle size and the surface energy of the colliding objects. Nonetheless, the effects of the velocity increase on the CoR of nanoparticle collisions deserve further investigation.

Thus, the objective of this study is to understand the effects of particle-surface adhesion force on the CoR of adhesive collisions of sub-10 nm particles on surfaces with different surface energies. We first study the CoR of a repulsive collision of silver nanoparticles on a silver surface to determine the yield velocity as a function of particle diameter (1 to 10 nm). Then, we study the effects of particle-surface adhesion force on the CoR for adhesive collisions. The adhesivity of the collision is changed by changing the attraction part of the Lennard-Jones potential between the particle and surface.

The rest of this paper is organized as follows. Section 5.2 introduces the MD simulation for nanoparticle collisions. Section 5.3 presents the results and discussion; Section 5.3.1 reports the yield velocities of sub-10 nm particles for purely repulsive collisions, and Section 5.3.2 reports the CoR for adhesive collisions. Finally, Section 5.4 presents the conclusions.

5.2 Model Description

Figure 5.1 shows the imaginary box for MD simulation, which is 123 Å in x and y directions and 204 Å in z direction. The simulation box contains 45116 to 80558 atoms, depending on the diameter of the nanoparticle inside the box. Silver is chosen as the material of both particle and substrate. Both the particle and the substrate are cut out of a *face centered cubic* grid. The particle radius, R, changes from 8 Å to 38 Å, and the size of the substrate is 121 Å in x and y directions and 50 Å in z direction. This size of substrate is large enough because further increase in the substrate size does not change the accuracy of results but increase cost of calculation.

The potential energy, U_i, of the ith silver atom in the substrate or particle is modeled using an embedded atom method (EAM) potential (*see* Eq. 4.1). The potential parameters developed by Foiles *et al.* [72] are used for our modeling of silver atoms because these parameters are validated and can represent the physical properties of the atoms.

The modified version of Lennard-Jones (LJ) potential is used to calculate the van der Waals (vdW) interaction energy between the particle atoms and the substrate atoms:

$$U_i^{LJ} = 4\varepsilon \left[\left(\frac{\sigma}{r_{ij}} \right)^{12} - C \left(\frac{\sigma}{r_{ij}} \right)^{6} \right] \tag{5.1}$$

where $\varepsilon = 7.9466$ kcal/mol, and $\sigma = 2.644$ Å. The coefficient C is a coefficient applied to the attractive part of the potential to reduce the attraction strength between particle and surface atoms. Figure 5.2 shows the interatomic Lennard-Jones potential for nonbonding Ag-Ag interaction for different C values.

The force acting on the ith atom in the particle is calculated by differentiation of the LJ potential (U_i^{LJ}) of that atom:

$$F = -\nabla U_i^{LJ}\left(r_{ij}\right) \tag{5.2}$$

According to Eq. 5.2, the negative and positive slopes of the potential curves in Figure 5.2 indicate repulsive and attractive forces, respectively.

This work is focused on purely repulsive and adhesive collisions. The purely repulsive collision is modeled with $C = 1$, and the potential is truncated at the cutoff distance of

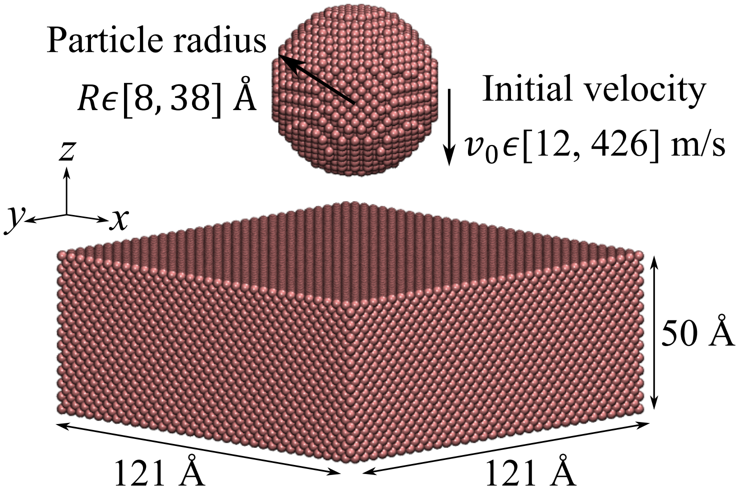

Figure 5.1: Simulation geometry for collision of a silver nanoparticle on a silver substrate.

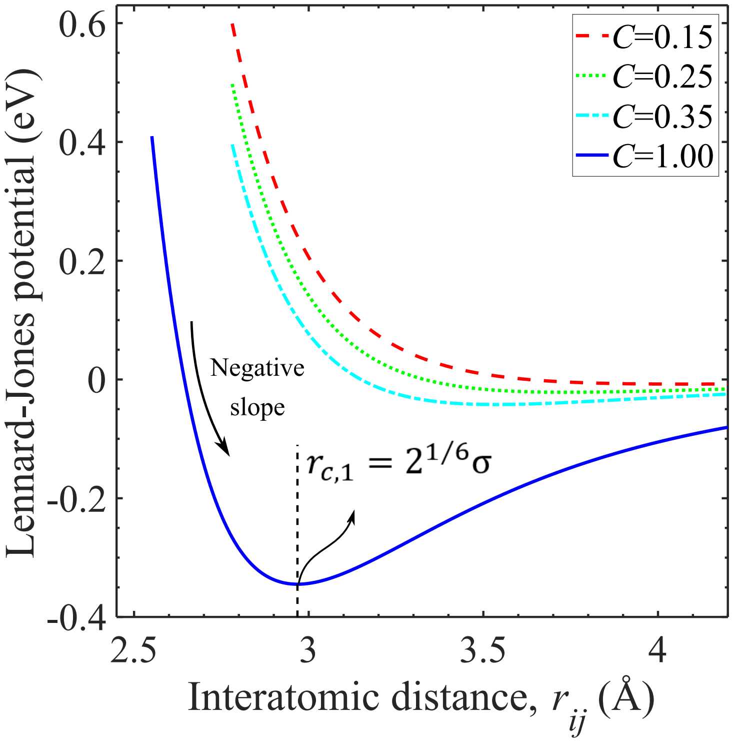

Figure 5.2: Interatomic potentials for van der Waals silver-silver interactions with different values of scaling factor C=0.15, 0.25, 0.35, and 1.

$r_{c,1} = 2^{1/6}\sigma \approx 2.967$ Å, the interatomic distance below which the slope of the curve with $C = 1$ is always negative [25]. Figure 5.2 shows that the slope of the curve for $C = 1$ is negative at $r_{ij} < r_{c,1}$, indicating only repulsive collisions between particle and surface (*see* Eq. 5.2). In comparison, an adhesive collision is modeled with a coefficient of $C < 1$, and the potential is truncated at a large cutoff distance of 6σ or 16 Å. The cutoff distance of 16 Å covers both the negative slope (repulsive interaction) and positive (attractive interaction) slope of the potential curves shown in Figure 5.2. Considering both repulsive and attractive interactions between the particle and the surface makes the contact between them sticky. The stickiness of the collision between the particle and the surface is controlled by reducing the attractive term $(\sigma/r_{ij})^6$ in Eq. 5.1 between particle and surface atoms by the coefficient C, which varies between 0.15 to 0.35 [87]. The curves with $C = 0.15, 0.25$, and 0.35 in Figure 5.2 are for the weakly adhesive, adhesive, and highly adhesive collisions, respectively. The graph of these potentials contains both negative and positive slopes for small and large values of interatomic distance (r_{ij}), respectively. The minimum point of the LJ potential shown in Figure 5.2, which separates the region with repulsion (negative slope) from the region with attraction (positive slope), is further increased (*see* Table 5.1). Therefore, with smaller value of C, not only the attraction force is weakened, but the domain of attraction where the NP is accelerated is further reduced, while the region of repulsion where the NP is being decelerated has expanded.

Table 5.1: The minimum point of the LJ potential for different values of C.

C	$r_{LJ,min}$
0.35	3.535
0.25	3.738
0.15	4.071

All MD simulations are performed using a MD code developed in the LAMMPS package [83]. Before starting, the nanoparticle is placed outside the LJ interaction range of the surface. All simulations start with a Maxwell-Boltzmann velocity distribution for all silver atoms at room temperature, 300 K. As a best practice in MD simulation, the system is initially equilibrated at 300 K using a canonical ensemble for 80 ps followed by simulation under a microcanonical ensemble for another 20 ps to ensure that the system reaches a stable thermal equilibrium state.

An initial velocity, v_0, in the range of 12 to 426 m/s, which covers both elastic and plastic regimes, is applied in the z direction to the center-of-mass of the equilibrated nanoparticle.

During a collision, two atomic layers at the bottom of the substrate remain fixed, and Langevin dynamics [62] is applied to the next eight layers. Newtonian dynamics is applied to the rest of the system. The block of Langevin atoms absorbs the energy from the collision and controls the temperature of other atoms in the simulation box that are governed by Newtonian dynamics [38]. The equations of motion for both Newtonian and Langevin atoms integrated with a velocity Verlet scheme with a time step of 1 fs. The time step of 1 fs is small enough to make sure that the displacement of atoms is sufficiently small in each step. Additionally, the simulations for some cases have been performed for the smaller timestep of 0.5 fs. No considerable difference was observed between the results for the small (0.5 fs) and large (1fs) time steps. Finally, the system is averaged over up to twelve independent runs by varying the initial thermal conditions to improve statistical accuracy. We increased the number of simulations until the randomness effects of the random seed number in the simulations disappear.

5.3 Results and Discussion

5.3.1 CoR and Yield Velocity for Purely Repulsive collisions

Figure 5.3a shows the simulated CoR of purely repulsive collisions using $C = 1$. The CoR of nanoparticles are obtained by varying the initial particle velocity from 12 m/s to 426 m/s for each particle radius, R, which ranges from 8 Å to 38 Å. For a purely repulsive collision, the energy loss is only due to plastic deformation. Without attraction force between colliding particles and surface, the impact velocity for a non-adhesive collision is equal to the initial particle velocity ($v_i = v_0$). For the initial particle velocities less than 36 m/s, the CoR for particles with radius smaller than 10 Å exceeds unity. This indicates that the particles gain translational kinetic energy from internal energy [88, 89], the reason behind if is that the thermal fluctuations of the particle atoms are transferred to the translational kinetic energy of the rebounding nanoparticles. In addition, the CoR scatters for small initial particle velocity up to 200 m/s. This is because nanoparticles are not perfect spheres due to their crystalline structure. Therefore, a slight rotation of the crystalline particle with respect to the surface affects the CoR of the collision [42].

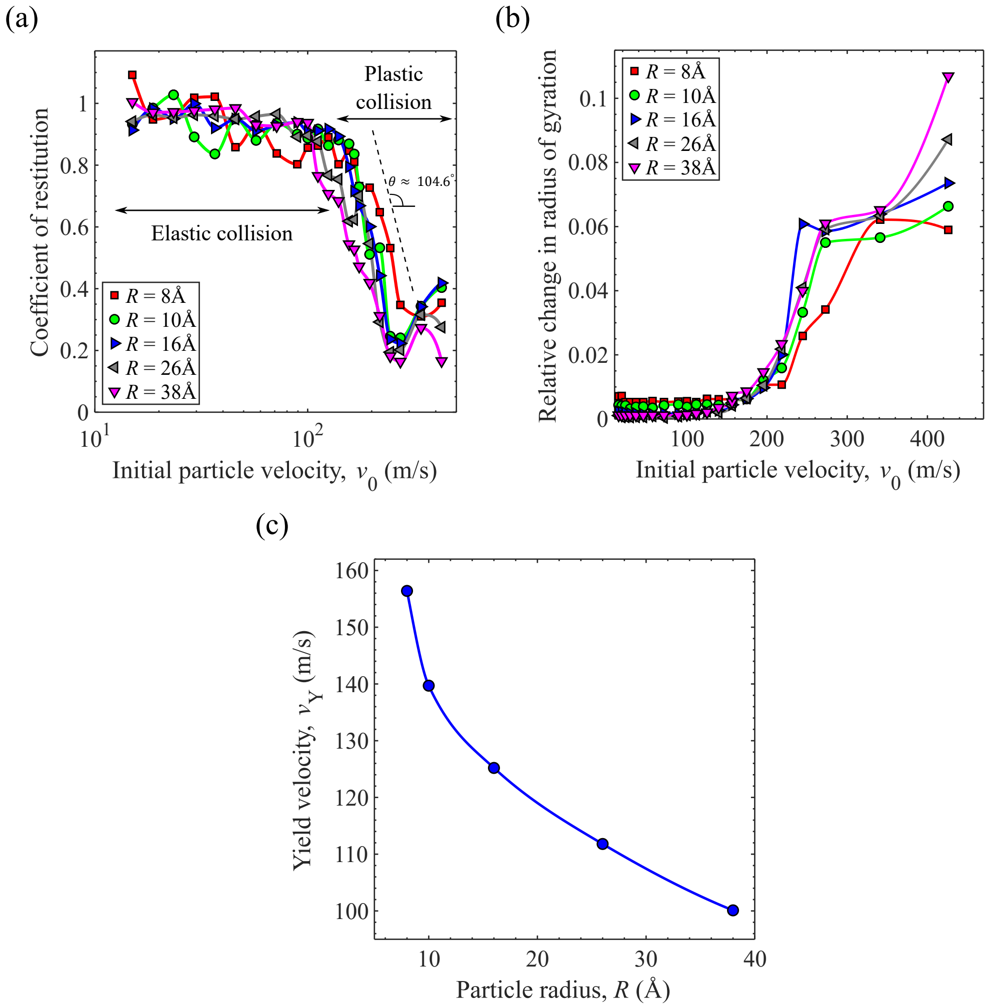

Figure 5.3: (a) CoR *vs.* initial particle velocity (v_0) for purely repulsive collisions; the onset of plastic deformation (yield) occurs at the critical velocity where the CoR drops roughly after the viscoelastic regime. (b) Relative change in radius of gyration *vs.* initial particle velocity. (c) Yield velocity *vs.* particle radius.

Quasi-elastic collisions are observed for small initial particle velocities, which is similar to those reported in previous studies [25, 63]. In a quasi-elastic regime, the CoR is close to, but less than, unity. When the nanoparticle gently collides on the surface, elastic energy is initially stored during the collision stage followed by its release during rebounding. After the gentle elastic collision, the nanoparticle returns to its original shape (*see* Figure 5.4a), and the net energy remains constant in the colliding-rebounding stage of the collision. Thus, the CoR remains close to unity. As the initial particle velocity increases from 12 m/s to its yield velocity, v_Y, the CoR remains close to unity, then the CoR drops roughly in the initial particle velocity. The critical velocity where the CoR drops is yield velocity, where the collision is changed from elastic regime to plastic regime. Therefore, above this critical velocity, the particle undergoes plastic deformation and permanent deformation is observed after collision (see Figure 5.4b). Figure 5.3c shows the yield velocity *vs.* particle size. As the particle size increases, the yield velocity increases, which indicates the particle experiences plastic deformation at lower impact velocities; this result indicates that larger particles deform more easily.

The CoR decreases for initial particle velocity (v_0) ranging from v_Y to about 272 m/s but increases for initial particle velocities higher than 272 m/s. This is expected because the rate of increase in plastic deformation drops when $v_0 > 272$ m/s. The degree of deformation can be characterized by evaluating the relative change in radius of gyration of the nanoparticle, $\Delta R_g/R_g$, which is plotted in Figure 5.3b. For a low-speed impact below the yield velocity, $\Delta R_g/R_g$ remains near zero, indicating that the collision is in a viscoelastic regime (*see* Figure 5.5a and 5.5b). The relative deformation quadratically increases as the initial particle velocity is above the yield velocity (*see* Figure 5.5c and 5.5d) until it slows down for $v_0 > 272$ m/s, a velocity at which the deformation changes to twinning regimes. Figures 5.5e and 5.5f show that, in the twinning deformation regime, the particle deforms like a pancake with a distorted structure. Therefore, when the particle velocity increases to 272 m/s or higher, the increase rate of energy loss due to plastic

(a) $v_0 = 111$ m/s

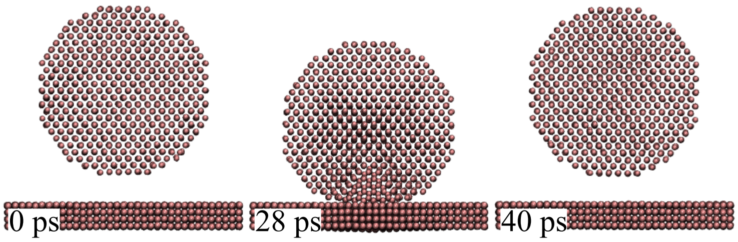

(b) $v_0 = 272$ m/s

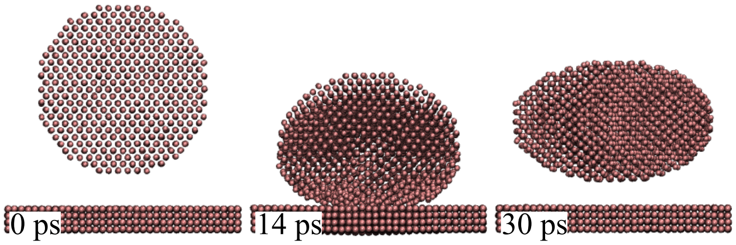

Figure 5.4: Structural change of nanoparticle ($R = 26$ Å) over time with initial particle velocities of (a) $v_0 = 111$ m/s, elastic collision and (b) $v_0 = 272$ m/s, with plastic deformation.

deformation slows down while the collision energy grows continuously. This results in a slight increase in the CoR for initial velocities higher than 272 m/s.

5.3.2 CoR of Adhesive Collisions

Figure 5.6 shows the CoR of adhesive collisions for different particle sizes and different initial particle velocities. The coefficient for adhesion strength C is 0.25 to reduce the stickiness of the collision. Figure 5.6 shows that the CoR of adhesive collisions for particles with radii ranging from 16 Å to 38 Å have the same trend as the CoR of purely repulsive collisions for particles with the same size (*see* Figure 5.3a). However, for low-speed impacts at $v_0 < 220$ m/s, the CoR of small particles with radii of 8 and 10 Å are smaller than those

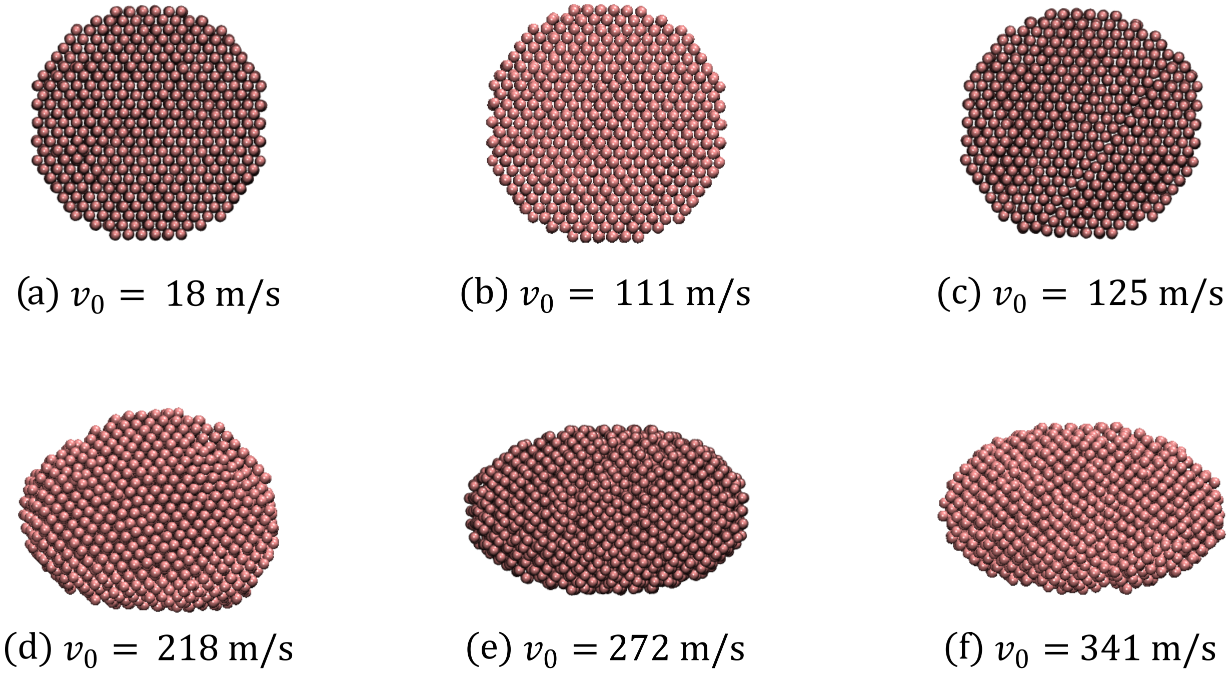

(a) $v_0 = 18$ m/s (b) $v_0 = 111$ m/s (c) $v_0 = 125$ m/s

(d) $v_0 = 218$ m/s (e) $v_0 = 272$ m/s (f) $v_0 = 341$ m/s

Figure 5.5: Deformation of nanoparticle with radius of 26 Å and initial particle velocities of (a) 18 m/s, (b) 111 m/s, (c) 125 m/s, (d) 218 m/s, (e) 272 m/s, and (e) 341 m/s. The yield velocity is 111.8 m/s for this particle size.

of larger particles.

For particles with radii ranging from 16 Å to 38 Å, the CoR is close to 0.8 for $v_0 < 220$, indicating a viscoelastic collision regime. In the case of adhesive collisions, the CoR in the viscoelastic regime for particles with radii from 16 Å to 38 Å is slightly less than the CoR for purely repulsive collisions (*see* Figure 5.3a) in the same particle size range. The reason is that the adhesion force is additionally applied to the particle accelerating the particle to a higher impact velocity causing some form of plastic deformation which dissipates its kinetic energy. As the initial particle velocity increases from 12 m/s to v_Y, the CoR

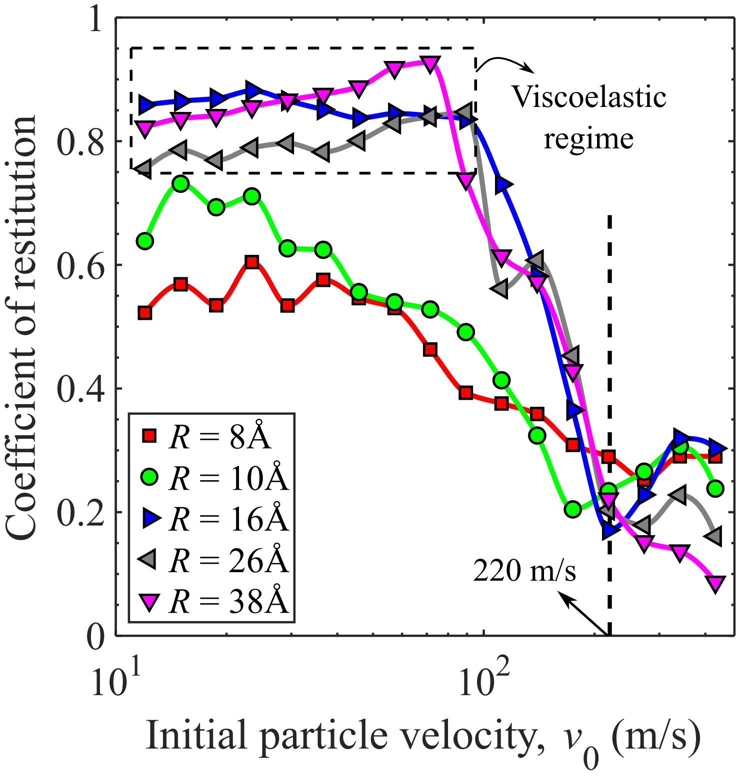

Figure 5.6: Coefficient of restitution *vs.* initial particle velocity v_0 for adhesive collisions with $C = 0.25$.

remains constant and then drops roughly with increasing the initial particle velocity. Like the CoR for purely repulsive collisions shown in Figure 5.3a, the velocity where the CoR drops indicates the onset of plastic deformation.

The CoR for particles with radii of 8 Å and 10 Å (red and green dots in Figure 5.6) is lower than those of larger particles for an initial velocity less than 220 m/s. Figure 5.6 also indicates that the viscoelastic regime for initial particle velocities of $v_0 < v_Y$, in which the CoR remains around 0.8 is no longer observed for small particles with radii of 8 Å and 10 Å.

Figure 5.7a shows the schematic of the particle velocity increase after entering the LJ interaction range of the surface. It is widely accepted that, in the case of adhesive collision, an attraction force along z axis is applied to the particle when it enters the LJ interaction range of the surface [26]. Figure 5.8 shows the evolution of the particle velocity over time for initial velocities of 89 m/s and 111 m/s, which results in rebound and adhesion, respectively. The attraction force increases the particle velocity from its initial value of v_0 to impact velocity, v_i, while the nanoparticle is approaching the surface. As a result, the impact velocity, v_i, is always higher than the initial particle velocity, v_0, for adhesive collisions. Due to the short-range of LJ interaction (*see* Eq. 5.1), a cutoff distance of 16 Å is considered for the LJ interaction; the attraction between two silver atoms disappears if the distance between two atoms is longer than the cutoff distance.

Figure 5.7b shows the total force applied to the unit mass of the nanoparticle (F/m) multiplied by the time of the collision (Δt) as a function of initial velocity. According to Newton's Second Law, the total force applied to the unit mass of the nanoparticle (F/m) multiplied by the time of the collision (Δt) is equal to change in the particle velocity from v_0 to v_i ($\frac{F}{m}.\Delta t = \Delta v$). Accordingly, Figure 5.7b shows that the value of Δv increases with decreasing particle radius R and initial particle velocity v_0, the reason behind which could be justified by the Newton's Second Law.

According to Newton's Second Law, the particle acceleration is the ratio of the particle-surface attraction force to the particle mass. The particle-surface attraction force (F) is proportional to the volume of the nanoparticle that is attracted by the surface, $F \propto V_a$, and the particle mass is proportional to the total volume of the nanoparticle, $m \propto V_t$. The ratio of the volume of the nanoparticle that is attracted by the surface to the total volume of the particle (V_a/V_t) is,

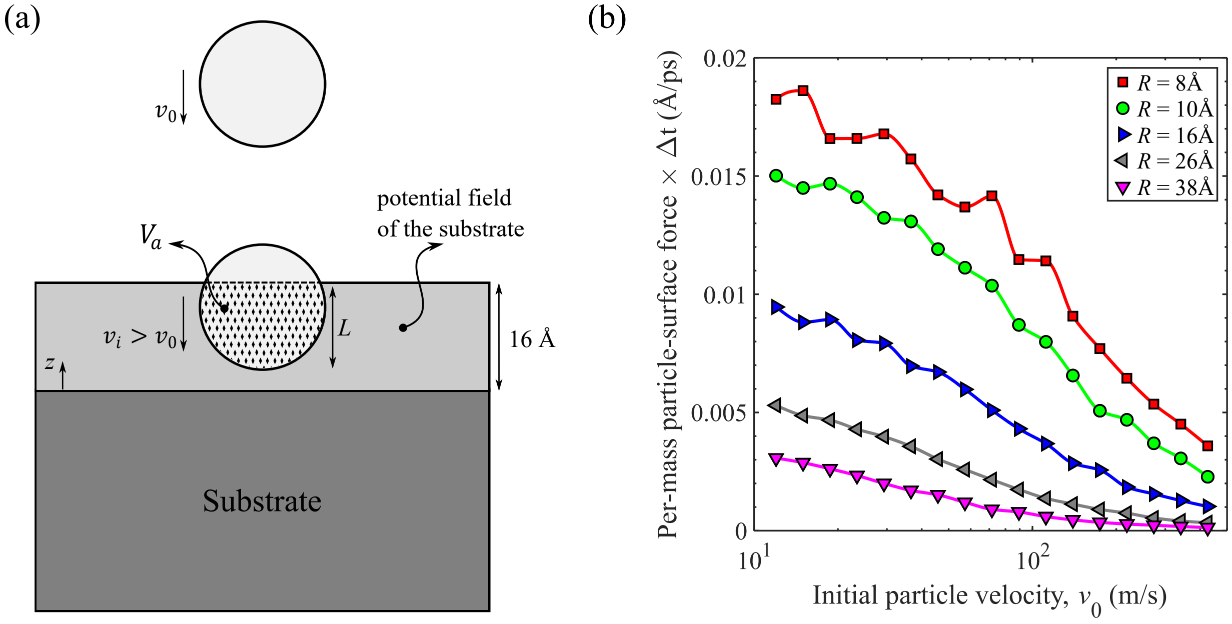

Figure 5.7: (a) Schematic of LJ interaction range of the surface and velocity increase of the particle. (b) Per unit mass particle-surface interaction as a function of initial particle velocity v_0.

$$a = \frac{F}{m} = \frac{V_a}{V_t} = \frac{3RL^2 - L^3}{4R^3} \tag{5.3}$$

where L is the penetration depth to the LJ interaction range of the surface and R is the particle size. Equation 5.3 can be integrated over the interaction range of the LJ potential:

$$a = \frac{1}{4R^3} \int_0^{16} \left(3RL^2 - L^3\right) dL = 1024 \left(\frac{R-4}{R^3}\right) \tag{5.4}$$

Figure 5.9 shows the average particle acceleration as a function of particle radius (R)

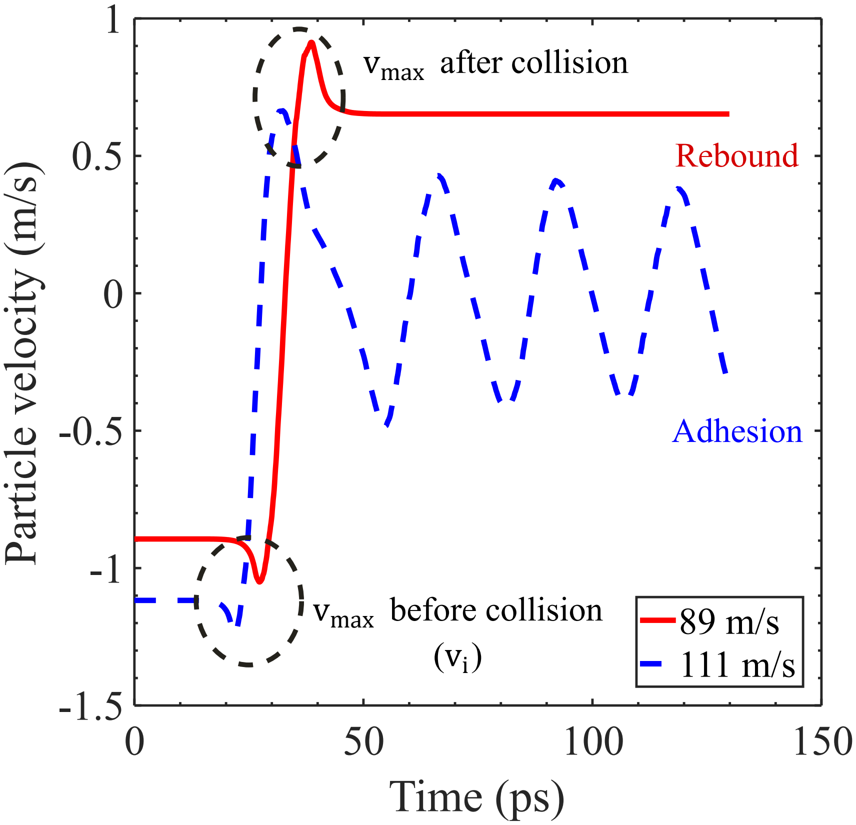

Figure 5.8: Evolution of the particle velocity over time for initial velocities of 89 m/s and 111 m/s.

calculated based on Equation 5.4. Figure 5.9 indicates that the attraction force applied to the unit mass of the particle, which is equal to the particle acceleration, increases with decreasing particle size. Therefore, as shown in Figure 5.7b, the increase in the initial velocity from v_0 to v_i increases with decreasing the particle size.

Equation 5.3 also shows that the particle acceleration is a function of the particle radius (R) and is independent of particle initial velocity (v_0). Therefore, the acceleration of particles with the same size remains constant as the initial velocity (v_0) increases. However,

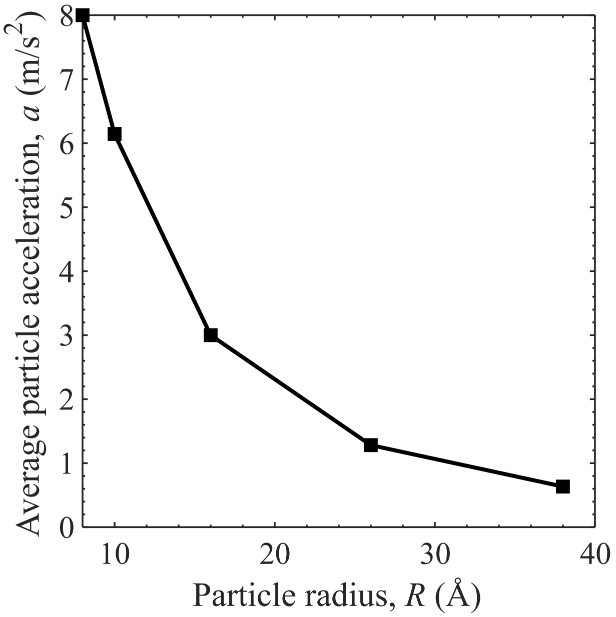

Figure 5.9: Average particle acceleration as a function of particle radius (R) for sticky collisions with C = 0.25.

increasing the initial particle velocity decreases the duration, Δt, that the nanoparticle is attracted by the surface. Therefore, as shown in Figure 5.7b, for each particle size, Δv decreases with increasing the initial velocity (v_0).

Figure 5.10a shows impact velocity *vs.* initial velocity (v_i *vs.* v_0) for different particle sizes. The impact velocity (v_i) increases with decreasing particle size for all initial impact velocities. This is because the acceleration, which is proportional to an increase in velocity from v_0 to v_i, increases with decreasing particle size. Therefore, v_i increases with decreasing particle size. As shown in Figure 5.10a, the impact velocity depends on particle size for impacts with initial velocity of $v_0 < 220$ m/s, but the degree of dependence becomes less and less as the initial particle velocity increases.

Figure 5.10a shows that v_i starts with size-dependent for $v_0 < 220$ and later becomes

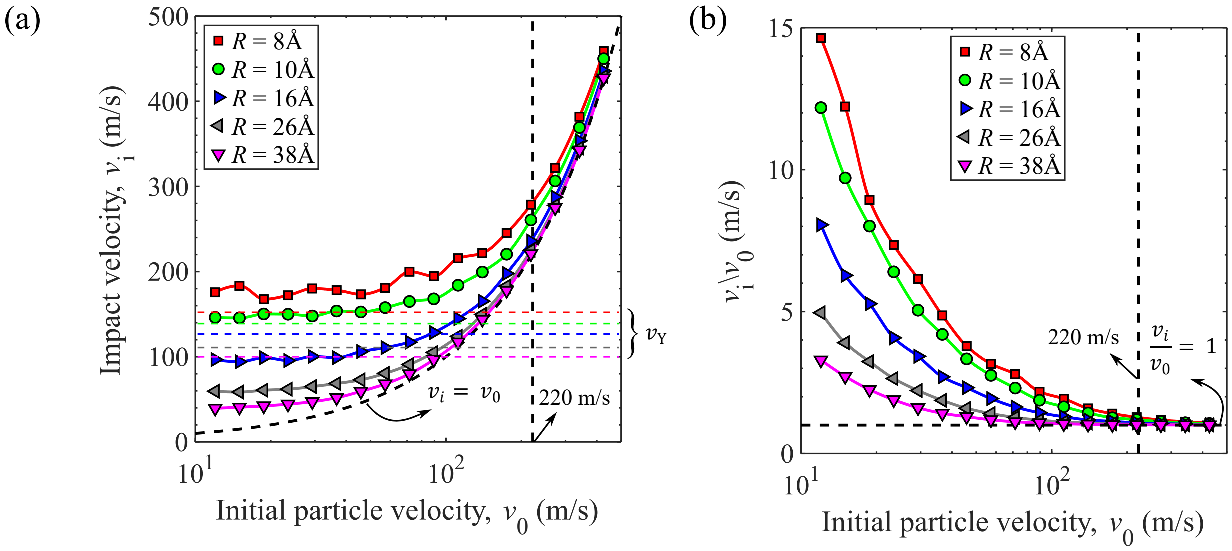

Figure 5.10: (a) Impact velocity *vs.* initial particle velocity. The dashed lines show the yield velocity for each particle size. (b) The ratio of impact velocity to initial particle velocity *vs.* initial particle velocity.

size-independent regardless of the increase in initial particle velocity. The reason is as follows. Based on the definition of acceleration $a = \Delta v \times \Delta t$, the increase in velocity from v_0 to v_i is proportional to $a \times \Delta t$. For high initial velocities, the time it takes for the particle to enter the LJ potential field of the surface is short. Because acceleration is only a function of particle size and is not affected by v_0, $\Delta v = v_i - v_0$ decreases as v_0 increases until it becomes nearly size-independent for $v_0 > 220$ m/s.

Figure 5.10b also shows the ratio of v_i/v_0 for all particle sizes and particle velocities. This ratio is higher for small particles than for the big ones for low-speed impacts at $v_0 < 220$ m/s then converges to unity as the particle velocity increases to $v_0 > 220$ m/s, indicating that the increase in velocity, Δv, becomes negligible at high particle velocities.

Here, the dependence of the CoR for adhesive collisions shown in Figure 5.6 is justified using the data in the Figure 5.10a and Figure 3c. Figure 5.3c shows that the yield velocity is $v_Y = 156.4, 139.7, 125.2, 111.8, 100.1$ m/s for particles with radius of $R = 8, 10, 16, 26, 38$ Å, respectively. Figure 5.10a shows that, by increasing the initial particle velocity (v_0) for particles with radii ranging from 16 Å to 38 Å, the impact velocity (v_i) remains below and then exceeds the yield velocity v_Y. If $v_i < v_Y$, the low-speed collisions remain viscoelastic, which results in a nearly constant CoR in Figure 5.6. However, as introduced in Section 5.3.1, as the initial particle velocity increases, v_i exceeds v_Y and the collision lies the plastic deformation regime. Therefore, the CoR of particles with radii ranging from 16 Å to 38 Å decreases because of the energy loss during plastic deformation (*see* Figure 5.6). For all initial particle velocities v_0, however, v_i is higher than 190 m/s and 146 m/s for particles with radii of 8 Å and 10 Å, respectively. The yield velocities for these particles are 156 m/s and 139 m/s, respectively. Therefore, the particles with radii of 8 Å and 10 Å undergo plastic deformation even their initial velocities are less than the yield velocity. The reason is that their impact velocities (v_i) are higher than their yield velocities. As a result, the kinetic energy loss of these particles increases during their plastic deformation. Therefore, the CoR for small particles are lower than those in the equivalent viscoelastic regime for bigger particles.

In addition, Figure 5.10a shows that the impact velocity for small particles with radii of 8 Å and 10 Å remains higher than that for bigger ones at $v_Y < v_0 < 220$ m/s. Thus, the degree of plastic deformation and the resultant energy loss, which increase with the particle velocity *see* Figure 5.3b), are higher for small particles than for the larger ones when initial velocity is less than 220 m/s. Therefore, the CoR for particles with radii of 8 Å and 10 Å are lower than those for bigger particles with radii in the range of 16 Å to 38 Å for low-speed impacts at $v_0 < 220$ m/s. The impact velocities for initial particle velocities higher than 220 m/s are size-independent (*see* Figures 5.10a and 5.10b). Therefore, the CoR for all particle sizes show the same trend as the purely repulsive collisions (*see* Figure 5.3a) and the CoR increases slightly for particles with radii ranging from 8 Å to 26 Å, and the rate of CoR decrease slows down for particles with a radius of 38 Å. As discussed for purely repulsive collisions in Section 5.3.1, the reason is that the rate of increase in the degree of plastic deformation slows down for initial velocities higher than 220 m/s.

The rest of this section explains the effects of particle-surface attraction strength on CoR. The coefficient C is 0.15 and 0.35 for weakly adhesive and highly adhesive collisions, respectively.

Weakly Adhesive collisions at $C = 0.15$

Figure 5.11a shows the CoR of weakly adhesive collisions for different particle sizes and initial particle velocities, where the coefficient C is 0.15. The CoR of these collisions approach that of the purely repulsive collisions introduced in Section 5.3.1. Therefore, when $C = 0.15$ the weakly adhesive collisions are more or less identical to the purely repulsive collisions discussed in Section 5.3.1 (*see* Figure 5.3a).

For small initial velocities (v_0) quasi-elastic collisions are observed as described in Section 5.3.1 for purely repulsive collisions. This indicates that the CoR in this viscoelastic regime remains close to unity, which is expected because of the weak attraction between the particle and the surface. As seen in Figure 5.11b, the weak attraction between the particle and the surface increases the particle velocity from v_0 to v_i while the particle is approaching the surface. However, the impact velocity (v_i) remains below the yield velocity v_Y (*see* Figure 5.3c) for low-speed impacts. Therefore, the collision of all particle sizes remains elastic at low-speed impacts at which the impact velocity remains below the yield

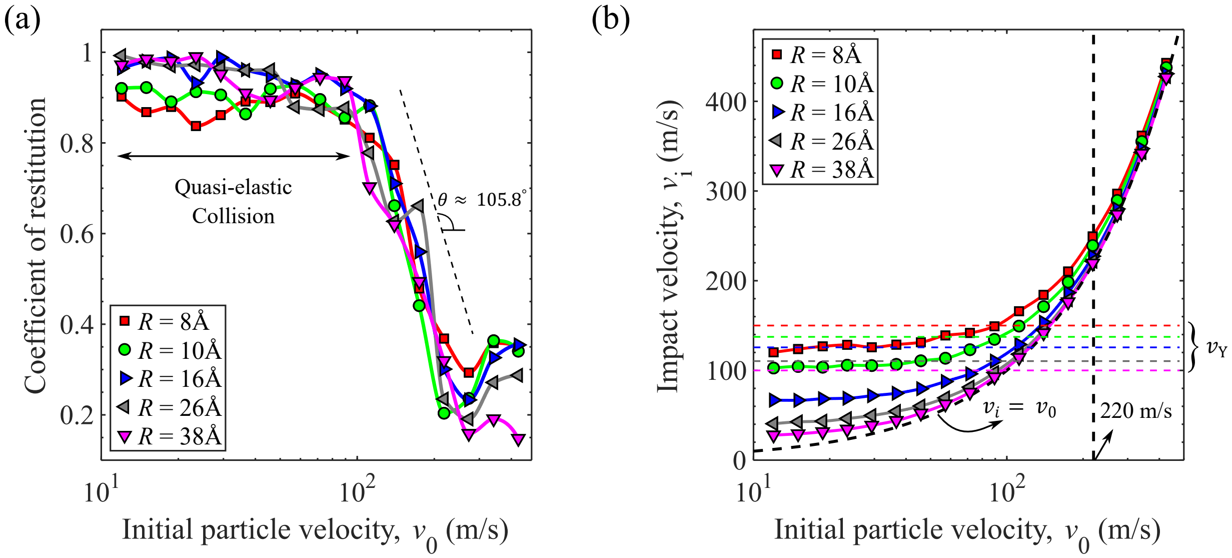

Figure 5.11: (a) Coefficients of restitution *vs.* initial particle velocity for weakly adhesive collisions with $C = 0.15$. (b) Impact velocity as a function of initial particle velocity. The dashed lines show the yield velocity for each particle size.

velocity (*see* Figure 5.3c). Therefore, the weakly adhesive collisions behave like the purely repulsive collisions. This conclusion is valid if the adhesion is reasonably weak at which the impact velocity remains below the yield velocity.

It should be noted that the CoR for weakly adhesive collisions in the viscoelastic regime (*see* Figure 5.11a) is slightly lower than those for purely repulsive collisions in the same viscoelastic regime (*see* Figure 5.3a). In addition, despite purely repulsive collisions, the CoR for weakly adhesive collisions does not exceed unity. The reason is that the slight energy loss arises from the adhesion force between particle and surface, which slightly decreases the CoR for weakly adhesive collisions compared to purely repulsive collisions.

Figure 5.11a shows that, as the initial velocity increases, the CoR remains close to unity in the viscoelastic regime and then drops in the initial velocity. As introduced in Section 5.3.1, the velocity corresponding to the drop is indeed the yield velocity where the collision is transferred from elastic to plastic regime. The CoR of the nanoparticles decreases at the same rate of the CoR decrease for purely repulsive collision (*see* Figure 5.3a). This indicates that the kinetic energy loss of rebounding nanoparticles due to the weak attraction is negligible compared with the energy loss from the plastic deformation. As a result, the CoR for the weakly adhesive collisions in the plastic deformation decays at a similar rate of the decrease of the CoR for purely repulsive collisions.

Highly Adhesive Collisions at $C = 0.35$

Figure 5.12a shows the calculated CoR for highly adhesive collisions for different particle sizes and particle velocities. The coefficient for adhesion strength, C, is 0.35 to strengthen the particle-surface adhesion. Relative decrease in CoR compared to the CoR of collisions with less adhesion at $C = 0.15, 0.25$ shown in Figure 5.11a and Figure 5.10 indicates that a nanoparticle with a stronger adhesion force is more prone to adhere to the surface.

Figure 5.12a shows that, for particles with radii of 16, 26, 38 Å, the CoR remains constant for initial velocities less than 71, 57, 45 m/s, respectively, indicating a viscoelastic collision. This viscoelastic regime can be justified by comparison of the impact velocities of these particles and their yield velocities. Figure 5.12b shows the impact velocity (v_i) *vs.* v_0 for different particle sizes. The attraction force accelerates the particle while it approaches the surface. For initial velocities corresponding to the viscoelastic regime shown in Figure 5.12a, v_i remains below the yield velocity v_Y (*see* Figures 5.3a and 5.12b). Therefore, the collision at $v_0 < 71, 57, 45$ m/s remains elastic for particles with radii of 16, 26, 38 Å and the CoR fluctuates around a constant value.

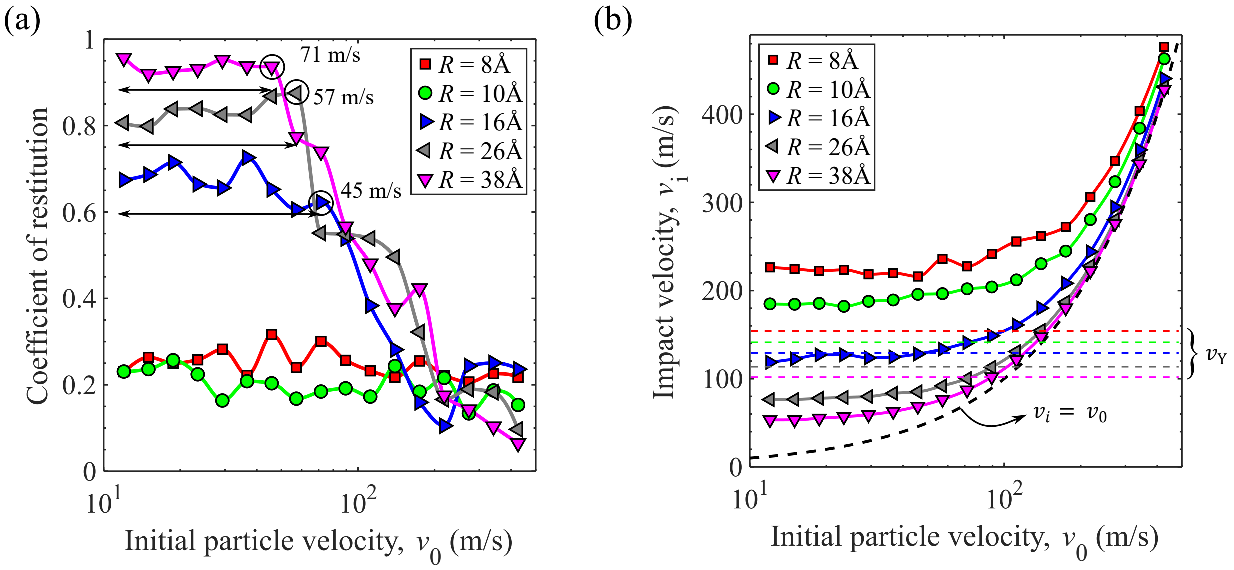

Figure 5.12: (a) Coefficient of restitution *vs.* initial particle velocity for $C = 0.35$. (b) Impact velocity *vs.* initial particle velocity. The dashed lines show the yield velocity for each particle size.

It should be noted that the CoR for $C = 0.35$ (*see* Figure 5.12a) decreases with decreasing the particle size in the viscoelastic regime, which is different from when C is 0.15 and 0.25. As shown in Figure 5.12a, the CoR for $C = 0.35$ in the viscoelastic regime decreases from 0.9 to 0.65 when the particle size decreases from 38 Å to 16 Å. According to Eq. 2.1, the CoR is inversely related to the ratio of the energy loss to the kinetic energy of the collision E_{loss}/KE_i. Without plastic deformation, the energy loss in the viscoelastic regime is mainly originated from the particle-surface attraction force. This particle-surface attraction force is applied to the nanoparticle during the rebounding stage and prevents the nanoparticle from moving away from the surface. The particle-surface attraction force during the rebounding stage is only applied to the atoms of the nanoparticle if their distance to the surface is less than 16 Å (*see* Figure 5.7a). Therefore, according to Eq. 5.3, the particle-surface attraction force in the rebounding stage (same as the collision stage) increases with decreasing the particle radius R. This suggests that the energy loss arises from the particle-surface attraction at the rebounding stage increases with decreasing the particle size. Additionally, kinetic energy of the collision KE_i is proportional to particle mass and as a result it increases with the particle size R. Subsequently, E_{loss} increases and KE_i decreases as the particle size decreases from 38 Å to 16 Å, which leads to decreasing of the CoR in the elastic regime as the particle size decreases from 38 Å to 16 Å. It is worth mentioning that this size-dependent CoR is no longer observed in viscoelastic regime for low-adhesive collisions at $C = 0.15$ and 0.25. The reason is that the kinetic energy of the collision increases because of the attraction force between particle and surface in the colliding stage. However, this particle-surface attraction force dissipates the kinetic energy of the collision during the rebounding stage. the energy loss from particle-surface attraction in the rebounding stage is insufficient to overcome the increase in the kinetic energy of the collision. Therefore, the CoR in the elastic regime (*see* Figure 5.11a and Figure 5.6) for particles with radii ranging from 16 Å to 38 Å changes slightly with the particle size, thanks to the small amount of this change, the dependence of the CoR on the size disappears.

Figure 5.12a shows that the CoR for particles with radii of 8 Å and 10 Å fluctuates around 0.2 for all values of v_0. This relatively low value of CoR indicates that the nanoparticles are prone to adhere to the surface even at initial particle velocities lower than the yield velocity. The reason is the significant velocity increase ($v_i > 185$ m/s) due to strong attraction between the particle and the surface, where the coefficient of attraction strength C increases to 0.35. As shown in Figure 5.12b, for all values of v_0, the impact velocity v_i is higher than 225 m/s and185 m/s for particles with radii of 8 Å and 10 Å, respectively.

Therefore, according to Figure 5.3b, the nanoparticle experiences plastic deformation after collision. Because the energy loss due to the particle-surface attraction also becomes appreciable for highly adhesive collisions, the energy loss from both mechanisms of plastic deformation and particle-surface adhesion dissipates almost all the initial kinetic energy of the colliding nanoparticle, which results in a low CoR around 0.2 for low values of v_0 (*see* Eq. 2.1). As the initial velocity increases, both the kinetic energy of the collision (KE_i) and the energy loss (E_{loss}) due to plastic deformation increase (*see* Figure 5.3b). Therefore, the CoR fluctuates around the constant value of 0.2 since both KE_i and E_{loss} increases (*see* also Eq. 2.1).

5.4 Summary

This chapter presents the collisional properties of silver (Ag) particles between 1.6 nm and 7.6 nm in diameter colliding on an Ag surface at initial velocities ranging from 12 to 426 m/s, representing the transition from the elastic to plastic collision regime. The yield velocity, a critical velocity above which the particle undergoes plastic deformation, for each particle size is obtained from the CoR for purely repulsive collisions. For purely repulsive collisions there is no attraction between the particle and the surface, and the only energy loss mechanism that can change the CoR is plastic deformation. For adhesive collisions, depending on the adhesivity of the collision and the particle velocity, the CoR of the collision depends on the particle size. Although, it was previously showed by Awasthi *et al.* [38] that the adhesion probability (which is inversely related to the CoR) increases with decreasing the degree of adhesion (increasing C), the effects of particle size for collisions with different degrees of adhesivity were not considered in their study. In this chapter, we showed that, in agreement with their results, the CoR decreases with increasing the adhesivity of the collision (increasing C), and also showed that the CoR depends on the particle size. In the case of adhesive collision, the particle accelerates because of the particle-surface attraction force when the particle enters the interaction range of the adhesive surface which is equal to the cutoff distance for the Ag-Ag LJ interaction. The acceleration decreases with increasing particle size. Particles with radii of 8 and 10 Å accelerate so that their impact velocities are greater than the corresponding yield velocities, even when the initial particle velocity is lower than the yield velocity. The particle acceleration leads the collision from elastic to plastic deformation regime if the initial particle velocity is lower than the yield velocity. The particle acceleration also increases the degree of plastic deformation if the initial particle velocity is already higher than the yield velocity. The energy loss due to the plastic deformation of small particles with radius of 8 Å and 10 Å for impacts at $v_0 < 220$ m/s reduces the coefficient of restitution of these particles compared to larger particles with similar initial velocities. As the stickiness of the collision increases, the CoR of particles with radii of 8 and 10 Å stays around 0.2 for all initial particle velocities. For bigger particles with radius from 16 Å to 38 Å the collision remains viscoelastic for low-speed impacts at which the impact velocity remains lower than the yield velocity. Nevertheless, the CoR in viscoelastic regime decreases with decreasing particle size. For weakly adhesive collisions with the coefficient of adhesion strength C equal to 0.15, the size dependency of CoR disappears, and the nanoparticles behaves as if they are non-adhesive.

Chapter 6

Conclusion and Future Work

The presented PhD thesis aimed to clarify the collision properties between nanoparticles and solid surfaces. The effects of several parameters such as air humidity, nanoparticle size, impact velocity, surface energy, etc. were examined on the nanoparticle collision dynamics. The main contribution of this research to the field of nanoparticle-surface collision is summarized in this chapter. The insights for future research to expand the work initiated in this research are also presented in this chapter.

6.1 Development and Validation of MD codes

A simulation setup to study the aerosol filtration process using MD simulations was developed in Chapter 3. Because modeling of a real filtration process is not possible using MD simulations, several assumptions were considered to simplify the system. Therefore, the aerosol filtration process was simplified as the collision of a single nanoparticle on a flat rigid substrate. The potential parameters for the interaction between all the types presented in the simulation box (Ag, O, H) were validated by repeating the results of previous experimental and numerical studied. The embedded atom model (EAM) for the interaction energy between the silver atoms was validated. The water-water interaction energy was also validated using TIP3P and TIP4P water models.

6.2 Effects of Humidity on Nanoparticle-surface Collision

The results of MD simulations show that, depending on the ambient conditions and surface properties of the substrate, condensed water layer can either increase or decrease the nanoparticle adhesion on the substrate. It was shown that the coefficient of restitution of 5-nm particles on a wet substrate depends on the thickness of the condensed water layer on the substrate, surface energy of the substrate, and impact velocity. Depending on the surface energy of the substrate and impact velocity, the coefficient of restitution for nanoparticles colliding on a substrate either increases or decreases with increasing the thickness of the condensed water layer on the substrate. For a high-energy substrate, the coefficient of restitution of the colliding nanoparticles first increases, then decreases by increasing the water layer thickness on the substrate. This was observed for the whole range of studied velocity $v_i \in [20 - 500]$ m.s^{-1}. However, for a low-energy substrate, the effects of condensed water layer thickness on the coefficient of restitution depend on the impact velocity. The nanoparticle rebounds from a low-energy and dry substrate for impact velocities lower than 300 m.s^{-1}. The coefficient of restitution decreases by increasing the thickness of the condensed water layer until the nanoparticle adheres to the substrate. The water layer thickness at which the nanoparticle adheres to the low-energy substrate depends on the impact velocity. For higher impact velocities, the nanoparticle adheres to the low-energy dry substrate. The coefficient of restitution first increases with the condensed water layer thickness, then decreases until the nanoparticle adheres to the substrate again. The change of the coefficient of restitution with respect to water layer thickness for both high- and low-energy substrates was explained by three mechanisms of translational kinetic energy dissipation of the colliding nanoparticles: particle-substrate interaction energy, particle-water interaction energy, and plastic deformation of the nanoparticle. The particle-substrate interaction energy decreases on a wet substrate because of the formation of a dense water layer near the substrate: the water layer acts as a buffer separating the nanoparticle from the substrate. The particle-water interaction energy continuously increases with increasing water layer thickness on the substrate. Plastic deformation of the nanoparticle also decreases or remains unaffected in wet conditions.

6.3 Effects of Particle Size on Nanoparticle-surface Collision

The collisional properties of sub-10 nm silver (Ag) particles colliding on an Ag surface at initial velocities ranging from 12 to 426 m/s was studied in Chapter 5. The yield velocity, a critical velocity above which the particle undergoes plastic deformation, for each particle size is obtained from the CoR for purely repulsive collisions. For purely repulsive collisions there is no attraction between the particle and the surface, and the only energy loss mechanism that can change the CoR is plastic deformation. In the case of adhesive collision, the particle accelerates because of the particle-surface attraction force when the particle enters the interaction range of the adhesive surface which is equal to the cutoff distance for the Ag-Ag LJ interaction. The acceleration decreases with increasing particle size. Particles with radii of 8 and 10 Å accelerate so that their impact velocities are greater than the corresponding yield velocities, even when the initial particle velocity is lower than the yield velocity. The particle acceleration leads the collision from elastic to plastic deformation regime if the initial particle velocity is lower than the yield velocity. The particle acceleration also increases the degree of plastic deformation if the initial particle velocity is already higher than the yield velocity. The energy loss due to the plastic deformation of small particles with radius of 8 Å and 10 Å for impacts at $v_0 < 220$ m/s reduces the coefficient of restitution of these particles compared to larger particles with similar initial velocities. As the stickiness of the collision increases, the CoR of particles with radii of 8 and 10 Å stays around 0.2 for all initial particle velocities. For bigger particles with radius from 16 Å to 38 Å the collision remains viscoelastic for low-speed impacts at which the impact velocity remains lower than the yield velocity. Nevertheless, the CoR in viscoelastic regime decreases with decreasing particle size. For weakly adhesive collisions with the coefficient of adhesion strength C equal to 0.15, the size dependency of CoR disappears, and the nanoparticles behaves as if they are non-adhesive.

6.4 Limitations of Current Work and Insights for Future Research

This section discusses the limitations of this thesis and accordingly provides the insights for future research.

As discussed in Chapter 4, during the collision of a nanoparticle on a wet surface, the capillary force applied to the nanoparticle strongly affects the coefficient of restitution of the collision. When a nanoparticle is placed on a wet surface, the capillary force that is applied to the nanoparticle depends on how the water behaves near the surface. It was also discussed in Chapter 4 that the interfacial solid/water structural behavior depends on the wettability of the solid surface. However, in this thesis, only two surfaces with different degrees of wettability were considered. A comprehensive research is still needed to study the collision of nanoparticles on wet surfaces with different levels of wettability, superhydrophobic to superhydrophilic.

The collision outcome is mainly characterized by the coefficient of restitution which according to Eq. 2.1 depends on the kinetic energy loss of the nanoparticle. Chemical reactivity between the colliding nanoparticle and the dry or wet surface is one of the important kinetic energy loss mechanisms through chemical bond formation between the nanoparticle and the surface. As a result, the adhesion of nanoparticles to the substrate is affected by this factor. The presence of unsaturated atoms on the surface of the particle makes the nanoparticle susceptible to form chemical bonds with the atoms of the surface or the water molecules in the system. Therefore, the effects of chemical reactivity between the particle and the surface on the collision dynamics should be investigated using classical MD with bond-order potential functions.

In this work, pristine nanoparticles and a model substrate were considered without any contamination on their outermost surfaces. However, in practical applications, because of the interaction with other components in air, the nanoparticles and the substrate may be contaminated. be contaminated. Therefore, the effects of contamination or impurity atoms is one factor that can be investigated in further studies. In case of contamination, two different scenarios may happen. If the presence of contamination causes chemical reactions between the nanoparticle and substrate, the actual molecules that cover and contaminate the surface should be added in the simulations. On the other hand, the contamination may not affect any chemical reactivity of the colliding nanoparticle and substrate. In such case the effects of contamination can be modeled by modifying the surface energy of the colliding objects [71]. The reason is that, due to small size of nanoparticles, the contamination could be considered as a layer that covers the surface of the nanoparticle or substrate and changes the surface energy of the colliding objects [53]. As reported by Shafrin and Zisman [53], the surface energy mainly depends on the outermost chemical groups of the solid. Usually, atoms which are a few atomic layers below the surface should have negligible effects on surface energy wettability. Changing the outermost chemical groups transforms a high-energy surface into another which demonstrates the wetting properties of a low-energy surface with the same material.

In this thesis, only the collision of a single and dry nanoparticle on dry or wet surfaces was investigated. However, the water content in air may condense on the surface of nanoparticles. Therefore, a wet nanoparticle or a droplet containing several nanoparticles may collide the surface. The collision dynamic of wet nanoparticles or a droplet containing several nanoparticles is different from the collision dynamics of a single and dry nanoparticle on a surface. Therefore, more research is needed to fully investigate the collision process at a humid environment.

As discussed in Chapter 1, the widespread use of nanoparticles in industry causes the dispersal of unwanted nanoparticles in the air. Long-time exposure to nanoparticles can cause pulmonary disease, fibrosis, and lung cancer [19, 5]. As a result, the dispersed nanoparticles in ambient air are considered as a major source of public health concern. Filtration is an effective method that removes aerosol particles from the air stream [20]. The principles associated with the filtration of micron particles have been validated in the literature [90]; however, the mechanisms of aerosol nanoparticle filtration are still unclear [91]. Since nanoparticle removal from the air stream takes place upon collision of nanoparticles on the surface of the filter fibers, investigating the collision dynamics of nanoparticles on the filter media is essential to investigate the effects of various parameters on the filtration process. The result on the nanoparticle-surface collision dynamics presented in this research provides fundamental insights for the mechanism of air borne nanoparticle filtration. In the process of nanoparticle filtration, the highest adhesion probability is desired. Therefore, the system conditions should be modified in a way that the CoR for the collision of nanoparticles to the surface of the fibers in the filter media decreases as much as possible. Therefore, future research can be performed to determine the system conditions for a filtration process in terms of relative humidity, nanoparticle size, and surface energy of the fibers in the filter media to increase the nanoparticle-surface adhesion and as a result, the filtration efficiency.

6.5 Publications

The publications authored by the candidate are listed as follows:

- Khodabakhshi, Milad, John Z. Wen, and Zhongchao Tan. "Coefficient of restitution for silver nanoparticles colliding on a wet silver substrate." Applied Surface Science 554 (2021): 149607. [76]
- Khodabakhshi, Milad, John Z. Wen, and Zhongchao Tan. "Coefficient of restitution for sub-10 nm silver particles colliding on adhesive silver surfaces." Journal of Computational Physics, submitted on July 1 2021.
- Milad Khodabakhshi, Zhongchao Tan, and John Wen. "Effects of Surface Energy of Substrate on Water Density Profile at a Solid Interface." Canadian Society for Mechanical Engineering (CSME) 2021 Congress.

References

[1] Antonina M Monaco and Michele Giugliano. Carbon-based smart nanomaterials in biomedicine and neuroengineering. *Beilstein journal of nanotechnology*, 5(1):1849–1863, 2014.

[2] Ganesh Venugopal, Andrew Hunt, and Faisal Alamgir. Nanomaterials for energy storage in lithium-ion battery applications. *Material Matters*, 5(2):42–45, 2010.

[3] Richard R Willis, Annabelle Benin, Randall Q Snurr, and AO Yazaydin. Nanotechnology for carbon dioxide capture. *Nanotechnology for the energy challenge*, pages 517–559, 2010.

[4] Ilka Gehrke, Andreas Geiser, and Annette Somborn-Schulz. Innovations in nanotechnology for water treatment. *Nanotechnology, science and applications*, 8:1, 2015.

[5] Chiu-sen Wang and Yoshio Otani. Removal of nanoparticles from gas streams by fibrous filters: a review. *Industrial & Engineering Chemistry Research*, 52(1):5–17, 2013.

[6] Xiaoxue Zhang, Ling Wang, and Erkki Levänen. Superhydrophobic surfaces for the reduction of bacterial adhesion. *Rsc Advances*, 3(30):12003–12020, 2013.

[7] JG Partridge, SA Brown, ADF Dunbar, R Reichel, M Kaufmann, C Siegert, S Scott, and RJ Blaikie. Templated-assembly of conducting antimony cluster wires. *Nanotechnology*, 15(9):1382, 2004.

[8] Hellmut Haberland, Zinetulla Insepov, and Michael Moseler. Molecular-dynamics simulation of thin-film growth by energetic cluster impact. *Physical Review B*, 51(16):11061, 1995.

[9] Milad Khodabakhshi and Ali Moosavi. Unidirectional transport of water through an asymmetrically charged rotating carbon nanotube. *The Journal of Physical Chemistry C*, 121(42):23649–23658, 2017.

[10] Ruling Chen, Min Liang, Jianbin Luo, Hong Lei, Dan Guo, and Xiao Hu. Comparison of surface damage under the dry and wet impact: molecular dynamics simulation. *Applied Surface Science*, 258(5):1756–1761, 2011.

[11] Ruling Chen, Yihua Wu, Hong Lei, Ranran Jiang, and Min Liang. Study of material removal processes of the crystal silicon substrate covered by an oxide film under a silica cluster impact: molecular dynamics simulation. *Applied surface science*, 305:609–616, 2014.

[12] Ruling Chen, Ranran Jiang, Hong Lei, and Min Liang. Material removal mechanism during porous silica cluster impact on crystal silicon substrate studied by molecular dynamics simulation. *Applied surface science*, 264:148–156, 2013.

[13] Anthony J Stace. Molecular dynamic simulations of the elastic and inelastic surface scattering of nanoparticles. *Physical Chemistry Chemical Physics*, 16(7):3077–3086, 2014.

[14] DJ Kenny, RE Palmer, CF Sanz-Navarro, and R Smith. Implantation depth of size-selected silver clusters into graphite. *Journal of Physics: Condensed Matter*, 14(8):L185, 2002.

[15] M Châtelet, A De Martino, J Pettersson, F Pradère, and H Vach. Argon cluster scattering from a graphite surface. *Chemical physics letters*, 196(6):563–568, 1992.

[16] Hai-Ping Cheng and Uzi Landman. Controlled deposition and classification of copper nanoclusters. *The Journal of Physical Chemistry*, 98(13):3527–3537, 1994.

[17] AI Ayesh, SA Brown, A Awasthi, SC Hendy, PY Convers, and K Nichol. Coefficient of restitution for bouncing nanoparticles. *Physical Review B*, 81(19):195422, 2010.

[18] Horngming Hsieh and RS Averback. Molecular-dynamics investigation of cluster-beam deposition. *Physical Review B*, 42(8):5365, 1990.

[19] Ken Donaldson, Robert Aitken, Lang Tran, Vicki Stone, Rodger Duffin, Gavin Forrest, and Andrew Alexander. Carbon nanotubes: a review of their properties in relation to pulmonary toxicology and workplace safety. *Toxicological sciences*, 92(1):5–22, 2006.

[20] Raheleh Givehchi and Zhongchao Tan. The effect of capillary force on airborne nanoparticle filtration. *Journal of Aerosol Science*, 83:12–24, 2015.

[21] Boris Khasainov, Marc Comet, Bernard Veyssiere, and Denis Spitzer. Comparison of performance of fast-reacting nanothermites and primary explosives. *Propellants, Explosives, Pyrotechnics*, 42(7):754–772, 2017.

[22] A Awasthi, SC Hendy, P Zoontjens, and SA Brown. Reentrant adhesion behavior in nanocluster deposition. *Physical review letters*, 97(18):186103, 2006.

[23] Giancarlo Cicero, Jeffrey C Grossman, Alessandra Catellani, and Giulia Galli. Water at a hydrophilic solid surface probed by ab initio molecular dynamics: inhomogeneous thin layers of dense fluid. *Journal of the American Chemical Society*, 127(18):6830–6835, 2005.

[24] Akira Akaishi, Tomohiro Yonemaru, and Jun Nakamura. Formation of water layers on graphene surfaces. *ACS omega*, 2(5):2184–2190, 2017.

[25] Yoichi Takato, Surajit Sen, and Jeremy B Lechman. Strong plastic deformation and softening of fast colliding nanoparticles. *Physical Review E*, 89(3):033308, 2014.

[26] Seung-chai Jung, Donguk Suh, and Woong-sup Yoon. Molecular dynamics simulation on the energy exchanges and adhesion probability of a nano-sized particle colliding with a weakly attractive static surface. *Journal of aerosol science*, 41(8):745–759, 2010.

[27] M Alonso, Y Kousaka, T Hashimoto, and N Hashimoto. Penetration of nanometer-sized aerosol particles through wire screen and laminar flow tube. *Aerosol Science and Technology*, 27(4):471–480, 1997.

[28] HTMY Ichitsubo, T Hashimoto, M Alonso, and Y Kousaka. Penetration of ultrafine particles and ion clusters through wire screens. *Aerosol Science and Technology*, 24(3):119–127, 1996.

[29] Chan Soo Kim, Li Bao, Kikuo Okuyama, Manabu Shimada, and Hitoshi Niinuma. Filtration efficiency of a fibrous filter for nanoparticles. *Journal of nanoparticle research*, 8(2):215–221, 2006.

[30] Xianliang Qiao, Tiantian She, Huiling Zhang, Xin Wen, Libo Niu, Luis Ricardez-Sandoval, Jingde Li, and Guoyi Bai. One-pot synthesis of porous silica-supported

ultrafine ni nanoparticles as efficient and stable catalyst for selective hydrogenation of benzophenone. *Applied Catalysis B: Environmental*, 259:118111, 2019.

[31] Xingwang Lan, Qing Li, Lili Cao, Cheng Du, Luis Ricardez-Sandoval, and Guoyi Bai. Rebuilding supramolecular aggregates to porous hollow n-doped carbon tube inlaid with ultrasmall ag nanoparticles: A highly efficient catalyst for co2 conversion. *Applied Surface Science*, 508:145220, 2020.

[32] Krishnendu Saha, Sarit S Agasti, Chaekyu Kim, Xiaoning Li, and Vincent M Rotello. Gold nanoparticles in chemical and biological sensing. *Chemical reviews*, 112(5):2739–2779, 2012.

[33] Abhilash Sugunan. *Fabrication and Photoelectrochemical Applications of II-VI Semiconductor Nanomaterials*. PhD thesis, KTH Royal Institute of Technology, 2012.

[34] Grigoriy Kimaev and Luis A Ricardez-Sandoval. Artificial neural network discrimination for parameter estimation and optimal product design of thin films manufactured by chemical vapor deposition. *The Journal of Physical Chemistry C*, 124(34):18615–18627, 2020.

[35] Ruling Chen, Jianbin Luo, Dan Guo, and Xinchun Lu. Energy transfer under impact load studied by molecular dynamics simulation. *Journal of Nanoparticle Research*, 11(3):589–600, 2009.

[36] Rafał Przekop and Leon Gradoń. Deposition and filtration of nanoparticles in the composites of nano-and microsized fibers. *Aerosol Science and Technology*, 42(6):483–493, 2008.

[37] Paolo Valentini and Traian Dumitrica. Molecular dynamics simulations of nanoparticle-surface collisions in crystalline silicon. In *Journal of Nano Research*, volume 1, pages 31–39. Trans Tech Publ, 2008.

[38] A Awasthi, SC Hendy, P Zoontjens, SA Brown, and F Natali. Molecular dynamics simulations of reflection and adhesion behavior in lennard-jones cluster deposition. *Physical Review B*, 76(11):115437, 2007.

[39] Aruna Awasthi. Impacts with initial rotation in nanocluster deposition. *e-Journal of Surface Science and Nanotechnology*, 6:307–311, 2008.

[40] A Awasthi, SC Hendy, and SA Brown. Oblique impacts and rebounds of lennard-jones clusters on solid surfaces. *Mathematics and mechanics of solids*, 15(7):771–781, 2010.

[41] Shintaro Sato, Da-Ren Chen, David YH Pui, et al. Molecular dynamics study of nanoparticle collision with a surface-implication to nanoparticle filtration. *Aerosol and Air Quality Research*, 7(3):278–303, 2007.

[42] Christian Schöner and Thorsten Pöschel. Orientation-dependent properties of nanoparticle impact. *Physical Review E*, 98(2):022902, 2018.

[43] Abrar H Quadery, Baochi D Doan, William C Tucker, Adrienne R Dove, and Patrick K Schelling. Role of surface chemistry in grain adhesion and dissipation during collisions of silica nanograins. *The Astrophysical Journal*, 844(2):105, 2017.

[44] M Suri and T Dumitrică. Efficient sticking of surface-passivated si nanospheres via phase-transition plasticity. *Physical Review B*, 78(8):081405, 2008.

[45] Yuchen Ma, Adam S Foster, and Risto M Nieminen. Reactions and clustering of water with silica surface. *The Journal of chemical physics*, 122(14):144709, 2005.

[46] AF Miguel. Effect of air humidity on the evolution of permeability and performance of a fibrous filter during loading with hygroscopic and non-hygroscopic particles. *Journal of Aerosol Science*, 34(6):783–799, 2003.

[47] Adam P Bateman, Helene Belassein, and Scot T Martin. Impactor apparatus for the study of particle rebound: Relative humidity and capillary forces. *Aerosol Science and Technology*, 48(1):42–52, 2014.

[48] Stephen W Stein, Barbara J Turpin, Xiaoping Cai, Po-Fu Huang, and Peter H Mcmurry. Measurements of relative humidity-dependent bounce and density for atmospheric particles using the dma-impactor technique. *Atmospheric Environment*, 28(10):1739–1746, 1994.

[49] Xudong Xiao and Linmao Qian. Investigation of humidity-dependent capillary force. *Langmuir*, 16(21):8153–8158, 2000.

[50] K Narayan Prabhu, Peter Fernades, and Girish Kumar. Effect of substrate surface roughness on wetting behaviour of vegetable oils. *Materials & design*, 30(2):297–305, 2009.

[51] KJ Kubiak, MCT Wilson, TG Mathia, and Ph Carval. Wettability versus roughness of engineering surfaces. *Wear*, 271(3-4):523–528, 2011.

[52] Robert Gordon Jackson, Mostafa Kahani, Nitin Karwa, Alex Wu, Robert Lamb, Robert Taylor, and Gary Rosengarten. Effect of surface wettability on carbon nanotube water-based nanofluid droplet impingement heat transfer. In *Journal of Physics: Conference Series*, volume 525, page 012024. IOP Publishing, 2014.

[53] Elaine G Shafrin and William A Zisman. Constitutive relations in the wetting of low energy surfaces and the theory of the retraction method of preparing monolayers1. *The Journal of Physical Chemistry*, 64(5):519–524, 1960.

[54] MA Ricci, F Bruni, P Gallo, M Rovere, and AK Soper. Water in confined geometries: experiments and simulations. *Journal of Physics: Condensed Matter*, 12(8A):A345, 2000.

[55] Morten Ø Jensen, Ole G Mouritsen, and Günther H Peters. The hydrophobic effect: Molecular dynamics simulations of water confined between extended hydrophobic and hydrophilic surfaces. *The Journal of chemical physics*, 120(20):9729–9744, 2004.

[56] Marie-Claire Bellissent-Funel. Water near hydrophilic surfaces. *Journal of molecular liquids*, 96:287–304, 2002.

[57] John Dore. Structural studies of water in confined geometry by neutron diffraction. *Chemical Physics*, 258(2-3):327–347, 2000.

[58] LF Scatena, MG Brown, and GL Richmond. Water at hydrophobic surfaces: Weak hydrogen bonding and strong orientation effects. *Science*, 292(5518):908–912, 2001.

[59] Youfeng Wang, Lan Chen, Rui Chen, Guolan Tian, Dexing Li, Chunying Chen, Xiujie Ge, and Guanglu Ge. Effect of relative humidity on the deposition and coagulation of aerosolized sio2 nanoparticles. *Atmospheric Research*, 194:100–108, 2017.

[60] SG Jennings. The mean free path in air. *Journal of Aerosol Science*, 19(2):159–166, 1988.

[61] Pei Zhao, Weitao Su, Reng Wang, Xiaofeng Xu, and Fengshan Zhang. Properties of thin silver films with different thickness. *Physica E: Low-dimensional Systems and Nanostructures*, 41(3):387–390, 2009.

[62] Gary S Grest and Kurt Kremer. Molecular dynamics simulation for polymers in the presence of a heat bath. *Physical Review A*, 33(5):3628, 1986.

[63] Yoichi Takato, Michael E Benson, and Surajit Sen. Rich collision dynamics of soft and sticky crystalline nanoparticles: numerical experiments. *Physical Review E*, 92(3):032403, 2015.

[64] John D Bernal and Ralph H Fowler. A theory of water and ionic solution, with particular reference to hydrogen and hydroxyl ions. *The Journal of Chemical Physics*, 1(8):515–548, 1933.

[65] Herman JC Berendsen, James PM Postma, Wilfred F van Gunsteren, and Jan Hermans. Interaction models for water in relation to protein hydration. In *Intermolecular forces*, pages 331–342. Springer, 1981.

[66] William L Jorgensen, Jayaraman Chandrasekhar, Jeffry D Madura, Roger W Impey, and Michael L Klein. Comparison of simple potential functions for simulating liquid water. *The Journal of chemical physics*, 79(2):926–935, 1983.

[67] HJC Berendsen, JR Grigera, and TP Straatsma. The missing term in effective pair potentials. *Journal of Physical Chemistry*, 91(24):6269–6271, 1987.

[68] Daniel J Price and Charles L Brooks III. A modified tip3p water potential for simulation with ewald summation. *The Journal of chemical physics*, 121(20):10096–10103, 2004.

[69] David J Kukulka, Benjamin Gebhart, and Joseph C Mollendorf. Thermodynamic and transport properties of. *Advances in Heat Transfer*, page 325, 1987.

[70] Qianli Ma and Haisheng Fang. Viscosity prediction of water-based silver nanofluid using equilibrium molecular dynamics. In *ASME International Mechanical Engineering Congress and Exposition*, volume 50619, page V007T09A048. American Society of Mechanical Engineers, 2016.

[71] Bo Liu, Renbing Wu, Julia A Baimova, Hong Wu, Adrian Wing-Keung Law, Sergey V Dmitriev, and Kun Zhou. Molecular dynamics study of pressure-driven water transport through graphene bilayers. *Physical Chemistry Chemical Physics*, 18(3):1886–1896, 2016.

[72] SM Foiles, MI Baskes, and Murray S Daw. Embedded-atom-method functions for the fcc metals cu, ag, au, ni, pd, pt, and their alloys. *Physical review B*, 33(12):7983, 1986.

[73] Murray S Daw, Stephen M Foiles, and Michael I Baskes. The embedded-atom method: a review of theory and applications. *Materials Science Reports*, 9(7-8):251–310, 1993.

[74] Seyed Moein Rassoulinejad-Mousavi and Yuwen Zhang. Interatomic potentials transferability for molecular simulations: A comparative study for platinum, gold and silver. *Scientific reports*, 8(1):1–10, 2018.

[75] M Li and SJ Zinkle. 4.20-physical and mechanical properties of copper and copper alloys. *Comprehensive nuclear materials*, pages 667–690, 2012.

[76] Milad Khodabakhshi, John Z Wen, and Zhongchao Tan. Coefficient of restitution for silver nanoparticles colliding on a wet silver substrate. *Applied Surface Science*, 554:149607, 2021.

[77] M Gensch and AP Weber. Rebound behavior of nanoparticle-agglomerates. *Advanced Powder Technology*, 28(8):1930–1942, 2017.

[78] Hiroto Kuninaka and Hisao Hayakawa. Simulation of cohesive head-on collisions of thermally activated nanoclusters. *Physical Review E*, 79(3):031309, 2009.

[79] Christian Schöner, Stephan Rennecke, Alfred P Weber, and Thorsten Pöschel. Introduction of a new technique to measure the coefficient of restitution for nanoparticles. *Chemie Ingenieur Technik*, 86(3):365–374, 2014.

[80] Michael P Allen and Dominic J Tildesley. *Computer simulation of liquids*. Oxford university press, 2017.

[81] GM Pound et al. Calculation of potential energy parameters form crystalline state properties. *PSSAR*, 30(2):619–623, 1975.

[82] FE Bartell and JT Smith. Alteration of surface properties of gold and silver as indicated by contact angle measurements. *The Journal of Physical Chemistry*, 57(2):165–172, 1953.

[83] Steve Plimpton. Fast parallel algorithms for short-range molecular dynamics. *Journal of computational physics*, 117(1):1–19, 1995.

[84] Kenneth Langstreth Johnson and Kenneth Langstreth Johnson. *Contact mechanics*. Cambridge university press, 1987.

[85] C Thornton. Coefficient of restitution for collinear collisions of elastic-perfectly plastic spheres. 1997.

[86] Sangrak Kim. Collision of polymer nano droplets: Molecular dynamics study. *Physics Procedia*, 34:66–69, 2012.

[87] Jean-Louis Barrat and Lydéric Bocquet. Large slip effect at a nonwetting fluid-solid interface. *Physical review letters*, 82(23):4671, 1999.

[88] Hiroto Kuninaka and Hisao Hayakawa. Super-elastic collisions in a thermally activated system. *Progress of Theoretical Physics Supplement*, 178:157–162, 2009.

[89] LB Han, Q An, SN Luo, and WA Goddard III. Ultra-elastic and inelastic impact of cu nanoparticles. *Materials Letters*, 64(20):2230–2232, 2010.

[90] Albert Podgorski, Anna Bałazy, and Leon Gradoń. Application of nanofibers to improve the filtration efficiency of the most penetrating aerosol particles in fibrous filters. *Chemical Engineering Science*, 61(20):6804–6815, 2006.

[91] Raheleh Givehchi, Zhongchao Tan, et al. An overview of airborne nanoparticle filtration and thermal rebound theory. *Aerosol and Air Quality Research*, 14(1):46–63, 2014.

[92] D Poulikakos, S Arcidiacono, and Shigeo Maruyama. Molecular dynamics simulation in nanoscale heat transfer: a review. *Microscale Thermophysical Engineering*, 7(3):181–206, 2003.

[93] Loup Verlet. Computer" experiments" on classical fluids. i. thermodynamical properties of lennard-jones molecules. *Physical review*, 159(1):98, 1967.

[94] William C Swope, Hans C Andersen, Peter H Berens, and Kent R Wilson. A computer simulation method for the calculation of equilibrium constants for the formation of physical clusters of molecules: Application to small water clusters. *The Journal of chemical physics*, 76(1):637–649, 1982.

[95] Franco Mario Capaldi. *Atomistic simulations of octacyclopentyl polyhedral oligomeric silsesquioxane polyethylene nanocomposites.* PhD thesis, Massachusetts Institute of Technology, 2005.

[96] MP Allen. Dj tildesley computer simulation of liquids, 1987.

[97] JM Haile, Ian Johnston, A John Mallinckrodt, and Susan McKay. Molecular dynamics simulation: elementary methods. *Computers in Physics*, 7(6):625–625, 1993.

[98] Alex D MacKerell Jr, Donald Bashford, MLDR Bellott, Roland Leslie Dunbrack Jr, Jeffrey D Evanseck, Martin J Field, Stefan Fischer, Jiali Gao, H Guo, Sookhee Ha, et al. All-atom empirical potential for molecular modeling and dynamics studies of proteins. *The journal of physical chemistry B*, 102(18):3586–3616, 1998.

[99] Furio Ercolessi. A molecular dynamics primer. *Spring college in computational physics, ICTP, Trieste*, 19, 1997.

[100] DA McQuarrie. Statistical mechanics, harper &, 1976.

[101] Roger W Hockney and James W Eastwood. *Computer simulation using particles.* crc Press, 2021.

[102] Marcella Iannuzzi, Alessandro Laio, and Michele Parrinello. Efficient exploration of reactive potential energy surfaces using car-parrinello molecular dynamics. *Physical Review Letters*, 90(23):238302, 2003.

[103] Michael W Mahoney and William L Jorgensen. A five-site model for liquid water and the reproduction of the density anomaly by rigid, nonpolarizable potential functions. *The Journal of Chemical Physics*, 112(20):8910–8922, 2000.

[104] Bertrand Guillot. A reappraisal of what we have learnt during three decades of computer simulations on water. *Journal of molecular liquids*, 101(1-3):219–260, 2002.

APPENDICES

Appendix A

Molecular Dynamics Simulation Technique

Molecular dynamics (MD) is a powerful computational tool capable of predicting atomic-scale material behavior. In MD, each atom is determined by the spatial location of its center of mass (x, y, z), and the mass of the atom is concentrated at this point. Thus, each point defined in the simulation box represents an atom of the material under investigation. Type and structure of atoms in the simulation box and the potential function (U) for modeling the interaction among them are two essential parameters in MD simulations. The interaction potential between each atom pairs in the simulation box is determined by a specific potential function. These functions could be derived based on empirical functions fitting experimental measurements or based on *ab initio* calculations [92]. The resulting potential function will be useful and reliable if it combines accuracy, simplicity, comprehensiveness, and cost-effective computation. In general, the total potential energy of the ith atom (U_i) could be defined as the sum of potentials between this atom and other atoms in the simulation box [80].

$$U_i = \sum_{i} U_1\left(\mathbf{r}_i\right) + \sum_{i}\sum_{j>i} U_2\left(\mathbf{r}_i, \mathbf{r}_j\right) + \sum_{i}\sum_{j>i}\sum_{k>j>i} U_3\left(\mathbf{r}_i, \mathbf{r}_j, \mathbf{r}_k\right) + \dots \tag{A.1}$$

The first term of Eq. A.1, $u_1\left(\mathbf{r}_i\right)$, represents the effect of an external field on the ith atom, while the remaining terms stand for atom-atom interactions. The terms containing interaction between three or more batches of atoms greatly increase the computational cost, although, they have negligible effects on the results compared to the first two terms. Therefore, they can be ignored when possible. As a result, in the absence of an external field, the total potential energy between atom i and atom j only includes the term related to binary interactions, and the total potential function is simplified as follows:

$$U_{ij} = \sum_{i}\sum_{j>i} U_2\left(\mathbf{r}_i, \mathbf{r}_j\right) = \sum_{i}\sum_{j>i} U\left(r_i, r_j\right) = \sum_{i}\sum_{j>i} U\left(r_{ij}\right) \tag{A.2}$$

The total interaction force between atom i and atom j ($\mathbf{F}_{ij}$), which depends only on the distance vector between atom i and j ($\mathbf{r}_{ij}$), is defined as the derivative of their interatomic potential energy (*see* Eq. A.3) [92]. Figure A.1 shows an image of vectors $\mathbf{F}_{ij}$ and $\mathbf{r}_{ij}$.

$$\mathbf{F}_{ij} = -\sum_{i\neq j} \frac{\partial U\left(r_{ij}\right)}{\partial \mathbf{r}_{ij}} \tag{A.3}$$

A.1 Equations of Motion

The equation governing the motion of each atom is defined by Newton's second law [92]:

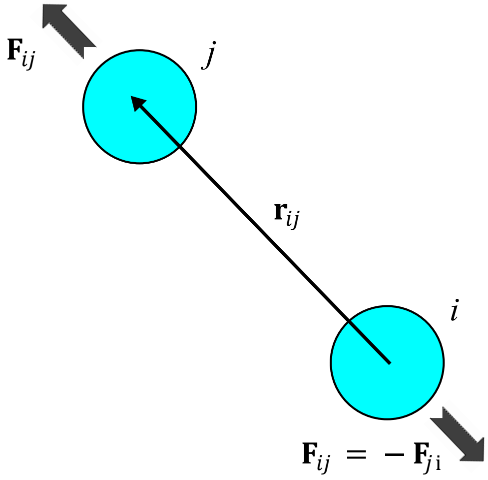

Figure A.1: Interatomic interaction between atoms i and j, with the distance vector $\mathbf{r}_{ij}$ between them.

$$\frac{\mathbf{F}_i}{m_i} = \frac{d\mathbf{r}_i^2}{dt^2} \tag{A.4}$$

where m_i and $\mathbf{r}_i$ stand for the mass and position vector of atom i. Equation A.4 must be modified so that the trajectory of each particle can be determined as a function of time. Velocity Verlet [93, 94] algorithm is the most common method of integrating atomic equations of motion in MD simulations:

$$\mathbf{r}\left(t+dt\right) = \mathbf{r}\left(t\right) + dt\mathbf{v}\left(t\right) + \frac{1}{2}\left(dt\right)^2\mathbf{a}(t) \tag{A.5}$$

$$\mathbf{v}\left(t+\frac{1}{2}dt\right) = \mathbf{v}\left(t\right) + \frac{1}{2}dt\ \mathbf{a}(t) \tag{A.6}$$

$$\mathbf{v}\left(t+dt\right)=\mathbf{v}\left(t+\frac{1}{2}dt\right)+\frac{1}{2}dt\ \mathbf{a}(t+dt) \tag{A.7}$$

where dt is the time step, $\mathbf{v}$ is the velocity vector, and $\mathbf{a}$ is the acceleration vector of the atom. In these equation series, the position and velocity of each atom are updated to $t+dt$. In the first equation, the position is calculated at $t+dt$ based on the values of $\mathbf{r}$, $\mathbf{v}$, and $\mathbf{a}$ at time t. Velocity calculation at $t+dt$ takes place in two steps. In the first step, using the acceleration at time t, the value of velocity at midpoint $t+\frac{1}{2}dt$ is calculated. Then, using the position vector at $t+dt$, the force, and subsequently, the acceleration is calculated at $t+dt$. Finally, in Equation A.7, the velocity is obtained at the moment $t+dt$.

A.2 Time Step (dt)

Choosing an appropriate time step depends sensitively on the system conditions. If the time step is too small, only a small portion of the path is traversed during each step. If the time step is too high, it will cause an error in the integration algorithm. The time step should be chosen such that while maintaining accuracy, it reduces the simulation time. It should be kept in mind that the time step must be smaller than one tenth of the largest interatomic frequency in the system. For flexible molecules, the highest frequency is related to the vibration of bond stretching between the atoms. However, such high-frequency motions have little effects on the overall behavior of the system. One solution is to freeze such vibrations by binding the bonds at their equilibrium distance and allow other degrees of freedom to change under the influence of existing intermolecular and intramolecular forces. With this method, a larger time step can be used. The convergence of the whole system's energy during the simulation is a suitable criterion for verifying the accuracy of the time step.

A.3 Thermodynamic Properties

In MD simulations, thermodynamic properties can be determined using the information obtained from the atomic motions. The properties obtained from the simulations have oscillatory behavior over time, so measuring a thermodynamic property means calculating its average over time. The average of a physical quantity can be calculated as follows [95].

$$\langle A \rangle = \frac{1}{\tau} \int_0^t A\left(t\right) dt \tag{A.8}$$

The main thermodynamics properties of a systems are the energy, temperature, and pressure of that system.

A.3.1 System Energy

The total energy (E) of a system consisting of N atoms is defined as the sum of the potential energy (U), and the kinetic energy (K).

$$\langle E \rangle = \langle U \rangle + \langle K \rangle = \langle \sum_{i}^{N-1} \sum_{j>i}^{N} u\left(r_{ij}\right) \rangle + \frac{1}{2} \langle \sum_{i}^{N} m_i v_i^2 \rangle \tag{A.9}$$

The potential energy is calculated based on Eq. A.2 at each step, and the average values are reported at different steps. The kinetic energy is also related to the particle mass and velocity. At each step of the simulation, the kinetic and potential energies are converted to each other, while, the total energy of the system is conserved. Accordingly, the convergence of energy is usually used to test the stability of the system.

A.3.2 System Temperature

One of the important thermodynamic properties is the temperature of the system. For an atomic system, temperature is related to the speed of each atom [80].

$$T = \frac{2\langle K \rangle}{3Nk_b} = \frac{\langle \sum_i^N m_i v_i^2 \rangle}{3Nk_b} \tag{A.10}$$

where k_b is the Boltzmann constant. The equation shows that $\langle K \rangle = (3N)\,\frac{1}{2}k_bT$, indicating that the degrees of freedom in each direction contribute equally to the average temperature. In other words, the kinetic energy of the system is divided equally between its degrees of freedom [96].

A.3.3 System Pressure

Another important physical quantity is pressure. The pressure is influenced by both kinetic and potential energies. The potential energy is usually calculated using the Clausius virial theorem. Virial is defined as the product of the position vector of the particles in the force exerted on them.

$$P = \frac{Nk_bT}{V} + \frac{1}{3V}\langle \sum_i^{N-1} \sum_{j>i}^{N} r_{ij}.\mathbf{F}_{ij} \rangle \tag{A.11}$$

The two terms of the right-hand side of Eq. A.11 show the kinetic energy and potential contribution, respectively [97]. In an ideal gas, only the forces due to the interaction between the atoms and the container wall affect the system behavior. Consequently, for an ideal gas, the second term, which refers to viral is zero. However, for real gases or liquids, the interatomic forces are not zero and affect the atoms and thus the pressure in Eq. A.11. Therefore, the contribution of the interatomic interactions should be considered to calculate the pressure of the system.

A.4 Force Calculation

The force acting on atom i is calculated by its potential energy arising from atom j [92].

$$\mathbf{F}_i = -\sum_{i \neq j} \frac{\partial u\left(r_{ij}\right)}{\partial \mathbf{r}_{ij}} \tag{A.12}$$

The pair interaction energy between atoms i and j, $u\left(r_{ij}\right)$, falls into two main categories: bonded and non-bonded. For each, a general potential function is needed to calculate the pair interaction energy. The parameters required to fit into the equation are determined by a prescribed force-field. The force-field parameters are determined on the basis of experimental data or quantum mechanics measurements.

A.4.1 Bonded Interactions

The bonded interactions arise from the bonds between the atoms of a molecule, holding them together. The general relation of the bonding interactions is as follows [98]:

$$U\left(r_i\right) = \sum_{bonds} K_b \left(r_b - r_0\right)^2 + \sum_{angles} K_\theta \left(\theta_b - \theta_0\right)^2 + \sum_{dihedrals} K_\phi \left[1 + \cos\left(n\phi_d - \gamma\right)\right] \tag{A.13}$$

where r_b, θ_b and ϕ_d are the instantaneous values of bond length, bond angle, and dihedral angle, respectively, and r_0, θ_0, and γ are the corresponding equilibrium values.

K_b, K_θ and K_ϕ are the stretching, bending, and dihedral spring constants, and γ is the period of the torsional potential. Equation A.13 shows that the bonded interaction includes three terms of bond stretching, angle bending, and dihedral. The bond stretching relates to the interaction energy that controls the distance between two bonded atoms. The angle bending correlates the equilibrium angle between three bonded atoms. The dihedral relates to the equilibrium position of four atoms that are bonded together.

many body potentials of embedded-atom-model (EAM)

A.4.2 Non-bonded Interactions

This type of interaction exists between all the atoms in the simulation box and is divided into two categories: van der Waals (vdW) and Columbus interaction energies. Various models have been proposed for calculating the vdW interaction such as Lennard-Jones (LJ) potential function. The Lenard-Jones (LJ) model is described as follows [99, 100]:

$$U_{LJ}(r_{ij}) = 4\varepsilon \left[\left(\frac{\sigma}{r_{ij}} \right)^{12} - \left(\frac{\sigma}{r_{ij}} \right)^{6} \right] \tag{A.14}$$

where r_{ij} is the distance of atoms, ε is the depth of the potential energy well, and σ is the interatomic distance at which the potential between two atoms becomes zero. The LJ parameters depend on the atom type and are determined by fitting the LJ curve to experimental data or measurements based on quantum mechanics studies. The LJ potential consists of two repulsive, $\left(\frac{\sigma}{r_{ij}} \right)^{12}$, and attractive, $\left(\frac{\sigma}{r_{ij}} \right)^{6}$, parts. If the distance between two atoms is too low, $r_{ij} < \sigma$, the potential is repulsive. By increasing the distance between them, $r_{ij} > \sigma$, the attraction part dominates, and the interaction becomes attractive.

When both i and j atoms are electrically charged, in addition to the vdW interaction, the Coulomb interaction will also appear between them. The functional form of this interaction is as follows:

$$U_C\left(r_{ij}\right) = k\frac{q_i q_j}{r_{ij}} \tag{A.15}$$

where k is the dielectric constant and q_i and q_j are the point charges of the particles i and j.

A.5 Cut-off Radius (r_c)

Despite the high accuracy of the MD method, its computational cost is still a serious problem. It is necessary to employ strategies to reduce computational costs while maintaining accuracy. In the case of non-bonded vdW interactions, the potential energy acting on each atom mainly originates from the nearby atoms. For example, for the LJ potential, the potential value at the cut-off radius of $r_c = 2.5\sigma$ is only 0.0016ε. Therefore, if only the interactions caused by atoms within the cut-off radius are considered, the computational cost will be reduced by $\frac{4}{3}\pi r_c^3/V$, which V is the volume of the simulation box. Therefore, choosing an appropriate cut-off radius reduces the computational cost considerably. In order to avoid the potential discontinuity at $r = r_c$, the constant value of the potential at this radius, $U\left(r_c\right)$, is subtracted from the potential interaction. The cut-off radius is applied as follows [99]:

$$U\left(r_{ij}\right)=\begin{cases}U\left(r_{ij}\right)-U\left(r_c\right) & r_{ij}\leq r_c\\ 0 & r_{ij}\geq r_c\end{cases} \tag{A.16}$$

A.6 Water Models

Despite the simple molecular structure, water exhibits complex and unusual behaviors. Numerous molecular models have been proposed to justify the properties of water under various conditions. The development of molecular water models has a long history. The first attempts in this regard relate to Bernal and Fowler's study in 1933 [64]. The modern development of molecular water models in computer simulations began in 1970, and many of the models used today were developed in 1980. In 1981, Berendsen *et al.* [65] proposed the SPC model. The more sophisticated TIP3P and TIP4P models were also introduced in 1983 [66]. In the SPC/E model [67], which is an extended SPC model, the polarization effects of water are also taken into account.

Generally, water models are numbered based on the interactive sites in the water molecule in that model. So far, water models with 3 to 6 interactive sites are developed. For the 3-site model, each atom of one molecule interacts with the atoms of the other molecule. As a result, a total of 9 interactions are calculated between every two molecules. Similarly, for 4-site model 10, for 5-site model 17, and for 6-site model 26, interactions are calculated between every two molecules. The computational cost of the simulations increases with the number of interactive sites. Therefore, 3-site water models are usually used in MD studies due to its low computational cost. Table A.1 summarizes the potential interaction parameters for some of the most common water models. Examples of 4-, 5, and 6-site water models are TIP4P, TIP5P, and TIP6P, respectively.

Table A.1: Potential parameters for some three site water models.

Parameters	Unit	TIP3P [101]	modified TIP3P [68]	SPC [65]	SPC/E [102]
σ_{OO}	Å	3.5365	3.150	3.5533	3.5533
ε_{OO}	kcal/mole	0.1521	0.1521	0.1553	0.1553
σ_{HH}	Å	0.0	0.4	0.0	0.0
ε_{HH}	kcal/mole	0.0	0.0461	0.0	0.0
σ_{OH}	Å	0.0	1.775	0.0	0.0
ε_{OH}	kcal/mole	0.0	0.0837	0.0	0.0
q_O	e	-0.834	-0.834	-0.82	-0.8476
q_H	e	0.417	0.417	0.41	0.4238
b_0^{OH}	Å	0.9572	0.9572	1.0	1.0
θ_0^{OH}	deg	104.52	104.52	109.47	109.47

One of the challenging behaviors of water is its unusual density at $T = 277$ K, which reaches its maximum at atmospheric pressure. So far, none of the mentioned models have been able to reproduce the correct water density at this temperature. The five-site TIP5P [103] model proposed in 2000, while maintaining high structural quality and thermal properties of water, is able to reproduce the water density correctly in this temperature range. During the last decades, a vast number of scientific research has been conducted to improve water models [104], and given the prospects ahead, much of the research will be addressed in the future.

Each molecular model of water is capable of reproducing one or more physical properties of water, such as radial distribution function, density variation, dipole moment, and so on. In fact, none of the models are able to reproduce all the physical properties of water. In addition, all classical molecular models consider only binary interactions in their calculations and neglect triple interactions, which account for about 14.5% of total internal energy, which is a drawback of the classical water models. However, the simulations performed by classical water models have had a great impact in many areas of physics and chemistry.

Molecular water models are divided into two simple and polarizable categories. Unlike polarizable models, simple models neglect the LJ interaction for hydrogen atoms. The Coulomb interaction, which results from the partial electric charge of hydrogen and oxygen, models the hydrogen bond between the water molecules. The intermolecular interactions for these models are described below [80].

$$V_{ij} = \sum_i \sum_j \frac{q_i q_j e^2}{4\pi\varepsilon_0 r_{ij}} + \frac{C_{12}}{r_{ij}^{12}} + \frac{C_6}{r_{ij}^{6}} \tag{A.17}$$

where i and j represents for the O and H atoms, and r_{ij} stands for their interatomic distance. Given that the internal bonds are kept frozen, bonded interactions do not appear in the above equation.

Appendix B

Rights and Permissions

The permissions to reuse the figures from other published papers are provided in this section.

Permission to reuse Figure 2.1:

American Physical Society
Reuse and Permissions License

09-Sep-2021

This license agreement between the American Physical Society ("APS") and Milad Khodabakhshi ("You") consists of your license details and the terms and conditions provided by the American Physical Society and SciPris.

Licensed Content Information

License Number:	**RNP/21/SEP/044325**
License date:	09-Sep-2021
DOI:	10.1103/PhysRevLett.97.186103
Title:	Reentrant Adhesion Behavior in Nanocluster Deposition
Author:	A. Awasthi et al.
Publication:	Physical Review Letters
Publisher:	American Physical Society
Cost:	USD $ 0.00

Request Details

Does your reuse require significant modifications: No

Specify intended distribution locations:	United States,Canada
Reuse Category:	Reuse in a thesis/dissertation
Requestor Type:	Student
Items for Reuse:	Figures/Tables
Number of Figure/Tables:	1
Figure/Tables Details:	FIG. 4. Page 3: The probability of sticking as a function of incident velocity for each cluster size.
Format for Reuse:	Electronic

Information about New Publication:

University/Publisher:	University of Waterloo
Title of dissertation/thesis:	Molecular Dynamics Simulation for Nanoparticle-Surface Collision
Author(s):	Milad Khodabakhshi
Expected completion date:	Sep. 2021

License Requestor Information

Name:	Milad Khodabakhshi
Affiliation:	Individual
Email Id:	m2khodab@uwaterloo.ca
Country:	Canada

American Physical Society
Reuse and Permissions License

TERMS AND CONDITIONS

The American Physical Society (APS) is pleased to grant the Requestor of this license a non-exclusive, non-transferable permission, limited to Electronic format, provided all criteria outlined below are followed.

1. You must also obtain permission from at least one of the lead authors for each separate work, if you haven't done so already. The author's name and affiliation can be found on the first page of the published Article.
2. For electronic format permissions, Requestor agrees to provide a hyperlink from the reprinted APS material using the source material's DOI on the web page where the work appears. The hyperlink should use the standard DOI resolution URL, http://dx.doi.org/{DOI}. The hyperlink may be embedded in the copyright credit line.
3. For print format permissions, Requestor agrees to print the required copyright credit line on the first page where the material appears: "Reprinted (abstract/excerpt/figure) with permission from [(FULL REFERENCE CITATION) as follows: Author's Names, APS Journal Title, Volume Number, Page Number and Year of Publication.] Copyright (YEAR) by the American Physical Society."
4. Permission granted in this license is for a one-time use and does not include permission for any future editions, updates, databases, formats or other matters. Permission must be sought for any additional use.
5. Use of the material does not and must not imply any endorsement by APS.
6. APS does not imply, purport or intend to grant permission to reuse materials to which it does not hold copyright. It is the requestor's sole responsibility to ensure the licensed material is original to APS and does not contain the copyright of another entity, and that the copyright notice of the figure, photograph, cover or table does not indicate it was reprinted by APS with permission from another source.
7. The permission granted herein is personal to the Requestor for the use specified and is not transferable or assignable without express written permission of APS. This license may not be amended except in writing by APS.
8. You may not alter, edit or modify the material in any manner.
9. You may translate the materials only when translation rights have been granted.
10. APS is not responsible for any errors or omissions due to translation.
11. You may not use the material for promotional, sales, advertising or marketing purposes.
12. The foregoing license shall not take effect unless and until APS or its agent, Aptara, receives payment in full in accordance with Aptara Billing and Payment Terms and Conditions, which are incorporated herein by reference.
13. Should the terms of this license be violated at any time, APS or Aptara may revoke the license with no refund to you and seek relief to the fullest extent of the laws of the USA. Official written notice will be made using the contact information provided with the permission request. Failure to receive such notice will not nullify revocation of the permission.
14. APS reserves all rights not specifically granted herein.
15. This document, including the Aptara Billing and Payment Terms and Conditions, shall be the entire agreement between the parties relating to the subject matter hereof.

Permission to reuse Figure 2.2:

American Physical Society
Reuse and Permissions License

09-Sep-2021

This license agreement between the American Physical Society ("APS") and Milad Khodabakhshi ("You") consists of your license details and the terms and conditions provided by the American Physical Society and SciPris.

Licensed Content Information

License Number:	**RNP/21/SEP/044326**
License date:	09-Sep-2021
DOI:	10.1103/PhysRevE.89.033308
Title:	Strong plastic deformation and softening of fast colliding nanoparticles
Author:	Yoichi Takato, Surajit Sen, and Jeremy B. Lechman
Publication:	Physical Review E
Publisher:	American Physical Society
Cost:	USD $ 0.00

Request Details

Does your reuse require significant modifications: No

Specify intended distribution locations:	United States,Canada
Reuse Category:	Reuse in a thesis/dissertation
Requestor Type:	Student
Items for Reuse:	Figures/Tables
Number of Figure/Tables:	2
Figure/Tables Details:	Page3. FIG. 1. Coefficient of restitution between nanoparticles as a function of collision velocity. FIG. 2. (a) Cluster-size dependence in yield velocity.
Format for Reuse:	Electronic

Information about New Publication:

University/Publisher:	University of Waterloo
Title of dissertation/thesis:	Molecular Dynamics Simulation for Nanoparticle-Surface Collision
Author(s):	Milad Khodabakhshi
Expected completion date:	Sep. 2021

License Requestor Information

Name:	Milad Khodabakhshi
Affiliation:	Individual
Email Id:	m2khodab@uwaterloo.ca
Country:	Canada

American Physical Society
Reuse and Permissions License

TERMS AND CONDITIONS

The American Physical Society (APS) is pleased to grant the Requestor of this license a non-exclusive, non-transferable permission, limited to Electronic format, provided all criteria outlined below are followed.

1. You must also obtain permission from at least one of the lead authors for each separate work, if you haven't done so already. The author's name and affiliation can be found on the first page of the published Article.
2. For electronic format permissions, Requestor agrees to provide a hyperlink from the reprinted APS material using the source material's DOI on the web page where the work appears. The hyperlink should use the standard DOI resolution URL, http://dx.doi.org/{DOI}. The hyperlink may be embedded in the copyright credit line.
3. For print format permissions, Requestor agrees to print the required copyright credit line on the first page where the material appears: "Reprinted (abstract/excerpt/figure) with permission from [(FULL REFERENCE CITATION) as follows: Author's Names, APS Journal Title, Volume Number, Page Number and Year of Publication.] Copyright (YEAR) by the American Physical Society."
4. Permission granted in this license is for a one-time use and does not include permission for any future editions, updates, databases, formats or other matters. Permission must be sought for any additional use.
5. Use of the material does not and must not imply any endorsement by APS.
6. APS does not imply, purport or intend to grant permission to reuse materials to which it does not hold copyright. It is the requestor's sole responsibility to ensure the licensed material is original to APS and does not contain the copyright of another entity, and that the copyright notice of the figure, photograph, cover or table does not indicate it was reprinted by APS with permission from another source.
7. The permission granted herein is personal to the Requestor for the use specified and is not transferable or assignable without express written permission of APS. This license may not be amended except in writing by APS.
8. You may not alter, edit or modify the material in any manner.
9. You may translate the materials only when translation rights have been granted.
10. APS is not responsible for any errors or omissions due to translation.
11. You may not use the material for promotional, sales, advertising or marketing purposes.
12. The foregoing license shall not take effect unless and until APS or its agent, Aptara, receives payment in full in accordance with Aptara Billing and Payment Terms and Conditions, which are incorporated herein by reference.
13. Should the terms of this license be violated at any time, APS or Aptara may revoke the license with no refund to you and seek relief to the fullest extent of the laws of the USA. Official written notice will be made using the contact information provided with the permission request. Failure to receive such notice will not nullify revocation of the permission.
14. APS reserves all rights not specifically granted herein.
15. This document, including the Aptara Billing and Payment Terms and Conditions, shall be the entire agreement between the parties relating to the subject matter hereof.

Permission to reuse Figure 2.3:

American Physical Society
Reuse and Permissions License

09-Sep-2021

This license agreement between the American Physical Society ("APS") and Milad Khodabakhshi ("You") consists of your license details and the terms and conditions provided by the American Physical Society and SciPris.

Licensed Content Information

License Number:	**RNP/21/SEP/044327**
License date:	09-Sep-2021
DOI:	10.1103/PhysRevB.76.115437
Title:	Molecular dynamics simulations of reflection and adhesion behavior in Lennard-Jones cluster deposition
Author:	A. Awasthi et al.
Publication:	Physical Review B
Publisher:	American Physical Society
Cost:	USD $ 0.00

Request Details

Does your reuse require significant modifications: No

Specify intended distribution locations:	United States,Canada
Reuse Category:	Reuse in a thesis/dissertation
Requestor Type:	Student
Items for Reuse:	Figures/Tables
Number of Figure/Tables:	1
Figure/Tables Details:	FIG. 11. The adhesion probability versus initial velocity of the 147 atom icosahedral cluster on the flat substrate for different C values.
Format for Reuse:	Electronic

Information about New Publication:

University/Publisher:	University of Waterloo
Title of dissertation/thesis:	Molecular Dynamics Simulation for Nanoparticle-Surface Collision
Author(s):	Milad Khodabakhshi
Expected completion date:	Sep. 2021

License Requestor Information

Name:	Milad Khodabakhshi
Affiliation:	Individual
Email Id:	m2khodab@uwaterloo.ca
Country:	Canada

American Physical Society Reuse and Permissions License

TERMS AND CONDITIONS

The American Physical Society (APS) is pleased to grant the Requestor of this license a non-exclusive, non-transferable permission, limited to Electronic format, provided all criteria outlined below are followed.

1. You must also obtain permission from at least one of the lead authors for each separate work, if you haven't done so already. The author's name and affiliation can be found on the first page of the published Article.
2. For electronic format permissions, Requestor agrees to provide a hyperlink from the reprinted APS material using the source material's DOI on the web page where the work appears. The hyperlink should use the standard DOI resolution URL, http://dx.doi.org/{DOI}. The hyperlink may be embedded in the copyright credit line.
3. For print format permissions, Requestor agrees to print the required copyright credit line on the first page where the material appears: "Reprinted (abstract/excerpt/figure) with permission from [(FULL REFERENCE CITATION) as follows: Author's Names, APS Journal Title, Volume Number, Page Number and Year of Publication.] Copyright (YEAR) by the American Physical Society."
4. Permission granted in this license is for a one-time use and does not include permission for any future editions, updates, databases, formats or other matters. Permission must be sought for any additional use.
5. Use of the material does not and must not imply any endorsement by APS.
6. APS does not imply, purport or intend to grant permission to reuse materials to which it does not hold copyright. It is the requestor's sole responsibility to ensure the licensed material is original to APS and does not contain the copyright of another entity, and that the copyright notice of the figure, photograph, cover or table does not indicate it was reprinted by APS with permission from another source.
7. The permission granted herein is personal to the Requestor for the use specified and is not transferable or assignable without express written permission of APS. This license may not be amended except in writing by APS.
8. You may not alter, edit or modify the material in any manner.
9. You may translate the materials only when translation rights have been granted.
10. APS is not responsible for any errors or omissions due to translation.
11. You may not use the material for promotional, sales, advertising or marketing purposes.
12. The foregoing license shall not take effect unless and until APS or its agent, Aptara, receives payment in full in accordance with Aptara Billing and Payment Terms and Conditions, which are incorporated herein by reference.
13. Should the terms of this license be violated at any time, APS or Aptara may revoke the license with no refund to you and seek relief to the fullest extent of the laws of the USA. Official written notice will be made using the contact information provided with the permission request. Failure to receive such notice will not nullify revocation of the permission.
14. APS reserves all rights not specifically granted herein.
15. This document, including the Aptara Billing and Payment Terms and Conditions, shall be the entire agreement between the parties relating to the subject matter hereof.

Permission to reuse Figure 2.6:

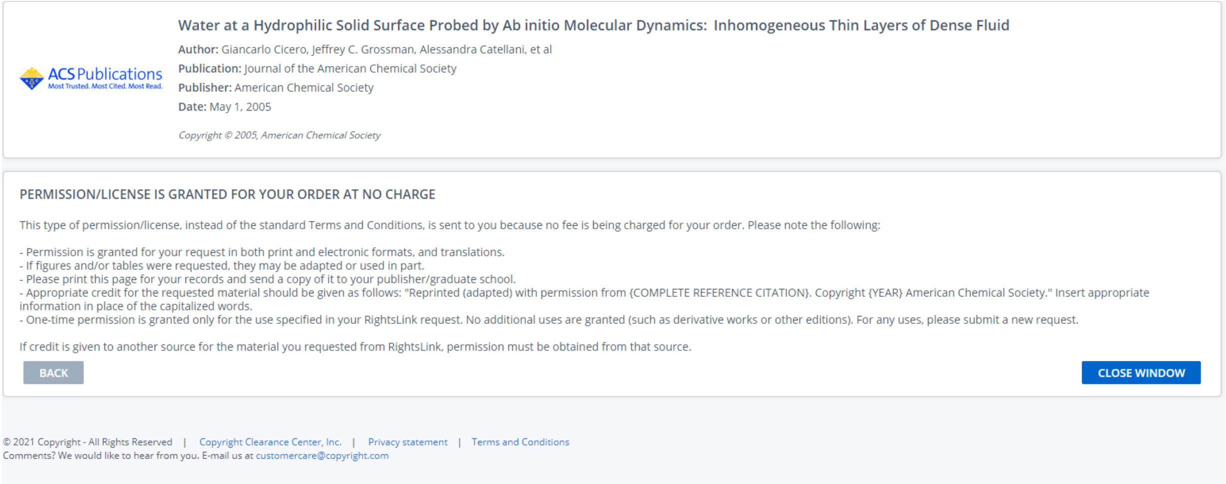

Water at a Hydrophilic Solid Surface Probed by Ab initio Molecular Dynamics: Inhomogeneous Thin Layers of Dense Fluid

Author: Giancarlo Cicero, Jeffrey C. Grossman, Alessandra Catellani, et al
Publication: Journal of the American Chemical Society
Publisher: American Chemical Society
Date: May 1, 2005

Copyright © 2005, American Chemical Society

PERMISSION/LICENSE IS GRANTED FOR YOUR ORDER AT NO CHARGE

This type of permission/license, instead of the standard Terms and Conditions, is sent to you because no fee is being charged for your order. Please note the following:

- Permission is granted for your request in both print and electronic formats, and translations.
- If figures and/or tables were requested, they may be adapted or used in part.
- Please print this page for your records and send a copy of it to your publisher/graduate school.
- Appropriate credit for the requested material should be given as follows: "Reprinted (adapted) with permission from {COMPLETE REFERENCE CITATION}. Copyright {YEAR} American Chemical Society." Insert appropriate information in place of the capitalized words.
- One-time permission is granted only for the use specified in your RightsLink request. No additional uses are granted (such as derivative works or other editions). For any uses, please submit a new request.

If credit is given to another source for the material you requested from RightsLink, permission must be obtained from that source.

© 2021 Copyright - All Rights Reserved | Copyright Clearance Center, Inc. | Privacy statement | Terms and Conditions
Comments? We would like to hear from you. E-mail us at customercare@copyright.com

Permission to reuse Figure 2.7:

AIP PUBLISHING LICENSE
TERMS AND CONDITIONS

Sep 09, 2021

This Agreement between Milad Khodabakhshi ("You") and AIP Publishing ("AIP Publishing") consists of your license details and the terms and conditions provided by AIP Publishing and Copyright Clearance Center.

License Number	5144810217142
License date	Sep 09, 2021
Licensed Content Publisher	AIP Publishing
Licensed Content Publication	Journal of Chemical Physics
Licensed Content Title	The hydrophobic effect: Molecular dynamics simulations of water confined between extended hydrophobic and hydrophilic surfaces
Licensed Content Author	Morten Ø. Jensen, Ole G. Mouritsen, Günther H. Peters
Licensed Content Date	May 22, 2004
Licensed Content Volume	120
Licensed Content Issue	20
Type of Use	Thesis/Dissertation

Requestor type	Student
Format	Electronic
Portion	Figure/Table
Number of figures/tables	1
Will you be translating?	No
Title	Molecular Dynamics Simulation for Nanoparticle-Surface Collision
Institution name	University of Waterloo
Expected presentation date	Sep 2021
Portions	Figure1, on page 9732
Requestor Location	Milad Khodabakhshi 275 Larch Street, Building G, Unit 112 Waterloo, ON N2L3R2 Canada Attn: University of Waterloo
Total	0.00 CAD

Terms and Conditions

AIP Publishing -- Terms and Conditions: Permissions Uses

AIP Publishing hereby grants to you the non-exclusive right and license to use and/or distribute the Material according to the use specified in your order, on a one-time basis, for the specified term, with a maximum distribution equal to the number that you have ordered. Any links or other content accompanying the Material are not the subject of this license.

1. You agree to include the following copyright and permission notice with the reproduction of the Material:"Reprinted from [FULL CITATION], with the permission of AIP Publishing." For an article, the credit line and permission notice must be printed on the first page of the article or book chapter. For photographs, covers, or tables, the notice may appear with the Material, in a footnote, or in the reference list.
2. If you have licensed reuse of a figure, photograph, cover, or table, it is your responsibility to ensure that the material is original to AIP Publishing and does not contain the copyright of another entity, and that the copyright notice of the figure, photograph, cover, or table does not indicate that it was reprinted by AIP Publishing, with permission, from another source. Under no circumstances does AIP Publishing purport or intend to grant permission to reuse material to which it does not hold appropriate rights.
   You may not alter or modify the Material in any manner. You may translate the Material into another language only if you have licensed translation rights. You may not use the Material for promotional purposes.
3. The foregoing license shall not take effect unless and until AIP Publishing or its agent, Copyright Clearance Center, receives the Payment in accordance with Copyright Clearance Center Billing and Payment Terms and Conditions, which are incorporated herein by reference.
4. AIP Publishing or Copyright Clearance Center may, within two business days of granting this license, revoke the license for any reason whatsoever, with a full refund payable to you. Should you violate the terms of this license at any time, AIP Publishing, or Copyright Clearance Center may revoke the license with no refund to you. Notice of such revocation will be made using the contact information provided by you. Failure to receive such notice will not nullify the revocation.
5. AIP Publishing makes no representations or warranties with respect to the Material. You agree to indemnify and hold harmless AIP Publishing, and their officers, directors, employees or agents from and against any and all claims arising out of your use of the Material other than as specifically authorized herein.
6. The permission granted herein is personal to you and is not transferable or assignable without the prior written permission of AIP Publishing. This license may not be amended except in a writing signed by the party to be charged.
7. If purchase orders, acknowledgments or check endorsements are issued on any forms containing terms and conditions which are inconsistent with these provisions, such inconsistent terms and conditions shall be of no force and effect. This document, including the CCC Billing and Payment Terms and Conditions, shall be the entire agreement between the parties relating to the subject matter hereof.

This Agreement shall be governed by and construed in accordance with the laws of the State of New York. Both parties hereby submit to the jurisdiction of the courts of New York County for purposes of resolving any disputes that may arise hereunder.

V1.2

Questions? customercare@copyright.com or +1-855-239-3415 (toll free in the US) or +1-978-646-2777.